OPTICAL - TO - OPTICAL INTERFACE DEVICE

A. D. JACOBSON

HUGHES RESEARCH LABORATORIES
3011 MALIBU CANYON ROAD
MALIBU, CALIFORNIA 90265

FEBRUARY 1973

CONTRACT NAS 5 - 11485
FINAL REPORT FOR PERIOD 1 JULY 1971 - 30 JUNE 1972

Prepared for
GODDARD SPACE FLIGHT CENTER
GREENBELT, MARYLAND 20771

1. Report No.	2. Government Accession No.	3. Recipient's Catalog No.

4. Title and Subtitle OPTICAL-TO-OPTICAL INTERFACE DEVICE	5. Report Date February 1973
	6. Performing Organization Code

7. Author(s) A.D. Jacobson	8. Performing Organization Report No.

9. Performing Organization Name and Address Hughes Research Laboratories 3011 Malibu Canyon Road Malibu, CA 90265	10. Work Unit No.
	11. Contract or Grant No. NAS 5-11485

12. Sponsoring Agency Name and Address Goddard Space Flight Center Greenbelt, MD 20771	13. Type of Report and Period Covered Final Report 1 July 1971 - 30 June 1972
	14. Sponsoring Agency Code

15. Supplementary Notes

16. Abstract

This report describes the work done on Contract NAS 5-11485 to develop the performance of a photoactivated dc liquid crystal light valve. The dc light valve is a thin film device that consists of two transparent electrodes, deposited on glass substrates, that enclose a thin film photoconductor (cadmium sulfide) and a thin layer of a nematic liquid crystal that operates in the dynamic scattering mode. The work was directed toward application of the light valve to high resolution non-coherent light to coherent light image conversion. The work was conducted in five parts: (1) Uniformity Studies, (2) Photoconductor Studies, (3) Liquid Crystal Scattering Studies, (4) Lifetime Studies, (5) Device Performance Studies. The goal of these studies was to improve the performance and quality of the already existing dc light valve device and to evaluate quantitatively the properties and performance of the device as they relate to the coherent optical data processing application. As a result of these efforts, device sensitivity was improved by a factor of ten, device resolution was improved by a factor of three, device lifetime was improved by two-orders of magnitude, undesirable "secondary" liquid crystal scattering effects were eliminated, the scattering characteristics of the liquid crystal were thoroughly documented, the cosmetic quality of the devices was dramatically improved, and the performance of the device was fully documented. These results satisfied or surpassed seven of the nine design goals that were set at the start of the program. The remaining two — unwanted scattering in the Fourier Transform Domain and device speed — were not fully satisfied. The report contains a full description of the work done on the program along with a full documentation of the performance of the device.

17. Key Words (Suggested by Author(s)) Light valve Electro-optics Liquid crystals Coherent optical data processing Real time imaging	18. Distribution Statement

19. Security Classif. (of this report) Unclassified	20. Security Classif. (of this page) Unclassified	21. No. of Pages 149	22. Price*

NASA-C-168 (Rev. 6-71)

TABLE OF CONTENTS

Preceding page blank

LIST OF ILLUSTRATIONS

LIST OF TABLES

SECTION I

INTRODUCTION, SUMMARY OF RESULTS, AND RECOMMENDATIONS

A.   INTRODUCTION

The following report describes the work done on Contract NAS 5-11485, Optical-to-Optical Interface Device Research Program. This report covers the entire contract effort, from 1 July 1971 through 30 June 1972. The primary goals of the program were to study and develop the state-of-the-art liquid crystal light valve that had been reduced to practice prior to the outset of the contract, and to deliver an improved device at the end of the program.

At the outset of the program we identified several device characteristics that required development if we were to improve the performance of the device. These included uniformity, sensitivity, and speed (both excitation and decay). In addition, we identified three aspects of the device that required study to better understand the nature and operation of the device. These included device lifetime, scattering properties, and the nature of the photoconductor/liquid crystal interface. The program was organized to explore all six of these aspects of the device, and in all cases the studies were carried out in depth. These studies are reported here with the aim of describing the tasks undertaken, the methods used, and the results obtained. The emphasis is on completeness so that the reader is fully informed on the sum and substance of the work performed. The body of the report is organized into five sections:

1.   Device Description Operation and Performance Evaluation

This section describes in full detail the design, fabrication, operation, and nominal performance of the deliverable item.

2. Uniformity Studies

A great deal of effort was directed toward the problem of reducing the background scattered light in the Fourier transform plane. Early in the program the problem was determined to be caused by liquid crystal misalignment. This section reports our efforts to produce single crystal-like alignment of the liquid crystal with the light device in the "off" state.

3. Photoconductor Studies

The sensitivity and the speed of the device depend on the nature of the photoconductor and on the nature of the interaction of the photo-conductor with the contiguous liquid crystal. A model that describes the behavior of the photoconductor in this device is presented in this section with an account of the experiments that led to improved device sensitivity.

4. Liquid Crystal Scattering Studies

To design the systems that accept this device, it is necessary to understand quantitatively the scattering performance of the device. This section describes a detailed experimental program to investigate the scattering properties of the liquid crystal. In particular, we studied the basic scattering patterns, the effect of polarization on the scattering patterns, the effect of the superimposed ac voltage on the scattering patterns, and the nature of the scattering domains.

5. Lifetime Studies

We recognized at the outset of the contract that the most serious problem that threatened the continuing development of these light valves was their limited lifetime. Consequently, we directed a major effort at gaining an understanding of the causes of the limited lifetime of the device. Our goal was to identify a means for resolving this problem. This section describes the experiments that characterized the problem and the ideas that those experiments generated toward the solution of this problem.

It is important to note that some of the device improvements reported herein (and evidenced in the delivered devices) are the result of work done on a parallel, inhouse research and development program.

The major contribution to that work was the development of room temperature, ester-base liquid crystal materials. This development was achieved in 1970 by Dr. Shi-Yin Wong of our laboratories. It was realized as the result of a 1970, Hughes Research Laboratories Internal Research and Development (IR&D) program, "Photochemistry: Liquid Crystal and Photochromic Studies." This program, directed toward basic research of liquid crystal systems, was intended to improve the photo and chemical stability of the then widely used Schiff base room temperature materials. Dr. Wong recognized that ester base materials held promise of being inherently more stable than Schiff base materials, and he set about synthesizing room temperature compositions. He accomplished his goal in 1970 when he synthesized mixtures, typified by the four-component system shown below:

2484-2

CH_3 —⟨O⟩— COO —⟨O⟩— C_4H_9

C_4H_9O —⟨O⟩— COO —⟨O⟩— OC_4H_9

$C_6H_{13}O$ —⟨O⟩— COO —⟨O⟩— OC_4H_9

$C_8H_{17}O$ —⟨O⟩— COO —⟨O⟩— OC_4H_9
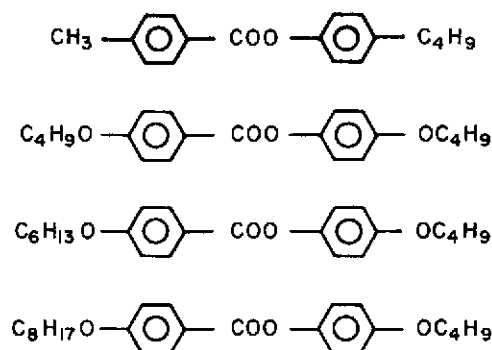
These basic liquid crystal studies have continued in parallel with various light valve device development programs. Their aim has been to improve our understanding of these materials and to explore new materials ideas, rather than to tailor specific materials for use in specific devices. Thus, this work is regarded to be outside the scope of the present program and is not reported here.

B. SUMMARY OF RESULTS

At the outset of the program we had a reduced-to-practice device that had more than adequate resolution (35 lines/mm), excellent contrast (500:1 in laser light), acceptable sensitivity (180 $\mu W/cm^2$), simplicity of fabrication, ease of use, and marginal speed (100 to 150 msec frame time). As pointed out above, it suffered from undesirable off-state scattering and enhanced scattering, from nonuniformities, and from seriously inadequate lifetime. In addition, we did not fully understand the operation of the device, nor did we have full quantitative knowledge of its operating performance. Therefore, at the outset of the program we established the following specific goals:

1. Improve the sensitivity by an order of magnitude.

2. Improve the speed (excitation plus decay) to better than 100 msec.

3. Improve the uniformity of the device by reducing the effect of fabrication defects and improving the uniformity of the liquid crystal layer.

4. Eliminate enhanced scattering.

5. Eliminate unwanted off-state scattering in the Fourier transform plane.

6. Identify the mechanisms that lead to lifetime failure of the device.

7. Evaluate quantitatively the performance of the device.

8. Acquire a quantitative understanding of the scattering performance of the liquid crystal in the device.

4

9.   Deliver an improved device that embodies the
       knowledge gained during the course of the
       program.

During the course of the program we were able to fulfill seven
of these goals, but fell short on the remaining two. Specifically, our
accomplishments were as follows:

1.   We improved the sensitivity of the device to the
       range 1 to 10 $\mu W/cm^2$.

2.   We learned how to fabricate defect-free light
       valves that are uniformly clear when viewed
       directly or when projected onto an image plane
       (but not when viewed in the Fourier transform
       plane. See below).

3.   We eliminated all traces of enhanced scattering.

4.   We identified the principal causes of lifetime
       failure. We found the following two causes:

       a.   Deterioration of the liquid crystal due
              to photo-induced effects, current-induced
              effects and impurity variations. The
              deterioration leads to the formation of
              gas bubbles and to decreased scattering
              efficiency.

       b.   Electrochemical reactions between the
              liquid crystal and the photoconductor
              that caused the photoconductor to disso-
              ciate into cadmium ions and free sulfur.
              Under the influence of the electric field,
              the cadmium crossed the liquid crystal
              layer and plated out on the counter electrode.
              The free sulfur formed an insulating layer
              that impeded the normal flow of current,
              thereby reducing the scattering of the device.

              Although our goal was merely to identify
              these mechanisms of lifetime degradation,
              we have been able, as a result of work done
              on our parallel inhouse program, to go
              beyond this goal and to prescribe corrective
              measures. In the case of the liquid crystal

degradation, during our IR&D program we found that use of an ester base liquid crystal alleviated these deleterious mechanisms because the ester base materials are substantially more stable than the then commonly used Schiff base materials, such as MBBA. Secondly, we found that the undesirable electrochemical activity at the CdS electrode could be substantially reduced by employing a chemically reversible dopant as the current carrying species in the liquid crystal. As mentioned in the introduction, both of these findings have been employed in the fabrication of the devices delivered to NASA, although they were done on the IR&D program.

5. We have fully evaluated the performance of these devices and have developed a complete understanding of their performance characteristics and the tradeoffs that characterize their operation. This knowledge forms the basis for the body of the report and will not be elaborated here.

6. A full quantitative study of the scattering characteristics of the device has been acquired. Apart from the details of these characteristics, which are reported in depth in Section V, we verified that the superimposed ac voltage directly alters the scattering characteristics of the liquid crystal in a way that improves contrast and increases device speed. Based on these observations, we have proposed a mechanism to explain these effects (see Section V-E.).

7. In the course of improving the sensitivity of the device, we arrived at a detailed model of the nature of the interface that exists between the liquid crystal and the photoconductor. Briefly, we found that a diode-like heterojunction forms at this interface, and that this junction can be photomodulated. The junction resistance aids the bulk resistance of the CdS in holding the voltage off the liquid crystal. Without this junction, the device would not operate nearly as well as it does. This model aided us in gaining some measure of control over the fabrication of these light valves. Although we still cannot provide a high yield of acceptable devices, we are now able to identify failure mechanisms and correct them with greater facility.

8.   We have delivered a device that embodies all of the characteristics listed above and, therefore, it represents a very substantial improvement over the device that existed at the start of this program.

We have to report two device characteristics that were not improved during the course of the program despite considerable efforts. The first is speed and the second is unwanted scattering in the Fourier transform plane. Speed was sacrificed when we chose to use the ester base liquid crystals. For reasons that we do not yet fully understand, this class of liquid crystals is substantially slower than an equivalent Schiff base material. However, due to its greatly enhanced stability, we chose to sacrifice some speed in the interest of longer lifetime when we fabricated the deliverable item. The speed of the present device (excitation plus decay) is approximately 500 msec at optimum operating conditions. Regarding the second problem area, we were unable to solve the residual scattering problem. We identified the difficulty: polycrystalline liquid crystal surface alignment in the device. However, due to the poor mechanical quality of the thermally evaporated CdS films, we could not successfully implement the alignment techniques that we believe will provide stable, single-crystal liquid crystal alignment in the off-state. Recourse to sputtered CdS films can resolve this difficulty.

C.   RECOMMENDATIONS

During the course of this program we learned the characteristics and idiosyncrasies of the photoactivated liquid crystal device. We learned how they work and we acquired greater control of their fabrication. As a result of this knowledge, we are in an excellent position to recommend a future course of action with respect to these devices. Specifically, we believe that to improve these devices further requires three distinct tasks:

1. Improve the quality of the ester liquid crystal
    and the presently used organo-metallic dopants
    to increase lifetime from the present 100 hours to
    several thousand hours. Seal the cell and develop
    modified addressing voltage waveforms that
    decrease net electrochemical reactions to assist
    in the improvement of lifetime.

2. Develop sputtered CdS films and implement
    the known techniques to obtain single-crystal
    homeotropic alignment of the liquid crystal.

3. Undertake basic studies of the liquid crystal,
    the photoconductor and the device structure
    to determine if enhanced speed can be realized
    from these devices.

A program to implement these tasks could improve the present
dc photoactivated liquid crystal light valve; however, it is difficult to
predict at this point how much improvement might be realized. The
principal result of the program just concluded has been to show that by
modifying the liquid crystal and the dopant used, it is possible to reduce
the electrochemical degradation of the device. Although this approach
will extend lifetime, we feel that a technique that defeats the lifetime
problem without placing composition requirements directly on the liquid
crystal would be far more desirable, because it would permit us more
freedom to exploit the liquid crystal properties for improving the
operating characteristics of the device.

DEVICE DESCRIPTION, OPERATION, AND PERFORMANCE EVALUATION

This section provides a detailed description of the structure of the dc photoactivated liquid crystal light valve, a description of the fabrication procedure, a discussion of the operation of the light valve, and a presentation of the data that characterize the performance of the light valve in operation. The intent of this section is to convey to the reader a practical working knowledge of this new device ranging from details about its construction to a description of its operation and, finally, to an evaluation of its performance.

A.   PHYSICAL DESCRIPTION OF COMPONENT PARTS

A photograph of both an assembled cell and the component parts is shown in Fig. 1. A schematic diagram of the cell that identifies the component parts is shown in Fig. 2. These parts consist of two glass substrates each of which is coated with tin doped indium oxide transparent electrodes. A thin film photoconductor (cadmium sulfide-CdS) is deposited on one of these substrates and a thin layer (6-25μ) of nematic liquid crystal is sandwiched between the two finished substrates. The following paragraphs describe the cell component parts.

1.   Substrates

The bases for both the CdS photoconductor and the transparent counter electrode are cut from tin doped indium oxide deposited on float glass purchased from Pittsburg Plate Glass Company, typically 100 Ω Nesatron. The quality and conductivity of this product varies widely; therefore, the substrates must be inspected for surface flatness, blemishes, chips, and conductivity. The sheets are cut into 1-1/4 x 1-3/8 in. rectangles

M9755
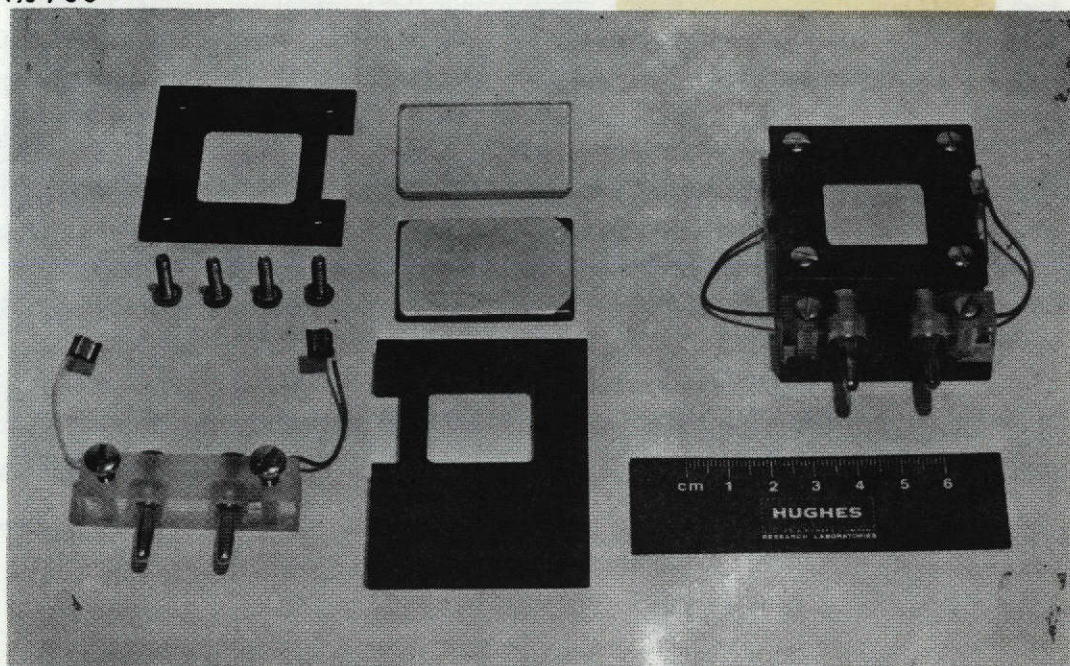
Fig. 1.   Exploded View of dc Photoactivated Liquid
Crystal Light Valve Device.

APPLIED
VOLTAGE

IMAGING
LIGHT

GLASS PLATES

CONDUCTIVE
NESA-COATINGS

LIQUID CRYSTAL

PHOTOCONDUCTIVE COATING
OVER THE CONDUCTIVE NESA COATING
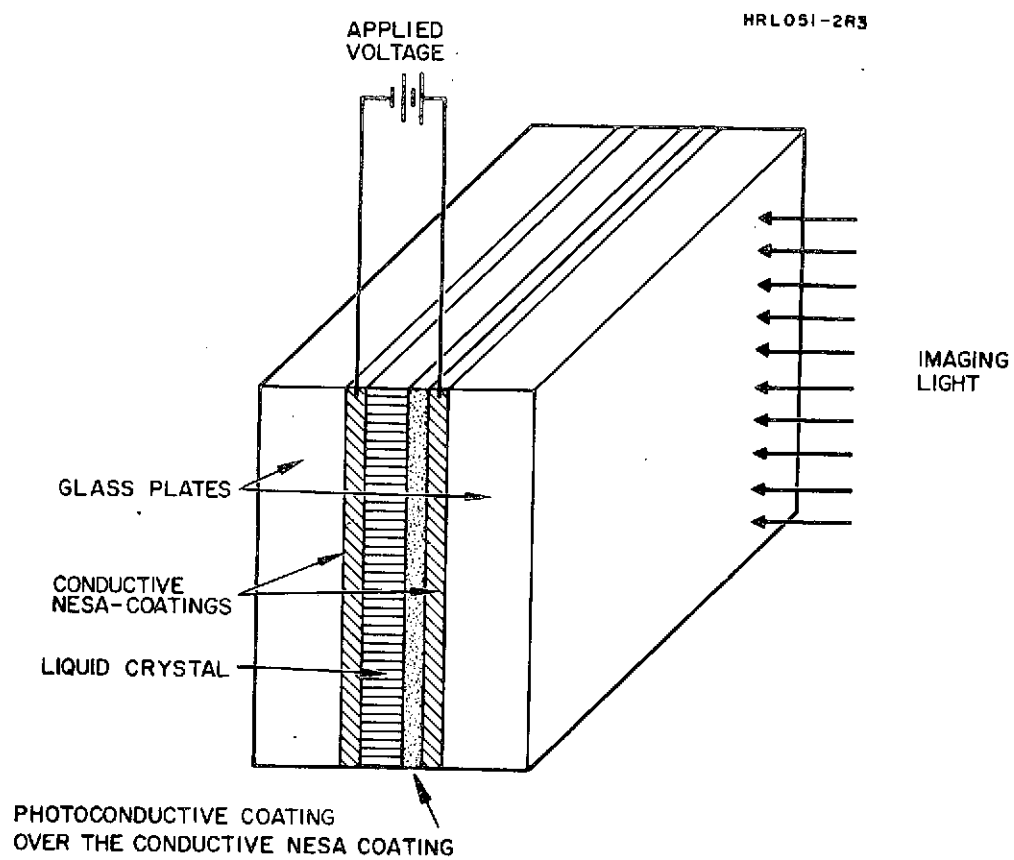
Fig. 2. Diagram of Cell Configuration.

and cleaned as follows:

    a.   2-Propanol degrease (10 to 20 min)

    b.   Ultrasonic clean with Micro cleaning solution
            (2 oz/gal.) (10 to 20 min)

    c.   Deionized water rinse

    d.   Ultrasonic clean with deionized water
            (10 to 20 min)

    e.   Deionized filtered water rinse

    f.   Oven dry at 60 to 120°C.

Then the CDS films are deposited in a liquid nitrogen trapped, diffusion-pumped vacuum system with a background pressure $< 5 \times 10^{-6}$ Torr. The evaporation material is ultrahigh purity CdS crystal chips from the Eagle-Picher Co. The evaporation source is a multi-baffled tantalum boat (Model SM-12, RD Mathis Co.). The baffled source prevents source material decrepitation while providing an easily stabilized oven for uniform deposition rates. The source-to-substrate distance is 30 cm and the substrates are held at 130°C as indicated by a thermocouple inserted in a small hole in a substrate. A He-Ne laser is used in an optical thickness monitor to observe both deposition rate and total film thickness. The films are typically 12 μ total thickness and are deposited at a rate of 2μ/hr.

The vacuum deposited CdS films are post-treated in a tube furnace in flowing hydrogen sulfide (H_2S) to increase the stoichiometry, thereby increasing the dark resistivity and photosensitivity. The procedure used is as follows:

    a.   Introduce substrates into furnace at 70°C in
            flowing nitrogen (N_2) at 2 SCFH.

    b.   Raise temperature of furnace to 300°C, then
            turn off N_2 and introduce H_2S(99. 9% pure) at
            2 SCFH.

    c.   Raise temperature to 475°C and continue
            processing for 30 min.

d. Lower temperature of furnace to 300°C in approximately 15 min, then turn off H_2S and introduce N_2.

e. Continue to purge furnace in N_2 until temperature is 70°C when samples are removed.

For good device performance, it is very important to avoid residual buildup of sulfur on the cooler ends of the tube; in subsequent processing, this buildup will be deposited on the substrates. To prevent this, the furnace insert tube is baked at 525°C between successive processes and the gas exit tube end is cleaned after every third process.

2. Cell Holders

The cell holders (Fig. 3(a) and (b)) are machined from 6061 aluminum stock and are black anodized prior to use. The base, or terminal block (Fig. 4), is machined from lucite to accept standard G-32 banana pins with wire lugs. Two-inch leads of stranded No. 26 Teflon-coated wire are soldered to the wire lugs and attached to the electrodes at their opposite ends by means of small alligator clips or small beryllium copper clips made from 1/4 x 5/8 x 0.020-in. thick sheet beryllium and bent into a U-shaped clip that slips over the end of the electrode (see Fig. 5). The terminal block is then attached to the holder by two 6/32 x 5/8 in. roundhead screws.

3. LC Material Studies

We have studied a number of liquid crystals with various conductivity range and with various dopants. Performance characteristics of the liquid crystals were examined with electro-optic cells which were made with two indium oxide substrates and 1/2-mil Mylar spacer with 1 in.^{2} aperture. We report here the composition and characteristics of those liquid crystals that we used extensively during the contract.

13

NOTE: ORIENTATION OF 45° BEVEL IMPORTANT

Fig. 3. Liquid Crystal Cell Holder.

14

8 X 32 CLEARANCE
HOLES 2 EA (typ)

6 X 32 CLEARANCE
HOLES 2 EA

2187-3

0.250

0.50

0.250

0.250

0.750

0.625

0.250

3/8 COUNTERBORE 0.250 DEEP

0.250

0.500

1.500

2.000
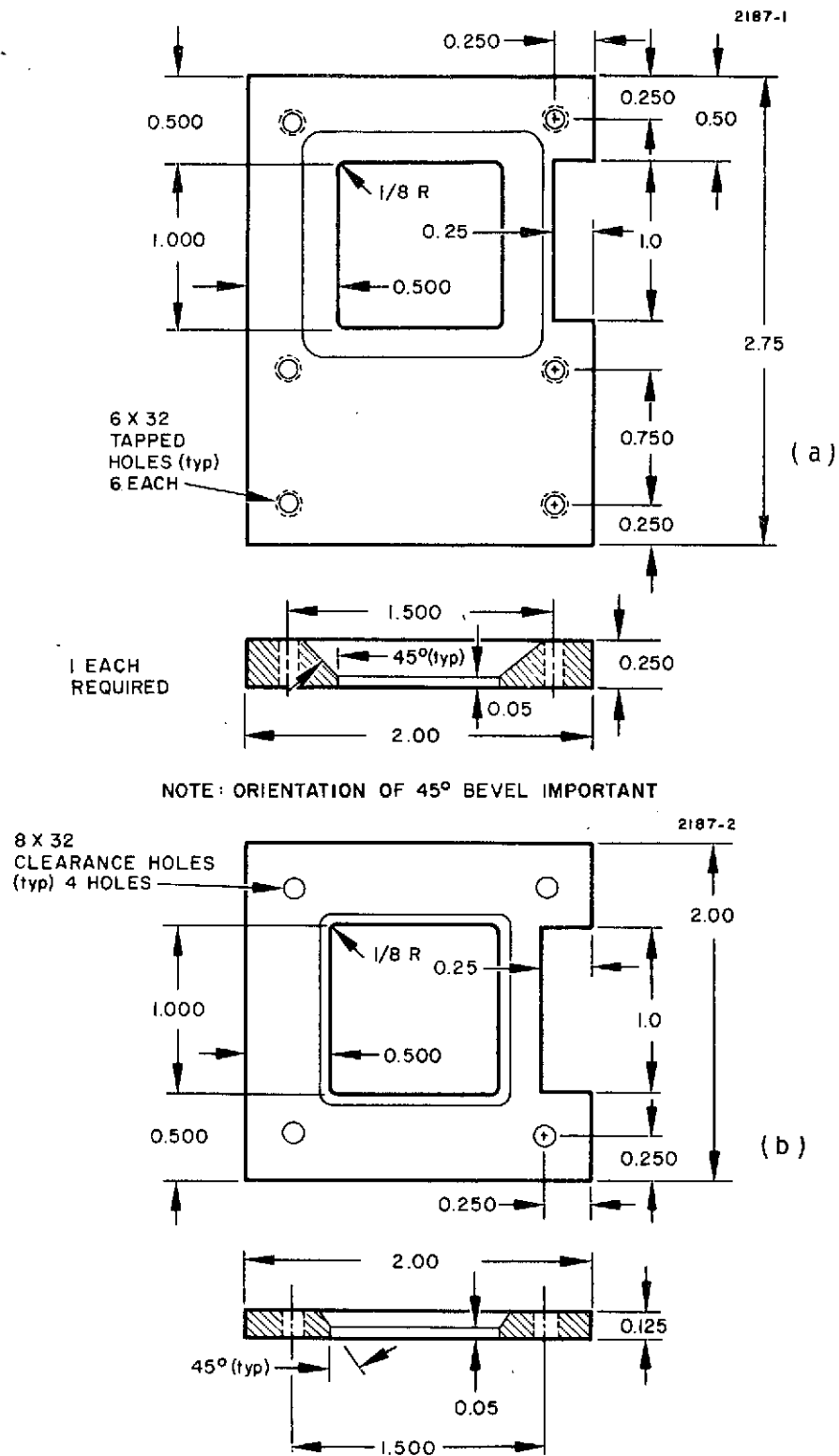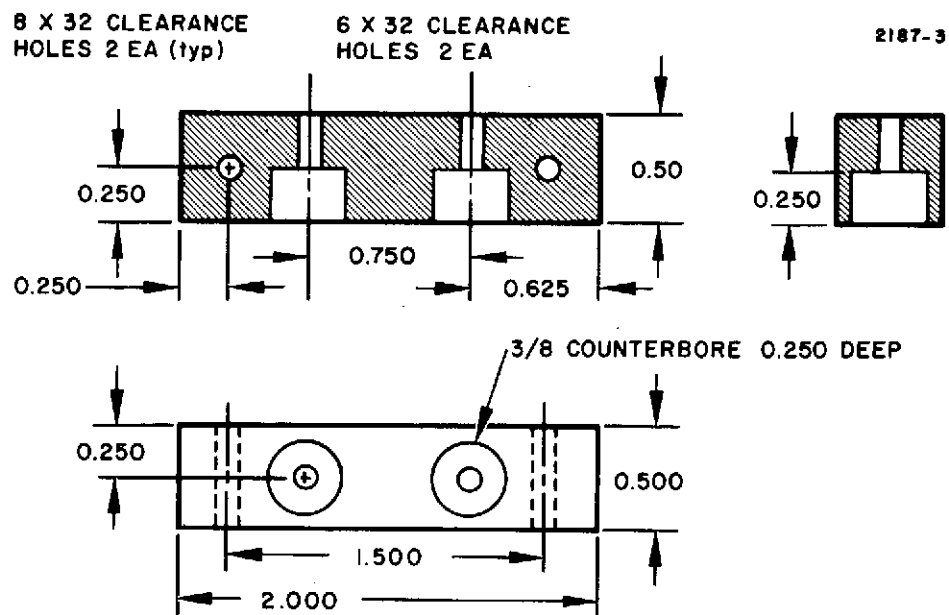
Fig. 4.   Liquid Crystal Cell Holder Base.
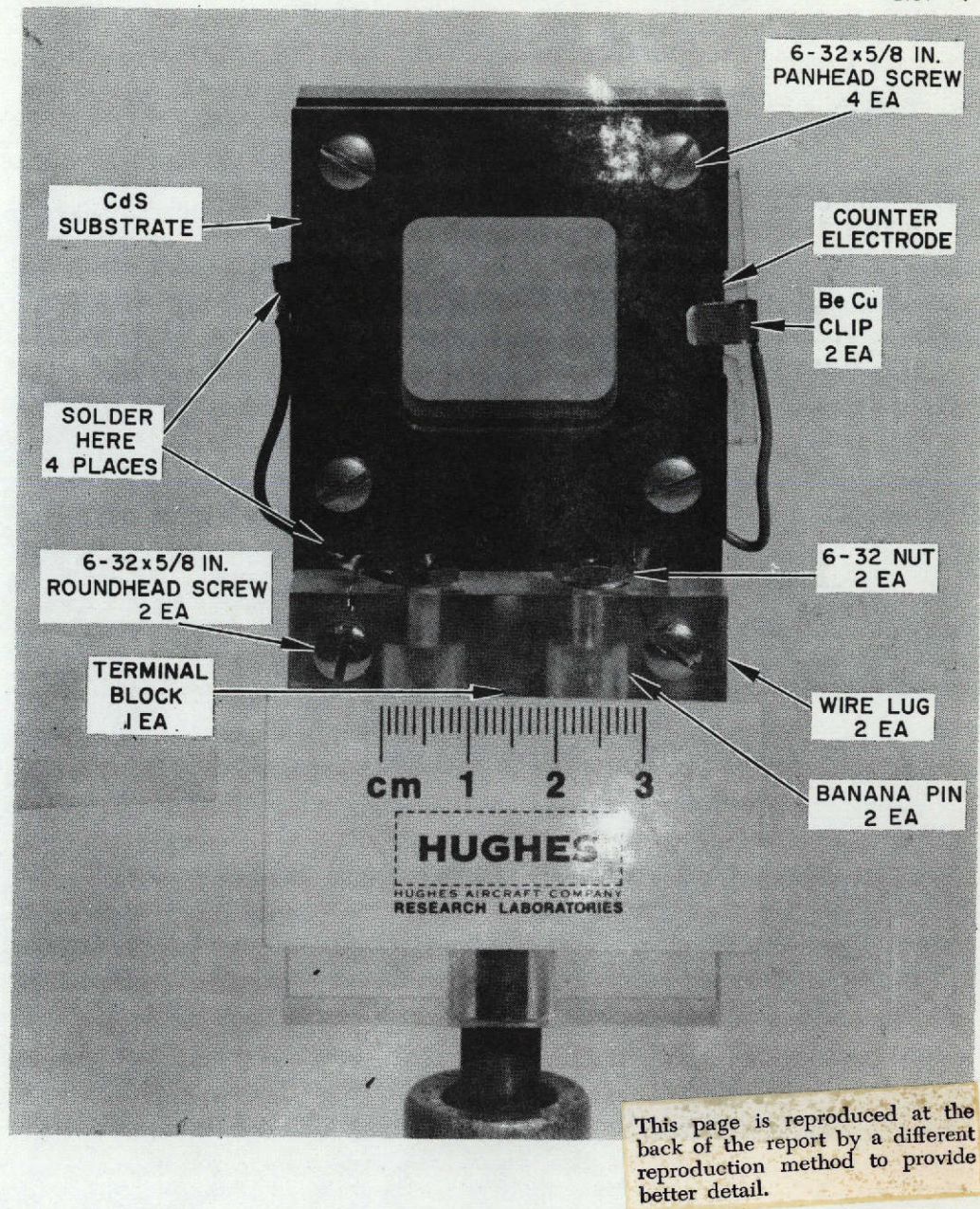
Fig. 5.   View of Assembled Cell.

a.   <u>MBBA (Nematic Range: 18 ~ 48°C)</u>

Scattering efficiency, threshold voltage, rise time and decay time were examined on MBBA with a conductivity range 10^8 to 10^{12} Ω-cm. Conductivity was varied by using unknown impurities that were introduced during preparation as well as by using HRL proprietary dopants.* One of the best liquid crystals (MBBA) showed the following characteristics:

Resistivity:	~3 x 10^9 Ω-cm
Scattering versus voltage curve is shown in Fig. 6	
Rise Time:	45 ms at 20 V dc
	20 ms at 30 V dc
	10 ms at 40 V dc
Decay Time:	800 ~ 900 ms
Threshold:	6 V
Lifetime at 20 V dc:	700 hr or more

This liquid crystal showed fairly good performance characteristics on indium oxide substrates. MBBA in general, however, has a number of disadvantages:

(1)   It is not stable in the presence of moisture.

(2)   It showed nonuniform scattering phenomena, which is called "enhanced scattering."

(3)   It showed grainy scattering on CdS substrates.

(4)   It led to very short device lifetimes on CdS substrates.

---

* Cobalt tetraphenylposphyrin complexes.
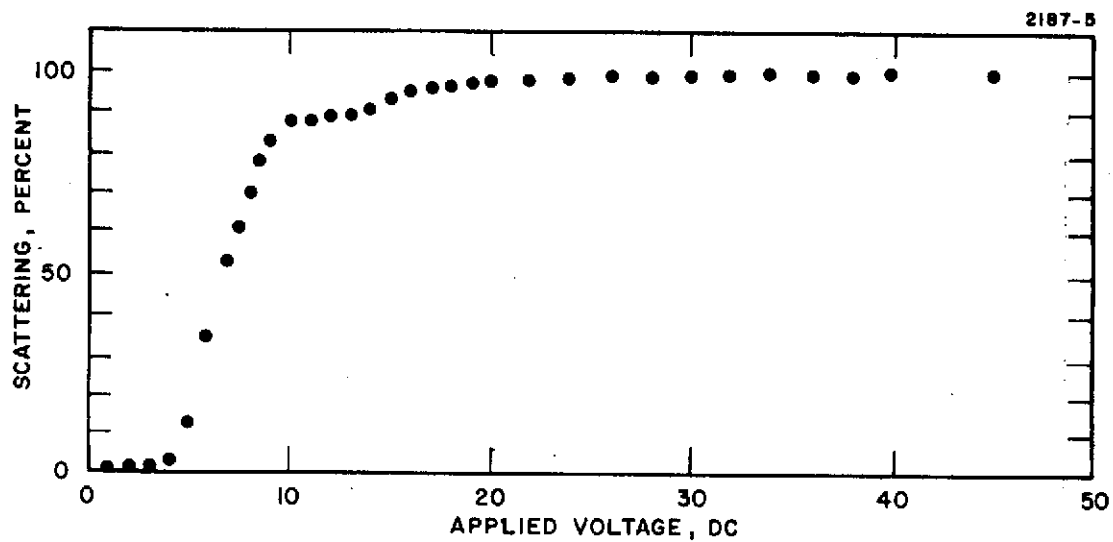
Fig. 6. S-V Curve for MBBA.

b. **Azoxy Compounds**

EM Phase IV (16 to 76°C), EM Phase V (-5~75°C), and these liquid crystals doped with HRL proprietary dopants, were studied. The liquid crystals without dopants did not scatter very well, but the doped one, which has resistivity of p ~ 10^9 Ω-cm, scattered quite well.

These liquid crystals on CdS substrate, however, destroyed the substrate immediately after dc potential was applied. Therefore, no further detailed study was made.
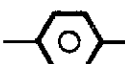
c. **Ester Compounds**

Ester compounds have generally higher chemical and photochemical stabilities than the other liquid crystals. One of the previously prepared HRL-proprietary ester mixtures[*] showed the following characteristics:

Nematic range:	10 - 50°C
Resistivity:	5 ~ 10 x 10^9 Ω-cm
Rise time (40 V):	~60 ms
Decay time:	~1. 5 sec
Threshold:	~5 V

The scattering characteristics of this material are shown in Fig. 7. This liquid crystal showed far superior lifetime when compared with Schiff base materials.

---

[*]This liquid crystal is a mixture of (by weight).

2187-31

Me —⟨O⟩— CO$_2$ —⟨O⟩— Bu	3
Bu O —⟨O⟩— CO$_2$ —⟨O⟩— O Bu	1
Hex O —⟨O⟩— CO$_2$ —⟨O⟩— O Bu	1.8
Oct O —⟨O⟩— CO$_2$ —⟨O⟩— O Bu	1.8

2187-6

Fig. 7.   Scattering Characteristics of Ester Compound.

B.   CELL ASSEMBLY TECHNIQUE

The following recipe describes, in detail, the procedure that we follow for assembling the light valve from the component parts previously described.

1.   The cell holder back is placed on a clean bench surface with the terminal block end toward the assembler and the notch to the left.

2.   The CdS substrate is placed on the holder with CdS surface up, the short edge of substrate flush with the left edge of the holder back and centered over the holder 1-in. aperture.

3.   Liquid crystal is applied in a narrow (~1/8 in.) strip across the width of the CdS substrate with a clean glass rod.

4.   A Mylar spacer, 1-1/2 x 2 x 0.00025-in. thick with 1-in. square aperture on center, is placed on this substrate so that the aperture edge almost touches this strip of liquid crystal (to keep the aperture completely clear and free of any liquid crystal).

5.   Another strip of liquid crystal then is put on top of the spacer in the same position as the original strip.

6.   The opposite electrode then is placed with one edge in the second strip of liquid crystal and the substrate is slowly lowered down onto the first substrate so the liquid crystal is spread over the entire cell evenly.

7.   The two substrates then are squeezed together so bubbles may escape, and the assembly is tightened into a cell holder. The entire light valve assembly is performed under a laminar flow hood to prevent dust from entering the cell during the fabrication process.

8.   The terminal block then is attached to the assembly.

9.   The CdS is scraped from the lower substrate in the area of the notch, and the wire clips are attached to the InO_3 surfaces of the respective electrodes.

This completes the assembly of the device.

C. OPERATING CdS LIGHT VALVES

The CdS light valves fabricated to date are laboratory models only, therefore they have operating characteristics that vary considerably. A quantitative description of the operating characteristics for a particular light valve is given in paragraph E, below. The conditions stated there should be regarded as nominal, because light valve performance varies from device to device. In view of this variability, we provide in this paragraph a qualitative discussion of the operation and expected performance of these devices in the form of a trade-off analysis to provide the reader with some feeling for the operation of these devices under off-nominal conditions. This discussion is not exhaustive; nevertheless, it should provide the required background for a more flexible and successful use of the devices. The input conditions that can be traded are the following: ac voltage, ac frequency, dc voltage, illumination light intensity, and projection light intensity. The output characteristics affected are: speed of excitation and decay, resolution, contrast, device uniformity, current (electrochemistry) and lifetime. The following paragraphs explain the effects of varying input conditions on the output of the cell and then describe the use of tradeoffs to obtain the desired output characteristics.

The following statements are restricted to CdS/ester liquid crystal light valves that contain a 6-μ thick layer of liquid crystal, such as the one sent to NASA as the deliverable item

1. Illumination and Projection Light

The typical illumination levels required to excite (or expose) the cells to saturation are upwards of 10 μ W/cm^2 of 510 nm wavelength projected on the CdS/liquid crystal interface from the liquid crystal side. The sensitivity of the cells varies as a function of cell processing and liquid crystal chemistry. Scattering has been observed with intensities as low as 0.5 μW/cm^2 on some cells; however, more typical figures are in the range 20 to 40 μ W/cm^2 to reach saturated scattering levels. The ratio of the sensitivity of the device (CdS in the presence of liquid crystal) at 510 μm (green) to that at 632.8 μm (red)

22

is approximately 250 (see Fig. 28, Section IV, a spectral sensitivity graph of typical CdS/liquid crystal function). Therefore, the intensity of the projection light (632.8 nm) must be held within a factor of 250 of the excitation light if background writeup of the device by the projector light is to be avoided. The foregoing applies for a given set of voltage conditions because, as explained later, the sensitivity of the cell is also a function of the amplitude of the ac voltage that is applied to the cell. The maximum projection light (632.8 nm) intensity for normal operating conditions is approximately 2.5 mW/cm^2; however, because the sensitivity of the CdS varies, the number must be regarded as nominal. A better practice is to adjust the laser light level for the particular cell that is in use.

2. Direct Current Voltage

Typical dc voltages for these cells vary from 20 to 40 V. The choice of dc voltage level is determined by the speed desired, by the ac voltage applied, and by the amounts of illumination and projection light used on the cell. The optimum scattering condition exists when the impedance of the liquid crystal is matched to that of the CdS liquid crystal junction so that the maximum voltage drop occurs across the photoconductor at points of nonillumination and across the liquid crystal at points of illumination. Therefore a tradeoff exists between dc voltage and illumination light over a range of several volts and several $\mu W/cm^2$. The major controlling factor of the acceptable range of dc voltage and illumination light intensity, however, is the amount of ac voltage that is applied (see the discussion of ac voltage below).

The dc voltage level determines the level of dc current that flows through the cell. Typical dc currents range from a few microamperes dark current to tens of microamperes when the cell is illuminated. These current levels apply to cells that are uniformly illuminated over the entire aperture. There is a current level tradeoff that must be considered. Higher dc voltages tend to improve (shorten) the response time of the cell. Higher dc voltage also increases the

current in the cell, which increases the scattering level in the cell which in turn improves both the contrast and the resolution of the cell. On the other hand, increased currents shorten the life of the cell. Hence, there is a tradeoff between cell performance and cell lifetime. Lifetime can be realized at the expense of response time, resolution, and contrast (See paragraph 4, below for additional remarks on lifetime).

A remaining note with regard to dc voltage relates to shorting the cell. Cells can be shorted and destroyed in several ways: by application of dc voltages in excess of 40 V[*]; by interruption of the circuit, which causes transients from the source to appear across the cell; or by inadvertently biasing the cell in the wrong direction at a high voltage. Care must be taken to insure that the clips are well contacted to the In_2O_3 layer on the substrates to prevent intermittent electrical contact and thereby over-voltage of the cell.

3. Alternating Current Voltage

Useful ac voltages vary over the range from approximately 30 to 60 V RMS at frequencies that vary from 5 to 20 kHz; the nominal value is 40 V RMS at 10 kHz. Application of ac voltage has two effects: first, it increases the threshold of the ac voltage at which the onset of scattering occurs, and secondly, it increases the "slope" of scattering versus dc voltage. Both effects serve to improve the scattering uniformity of the cell, thereby improving the cosmetic quality of the device. Another desirable side effect of ac voltage is that the speed of response is improved both excitation and decay. Speed of excitation improves because higher ac voltage permits the use of higher dc voltage.

---

[*] The tolerable over-voltage varies from cell to cell. Although we have cells that have survived in excess of 100 V, it is wise not to run these devices over 40 Vdc since device performance (particularly lifetime) tends to deteriorate at high voltage anyway.

Time of decay decreases because ac fields on the cell assist in returning the liquid crystal to equilibrium after the photocurrent has been turned off. Speed may also be increased as a function of ac frequency because changing the frequency changes the cell capacitance, which affects the external circuit time-constant. Resolution and contrast can sometimes be improved by varying the ac frequency, but this optimization must be done experimentally because we do not have an adequate understanding of this effect at present.

4. Operation for Maximum Lifetime

The liquid crystal light valves presently being made in our laboratory have liquid crystal impedance which is matched to that of the CdS photoconductor to optimize the heterojunction diode that forms at the interface between these materials (see Section IV). In this way, we optimize the resolution, contrast, and lifetime characteristics of the light valve. In particular, to obtain maximum lifetime, several conditions must be maintained. They are as follows: The projection light (6328 Å) intensity should be kept below 3 mW/cm^2. High voltage bias (in excess of 40 V avg) of either polarity should not be applied to the cell because high electric fields and high currents may cause irreversible etching or metal ion deposition of the electrodes. When the cell is used in normal operation, the net current is quite low (< 10μA), because the average ac current[*] is of the same magnitude as the current associated with the dc voltage, but it is of opposite polarity. Therefore, neither ac nor dc voltages should be applied separately except during turn-on/off). For normal operation, applied ac voltage of 40 V RMS at 10 kHz will give ac currents of from 6 to 10 mA RMS. Illumination light intensity must be high enough to saturate the photoconductor. The dc voltage required to give good contrast varies between 30 and 40 V when

---

[*] The nonzero value of the average ac current, mentioned here, is caused by the rectification properties of the heterojunction at the liquid crystal/CdS interface.

above conditions are met. Small changes in voltage (1 to 2 V) will produce substantial changes in contrast. The net current of the device decreases slowly in amplitude with time if the light valve is used continuously without respite. This condition can be offset by slightly increasing the dc voltage to maintain constant contrast. A diagram of a typical operating and monitoring setup is shown in Fig. 8.

5. Cell Rejuvenation After Use

The present devices are used best for relatively short times, several hours or less of continuous operation. Used in this way, they can be reused repeatedly with good performance, thereby achieving long total operating lifetimes. If it is necessary to use a light valve continuously for a period in excess of 8 hr, it may be necessary to rejuvenate it. By placing the cell in a warm, dry environment for 3 to 4 wk, its operating properties can be fully restored, provided that no permanent damage occurred during its period of use. To avoid permanent damage due to overuse under normal operating conditions, we suggest not to operate the device continuously for more than 8 hours. As the cell ages with continued use, the desired contrast may not be achievable with slight increases of dc voltage due to background scattering caused by leakage currents. In this event, the cell may be rejuvenated by placing it in a nitrogen oven at 66°C for approximately 24 hr and slowly cooling it to room temperature upon removal. This process has been repeated several times to date; it is very effective if the electrodes have not been etched by high current density. At the present time, etching of the electrodes cannot be reversed by the rejuvenation process. Therefore, the current should be kept less than safe maximum at all times. Unfortunately, local current effects can do the damage, hence it is difficult to prescribe an effective limiting current for the cell as a whole. As a matter of general precaution, the current should be kept below 50 a/cm^2. However, this does not generate that the cell will not suffer permanent damage.

D. LIMITATIONS WHEN OPERATING CdS LIGHT VALVES

1.   The maximum temperature for operation is approximately 52°C because at this transition point the liquid crystal changes to the isotropic state and will not scatter. Heating above 52°C will not damage the liquid crystal. The cell will again become operable upon cooling below 52°C.

AC POWER SUPPLY
($\approx$ 40 V RMS*)
10 kHz

DC POWER SUPPLY
($\approx$ 40 VDC MAX*)

DC

I_{DC}

YEL

LIQUID CRYSTAL

CdS

I_{AC}

500-520 nm
IMAGING
LIGHT

COHERENT
PROJECTION
LIGHT
632.8 nm

In_2O_3
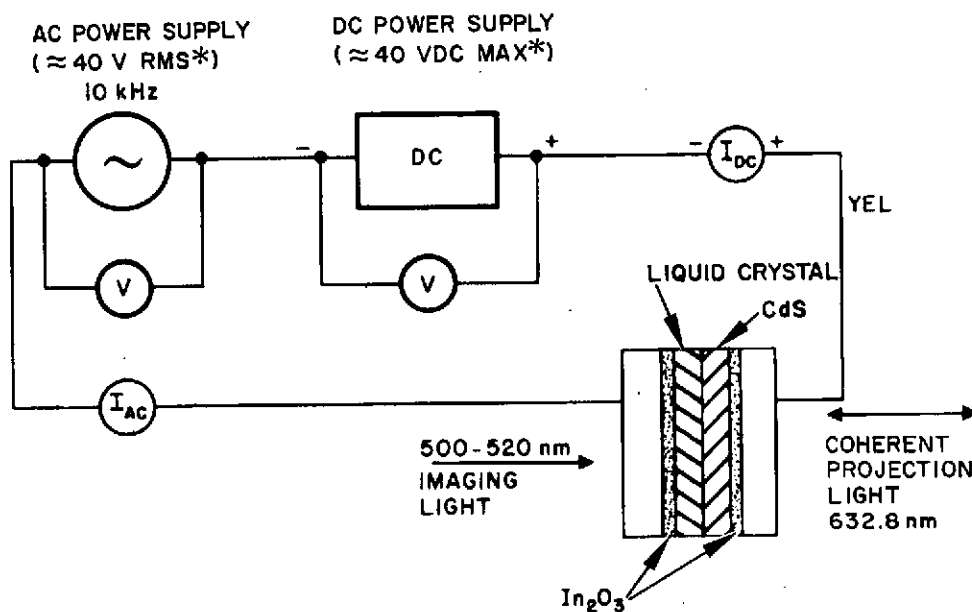
1. MAXIMIZE IMAGING LIGHT
   AND MINIMIZE DC CURRENT
2. DO NOT RUN CELLS W/DC
   ONLY OR AC ONLY

* SEE DATA SHEETS AND/OR
  OPERATING INSTRUCTIONS

Fig. 8. Schematic of Electrical Operating and
Monitoring Circuit.

2. Cells must not be subjected to severe pressure changes or else bubbles will appear in the aperture because the cells are not sealed.

3. Mechanical distortion of the cell by rough handling or uneven tightening of holder screws may cause both bubbles and electrical shorts.

4. The liquid crystal is degraded by moisture and should be stored in a clean, very dry area.

E. DEVICE PERFORMANCE EVALUATION

1. Testing Procedure and Equipment

This subsection describes the equipment and the procedures used in testing the crystal light valves (CLV's) for the following properties:

1. Percent transmission versus exposure light level at fixed aperture

2. Resolution versus input light level at fixed light blocking aperture diameter.

3. Speed (write up to 80% scattering) versus input light level

4. Current ratios illuminated (full gate) versus dark

5. Decay time.

a. Test Setup Description

The CLV test facility consists of two basic systems, the optical system and the electrical system; therefore, we describe them separately.

The optical system (Fig. 9) uses a tungsten filament incoherent illumination source that is varied in intensity by adjusting the input voltage and by inserting neutral density filters in the output beam. A 510-nm interference filter with narrow passband characteristics (Fig. 10) is used to set the illumination wavelength and an Ilex No. 4
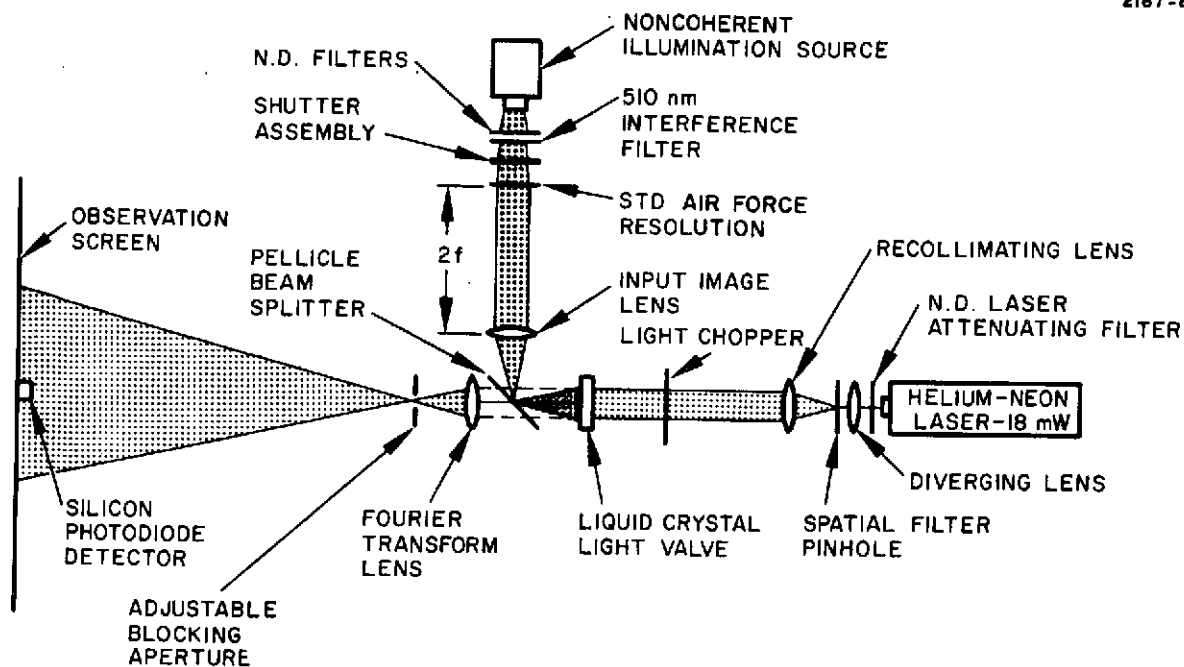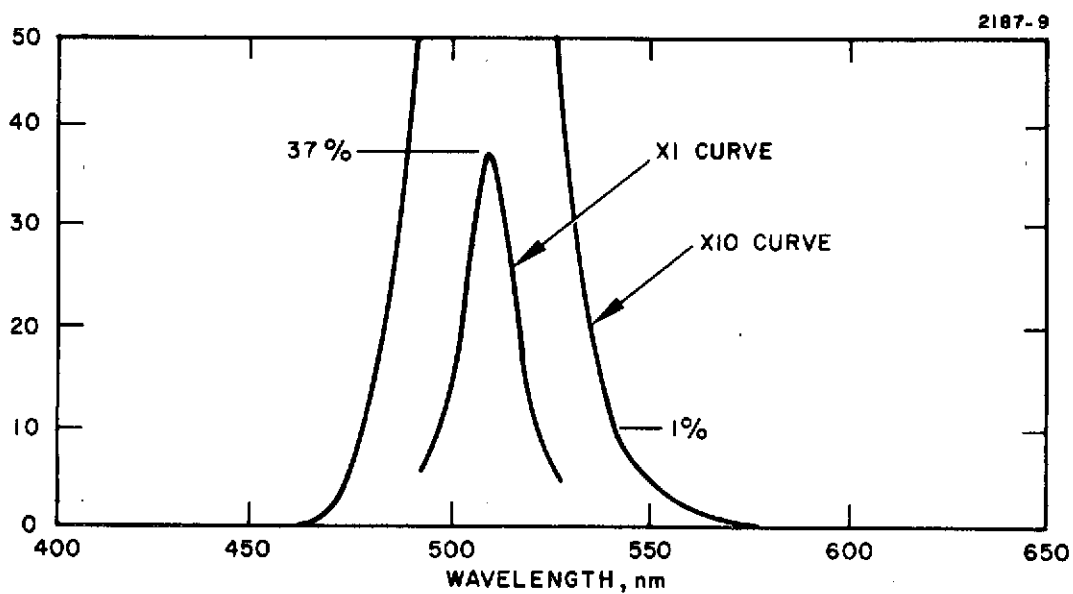
Fig. 9. Coherent Light Valve Optical System.

Note: Credit - Optics Technology, Inc. for data.
          Set No. 3473 ⎯⎯ Filter No. 500.

Fig. 10. 510-nm Interference Filter Set with Narrow
          Passband Characteristics.

universal shutter is used to shutter the illumination beam. The
Standard Air Force Resolution Chart and input imaging lens (f = 80 mm)
are adjusted to focus the inverted, positive, one-to-one image through
the liquid crystal on the interface of the liquid crystal/cadmium sulfide
layer. A pellicle beamsplitter at 45° to, and centered in the inter-
section of the optical axes is used to hold the input image into the device.
Care must be taken in aligning the illumination light axis at 90° to the
projection beam axis in the horizontal plane and also at 45° to the
pellicle beamsplitter in its vertical and horizontal planes to achieve
well focussed chart imaging over the entire cell aperture. Errors in
alignment are minimized by positioning the high resolution portion of
the resolution chart on or near both axes. The projection light
amplitude (632.8 nm) is adjusted by placing N. D. filters in front of the
first diverging lens; it is limited to 2 mW/cm^{2}, maximum, at the cell.
The expanded, spatially filtered, recollimated laser beam passed
through the liquid crystal cell from the cadmium sulfide side to be
scattered by the liquid crystal spatial modulation. The scattered laser
light passes through the pellicle beamsplitter to the transform lens
(f = 63 mm) and is blocked by the adjustable blocking aperture which is
placed at the focal plane of the transform lens. The transform
lens and blocking aperture are adjusted so the inverted negative image
from the cell is focused on the output screen at approximately 20X
magnification to facilitate reading of high resolution points on the
reproduced resolution chart image. A silicon photodiode detector is
placed in the center of a block on the resolution chart image to be used
for measuring response times and contrast ratios.

The electrical system used for exciting the cell (Fig. 11) consists
of ac and dc power supplies connected in series to give dc excitation with
a superimposed alternating bias voltage all in series with appropriate
ac and dc current monitors.

      b.   Procedures for Calibration of the System and Testing of
               Cells

The illumination light intensity and the projection light
intensity at the cell are measured by substituting a calibrated thermopile

D.C. CURRENT METER	AC CURRENT METER	0-100 VAC 50 Hz-10 kHz AC SUPPLY	0-100 V D.C. SUPPLY

NESA GLASS
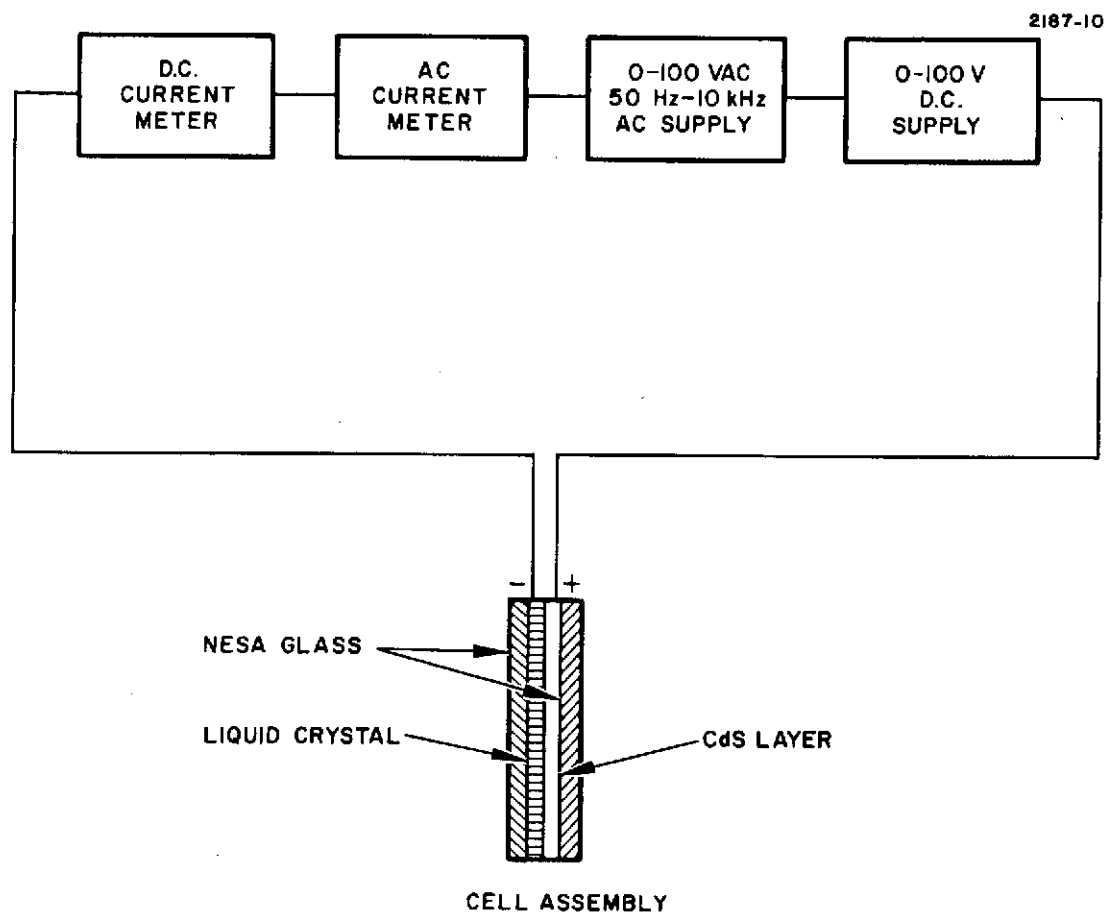
LIQUID CRYSTAL

CdS LAYER

CELL ASSEMBLY

Fig. 11. Electrical System Used for Exciting the Cell.

and/or a calibrated silicon photodiode in the plane of the liquid crystal cell. Contrast ratios or relative transmission and light efficiency are measured by reading the amplitude ratios of the output of a silicon photodiode placed in the output plane of the system at the observation screen. The photodiode is biased to read current linearly over a wide amplitude range. The spatial frequency limit of the output of the system is measured by substituting the Standard Air Force Resolution Chart in place of the liquid crystal cell and observing visually the maximum legible resolution (for a given diameter blocking aperture) on the output screen. Eye resolution of the observer is assumed to be 8 lines/mm or better at 25 to 30 cm, therefore at 20X magnification the observer should be capable of reading resolution of the cell up to 160 lines/mm. Blocking aperture diameters are measured by closing an iris diaphragm onto a gauge pin of preselected diameter. Response times are measured by photographing or visually observing the oscilloscope trace of the output of the silicon photodiode in the output plane while the illumination light is shuttered. Frequency response of the silicon photodiode is 10 kHz or better. Response times are measured by two methods. Cycle times are measured by adjusting the illumination light shutter to a speed setting which gives the desired percent transmission in a given cycle, usually about 80%. Write up and decay times measured individually require setting the shutter to the time position and operating open or closed to obtain saturation or decay, respectively.

2.   Test Results

The results of these measurements are shown graphically in Figures 12 through 15. These results were recorded for a single device and can be regarded only as nominal performance figures. Subsequent testing is required to document more fully the range of performance that can be expected from these devices. The technical description of the test cell fits that given above. The designation of

the particular cell used in these experiments is 1H1. The physical characteristics of the cell are as follows:

Liquid crystal:	Ester - no dopants (see Section II-A)
Aperture design:	Standard
Cell holder:	Standard, unsealed (see Section II-A)
Liquid crystal thickness:	1/4 mil
Photoconductor thickness:	12 μ.

The data that we present includes resolution and time response, all plotted versus excitation exposure level for several different cell voltages. In addition, it includes Table of off/on current ratios which serve as a figure of merit for the quality of cell. We discuss each of these data types separately.

a.   Sensitometry (Transmission Versus Excitation Exposure)

Figure 12 shows the sensitometry data for the deliverable light valve. Here we have plotted the light transmitted by the cell, as a function of excitation light intensity for several different cell voltages. We used tungsten light that had been filtered by the green filter whose passband is depicted in Fig. 10. The transmitted light is plotted relative to that with no excitation light present. Basically, these curves measure the response of the cell to the excitation illumination. The main points to observe here are that the cell voltage threshold is approximately 30 Vdc. At 20 Vdc, the sensitivity of the cell is seriously lacking, that is, excessive amounts of excitation light are required to elicit a nominal response from the cell. The scattering at 40 Vdc is somewhat stronger. Also, the excitation light level for almost full scattering is somewhat lower at 40 V than at 30 V; however, the differences are not that great. Moreover, 40 Vdc is an undesirably high voltage for continuous operation of the light valve, as discussed above. Therefore, the proper operating voltage for these cells is between 30 Vdc and 40 Vdc and should be held toward the low end of this range, if possible. These curves show that the minimum transmission of 0.02, which corresponds
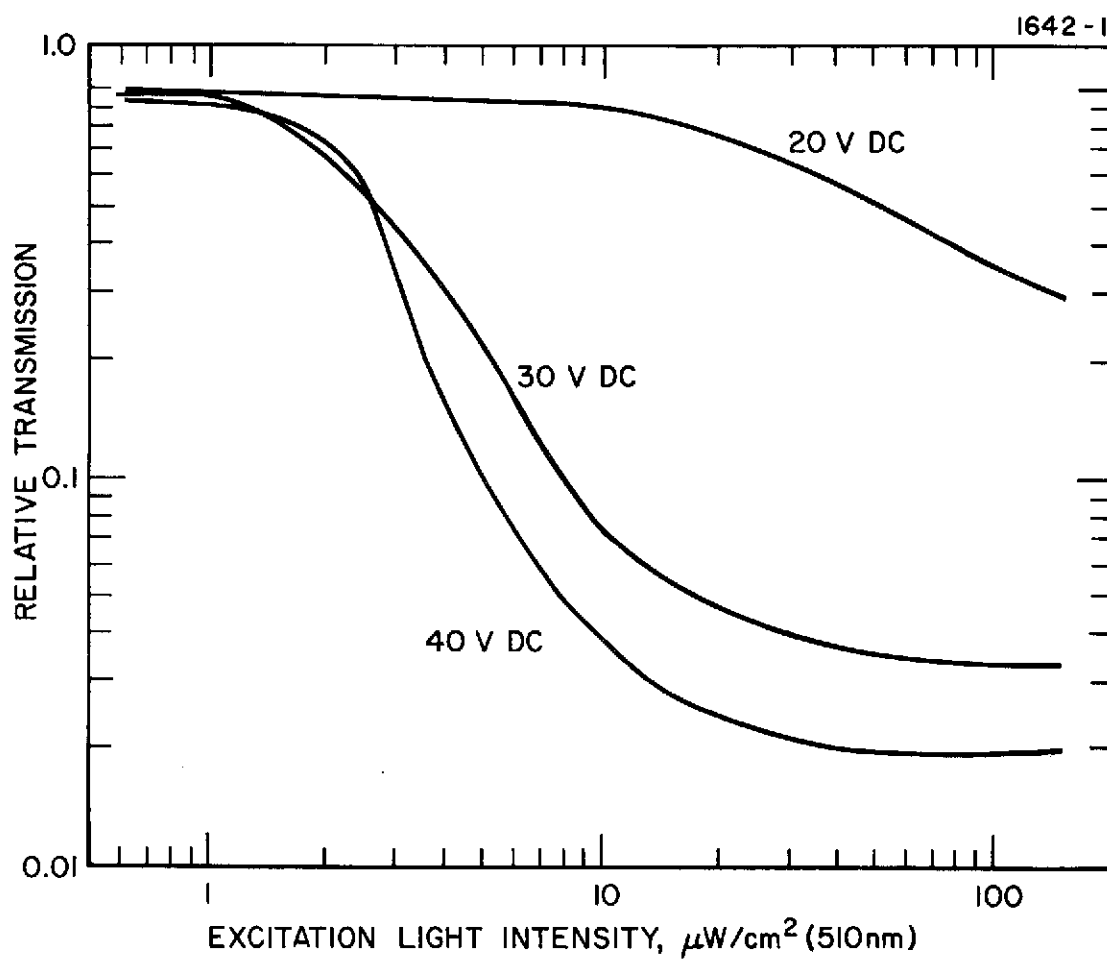
Fig. 12. Coherent Light Valve Sensitometry: Transmission Versus Exposure.

to a contrast ratio of 50:1,*occurs at about 20 μW/cm^2. Typically, the ac voltage is set 5 to 10 V (rms) higher than the dc voltage and is operated at 10 kHz. The ac voltage serves to improve both the contrast. the resolution, and the speed of the cell. It does this at the expense of both sensitivity and dc voltage threshold. In the presence of an ac voltage, the sensitivity decreases and the dc voltage threshold increases.

b.   Resolution

Figure 13 shows a plot of resolution in lines/mm versus excitation light intensity for the same voltages as before. We obtained these data by projecting the Air Force Resolution Chart and then recording the line group that could be resolved by the unaided eye. Here again we see the effect of below-voltage threshold operation. At 20 Vdc, we obtain poorer resolution at higher excitation levels. At the two higher voltages we obtain almost equal maximum resolution of 60 lines/mm. The maximum resolution occurs at an exposure of approximately 20 μW/cm^2, and the resolution remains high over a relatively large range of excitation light values. The decline of resolution at low light levels is caused by loss of contrast due to inadequate exposure and at high light levels by spreading of the image caused by over-exposure. These curves clearly indicate that operation of the device in the vicinity of 30 Vdc is highly desirable. Here we see that over-voltage not only endangers the life of the cell, but also leads to poorer performance due to over-exposure. Comparing these results with the sensitometry data, we see, as expected, there is a tradeoff between contrast and resolution at high exposure values and/or at high cell operating voltages. On the other hand, at low excitation, both contrast and resolution deteriorates due to under-exposure. As mentioned above, optimum operation is realized at approximately 30 Vdc at exposure light levels in the vicinity of 20 μW/cm^2. (Note that this represents an order of magnitude improvement in sensitivity over the sensitivity observed with these devices at the start of the program.) In all cases, the ac voltage

---

*This contrast is fixed by the diameter of the blocking aperture and should not be regarded as the characteristic limit of the device. (See Fig. 15).
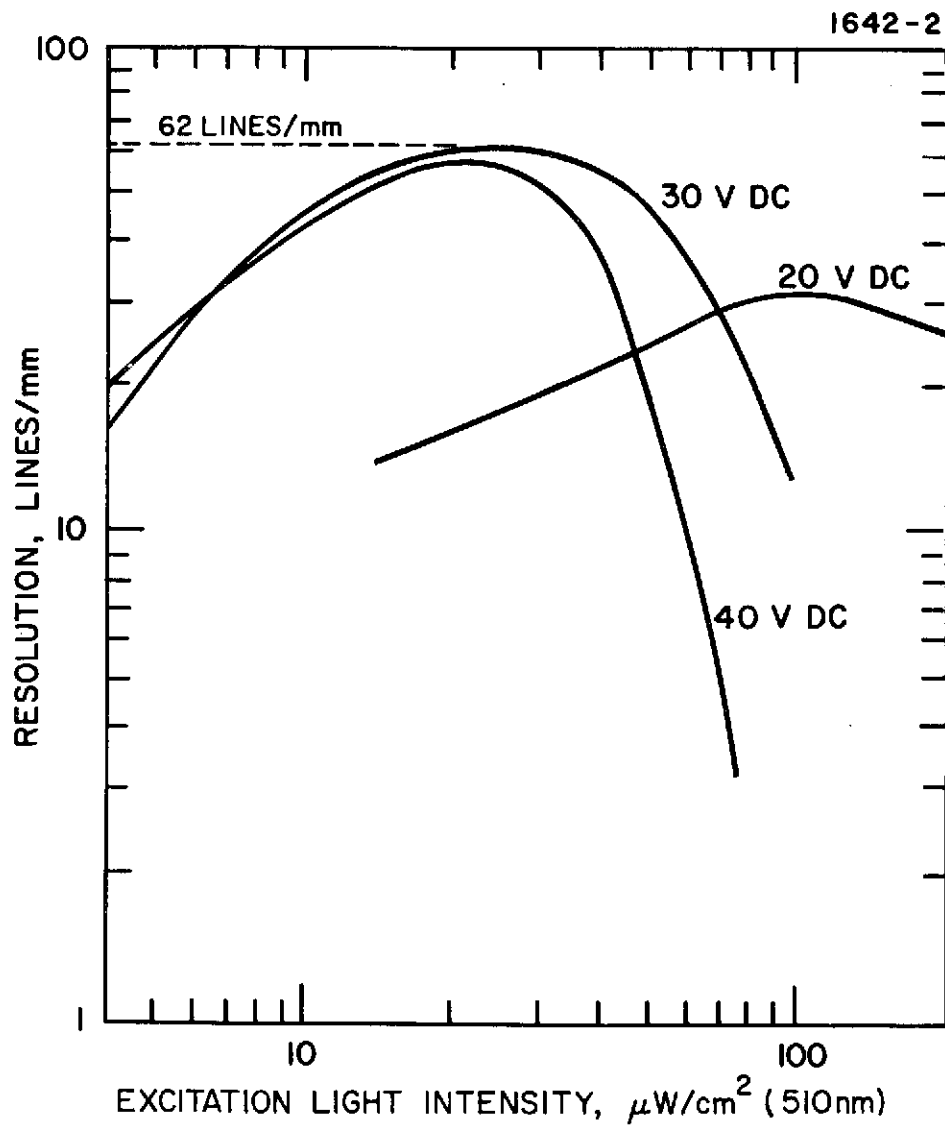
Fig. 13. Coherent Light Valve Resolution Plotted
Versus Exposure.

c.   Excitation Time

The excitation time is plotted versus excitation light level in Fig. 14. The excitation time is the time required by the cell to achieve 80% of full scattering at the particular set of operating conditions from the time the excitation light is first switched on. As seen in Fig. 14, the time is typically in the tens to hundreds of milliseconds range and is reduced as the operating voltage increases, or as the excitation light intensity increases. Looking at the 40 Vdc curve, we see that at 20 $\mu W/cm^2$, approximately 80 msec are required to excite the cell. This time is strongly affected by liquid crystal chemistry. The ester liquid crystals are appreciably slower than the Schiff base liquid crystals such as MBBA. Similarly, at the preferred operating voltage of 30 Vdc, the excitation time is approximately 150 msec at an exposure level of 20 $\mu W/cm^2$. By turning to higher light levels and lower voltages, the cell speed can be improved, but at the expense of resolution and contrast.

d.   Current Ratios : Illuminated Full Gate Versus Dark

Current ratios have been used extensively to characterize cell performance. The ratios measured most commonly are the full-gate saturated current versus the dark current under two different conditions with 20 Vdc applied to the cell. One condition is with the projection light on (helium-neon laser 2.5 mW/cm^2) and the other is with the projection light off. To first approximation, these currents reflect the following characteristics:

(1)   Illumination-on and projection-light-on current determines the series resistance of the bulk CdS. the liquid crystal, and the on-junction.

(2)   Illumination-off and projection-light-on current determines the series resistance of the bulk CdS, the liquid crystal, and the resistance of the off-junction under the influence of the projection light. This value is dominated by the junction resistance, therefore it determines the red sensitivity of the junction.
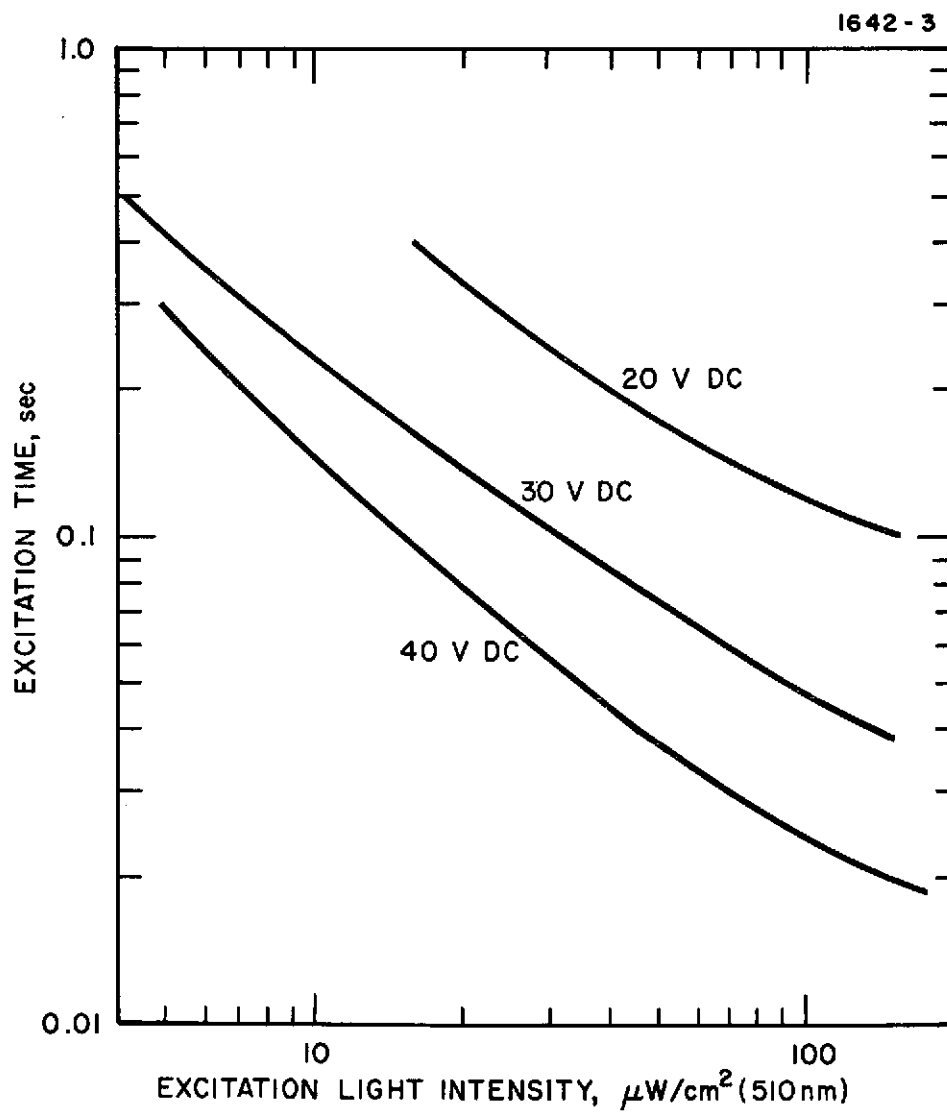
Fig. 14.   Coherent Light Valve Response Time Plotted
Versus Exposure.

(3)   Illumination-on, projection-light-off gives the series resistance of the bulk CdS, the liquid crystal, and the on-junction without the added conductance caused by the projected light.

(4)   Illumination-light-off and projection-light-off gives the dark resistance of the junction. Typical values of device current and current ratios for full one inch aperture, at 20 Vdc, in a well impedance matched cell are as follows:

Illumination light and projection light on   15 μa

Illumination light off, projection light on   0. 5 μa

                                              Ratio: 30

Illumination light on, projection light off   15 μa

Illumination light off, projection light off   0. 05 μa

                                              Ratio: 300

Light valves with current ratios that approximate the above values give good optical and lifetime performance.

e.   Decay Time

The decay time performance of dynamic scattering light valves is difficult to describe precisely, because it is affected by a complex interaction of the component elements of the light valve. For example, the conductivity and viscosity characteristics of the liquid crystal vary with composition, the bulk and surface conductivity and photosensitivity of the CdS substrate vary with processing and material purity and finally, the junction formed at the CdS/liquid crystal interface varies in behavior as a function of the joint characteristics of the two materials. Our tests, however, have provided some understanding of decay time and we can make some general statements about it. For a given cell, decay time is dependent upon ac voltage, dc voltage, and illumination intensity. As a general rule, the higher the ratio of ac to dc voltage, the faster the decay, and secondly, the higher the intensity of the illumination light (510-nm wavelength) the greater this effect becomes. Table I snows decay time behavior of the test cell described above.

TABLE I

Decay Time Behavior of Tested Cells

Vac 10 kHz rms	Vdc	ac-dc Ratio	Illumination Intensity ($\mu W/cm^2$)	Decay Time (ms)
40	20	2	16	400
40	30	1.33	16	400
50	40	1.25	16	450
40	20	2	44	200
40	30	1.33	44	400
50	40	1.25	44	500
40	20	2	150	150
40	30	1.33	150	400
50	40	1.25	150	600

T887

f.   Optics Considerations

Figure 15 depicts the effect of blocking aperture diameter on the performance data. It is included to provide some feeling for the effect of the test system optics on the measured data. The heavy curves in Fig. 15 represent the data shown in the previous three figures for the case of 30 Vdc across the cell. The aperture diameter was set at 0.125 in. for those measurements. The dashed curves shown here were taken at an aperture of 0.048 in. These figures show the expected result, viz., improved contrast: the transmitted light at saturation increased from 50:1 at the larger aperture to 100:1 at the smaller. At the same time, the resolution decreased from 62 lines/mm to approximately 46 lines/mm. Note also the narrowing of the resolution curve at high exposure values associated with the smaller aperture. This can be attributed to an increased sensitivity to the loss of resolution associated with over-exposure of the light valve at small aperture.

40
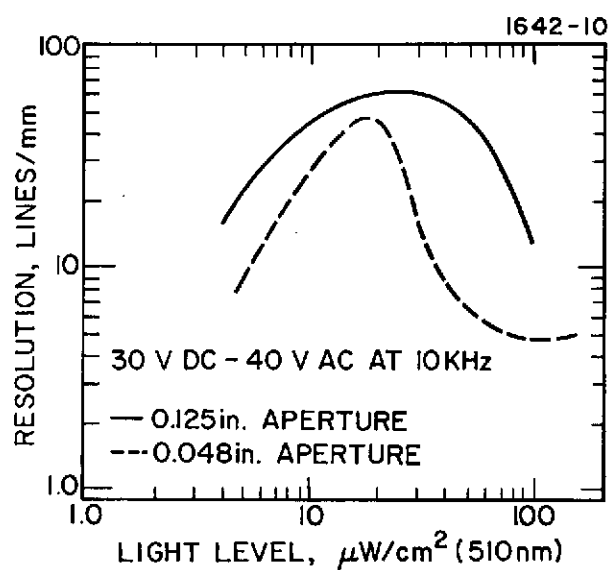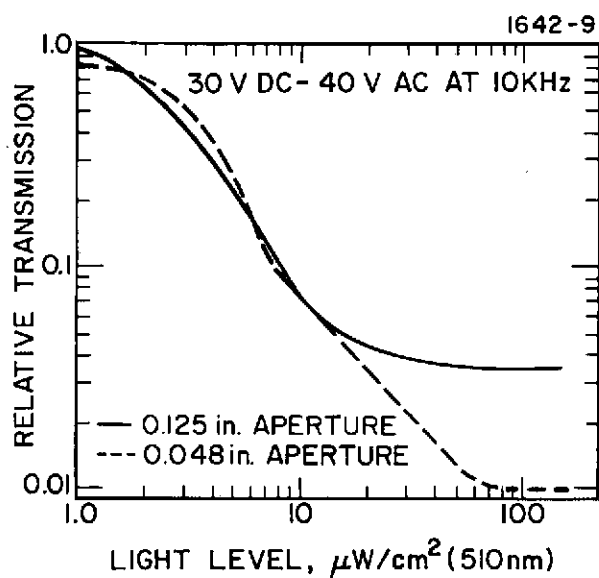
Fig. 15. Coherent Light Valve Sensitometry and Resolution Plotted Versus Exposure for Different Blocking Aperture Diameters.

3.   Performance Characteristics

Using the curves shown in Figs. 12 through 15, we can arrive at a set of performance characteristics for the deliverable item. These characteristics are selected for a single set of operating conditions on the basis of optimum performance, given the nature of the tradeoffs involved, viz.: contrast vs. sensitivity, resolution vs. contrast, resolution and sensitivity vs. speed, etc.

Operating voltage	30 Vdc
	40 Vrms at 10 kHz
Sensitivity (for maximum contrast)	20 μW/cm^2 at 510 nm
Resolution	60 lines/mm
Excitation time	150 msec
Decay time	400 msec
Readout light intensity	> 3 mW/cm^2 at 632.8 nm
Maximum contrast[*]	30:1 (0.125-in. aperture behind 63-mm fℓ transform lens)

---

[*] Note that a contrast of 100:1 can be realized with resolution of 46 lines/mm by recourse to the smaller, 0.048-in. blocking aperture. These characteristics are within the design goals specified by NASA at the outset of the program.

SECTION III

UNIFORMITY AND ALIGNMENT STUDIES

A.   OBJECTIVE

The objective of these studies was to develop techniques for constructing liquid crystal light valves with the uniformity and optical quality required for coherent optical system applications. The studies were carried out on both light-activated and non-light-activated light valves. This section discusses the basis for our approach to the uniformity problem, describes the experimental techniques that we employed, reviews the results that we obtained from the experiments, and summarizes the conclusions that we drew from these results.

B.   APPROACH

A light valve employed in a coherent optical system must not introduce unwanted modulations to either the amplitude or phase of the coherent wavefront. This means that, when not activated or when uniformly activated, the light valve must only create uniform amplitude or phase variations over the entire active area of the device.

Nematic liquid crystals are birefringent and behave as uniaxial crystals with either positive or negative dielectric anisotropy. (That is, the liquid crystal molecules are rod-like, and the induced dielectric constant that is parallel to the molecular axis, $\epsilon_{||}$, is either greater or less than the induced dielectric constant that is perpendicula to the molecular axis, $\epsilon_{\perp}$. If $\epsilon_{||} > \epsilon_{\perp}$ the liquid crystal is said to have positive dielectric anisotropy and if $\epsilon_{\perp} > \epsilon_{||}$, the liquid crystal is said to have negative dielectric anisotropy.) Thin layers of liquid crystal molecules of the sort employed in the light valve devices

tend to form domains with uniform molecular alignment within a domain, but with random molecular alignment from domain to domain. The random alignment of the birefringent domains leads to an undesirable phase modulation of a coherent wavefront passed through the light valve. Therefore, to achieve the desired uniformity and optical quality, it is necessary to cause the liquid crystal molecules to form a single domain within the active area of the cells.

The dominant forces that cause alignment of the liquid crystal molecules in the thin layers employed in light valves are the surface forces. Applied fields can influence the orientation of molecules remote from the surfaces of the films, but not the molecules at the film surfaces (for practical field strengths). Thus, in order to cause the liquid crystal molecules to form one large domain, it is necessary to prepare the surfaces that contact the liquid crystal film in such a way that they induce uniform molecular alignment. This implies that careful substrate material selection, cleaning procedures, and surface treatments are required to achieve the desired uniformity and optical quality. Based on this reasoning, we designed an experimental program to evaluate commercially available as well as inhouse fabricated transparent electrodes, to establish reliable and effective cleaning procedures, and to develop surface treatments and light valve assembly techniques that would yield uniformly aligned liquid crystal films.

Tin-doped In_2O_3 transparent electrodes on glass substrates are available from several sources (e.g., Pittsburg Plate Glass, Corning Glass, OCLI, etc.), and can be fabricated within the Hughes Research Laboratories. A number of these substrates, including some fabricated by HRL, were evaluated for scratches, pits, and other blemishes, by optical and by scanning electron microscopy. We found that none of the commercial sources reliably produce high quality substrates. However, nearly defect-free transparent electrodes can be found among the generally poor quality from the commercially available materials and very high quality transparent electrodes can be fabricated at HRL if float glass is employed as the basic substrate.

44

The substrate cleaning procedures developed during these studies were described in Section II and have been used for all experiments described in this section unless otherwise noted. The cell assembly techniques that were developed early in the uniformity studies are also described in Section II. These techniques were followed during the uniformity experiments with the exception that a laminar flow-clean bench was not always available.

C.   MOLECULAR ALIGNMENT TECHNIQUES

Two general approaches to uniform molecular alignment of liquid crystals are well known in the art.[1-5] The first approach is to rub the substrates in a single direction before applying the liquid crystal. This technique is found to cause the liquid crystal to align on the substrates with the long axis of the molecules parallel to the direction of rubbing (homogeneous parallel alignment). Various materials have been used for rubbing the substrates including paper, cotton, foam rubber, and leather. This approach must be considered an art, and there is no general agreement on whether the alignment is induced because of mechanical effects, e.g., minute surface scratches, or because of contaminants that are prealigned by the rubbing. The second approach is to add a surface active agent (surfactant) that forms an oriented thin layer (usually a monolayer) on the substrate. The orientation of the surfactant layer then induces the desired orientation in the liquid crystal layer. This approach usually results in the liquid crystal aligning with its long axis perpendicular to the substrate, homeotropic alignment.

Our initial efforts were directed toward the rubbing approach; however, we did not achieve satisfactory results with this approach. As a result, the bulk of the experiments were performed with surfactants. Surfactants are of great commercial importance, and the surface

chemistry associated with them has been widely studied[6]; but the
selection of a suitable surfactant is still largely an empirical task.
A brief review of the chemistry of surfactants is helpful in understand-
ing how we conducted the search for a suitable material.

Surface activity can be defined as the tendency of a solute to
concentrate at an interface. Molecules exhibiting surface activity
usually have two segregated portions, one of which has sufficient
affinity for the solvent to bring the entire molecule into solution and
the other of which is rejected by the solvent. Therefore, the rejected
portion tends to concentrate at an interface so that it will not be in
contact with the solvent molecules. Soaps in water are the most
common surfactants. A typical surfactant molecule has a long polar
hydrocarbon chain with a nonpolar group in one end. There are
surfactants that are soluble in hydrocarbon solvents and others that
are soluble in water. The present studies were primarily on the
water soluble surfactants.

The water-soluble surfactants can be classified as follows:

1.   Anionic - surfactants that ionize in solution
        with the long chain carrying a negative
        charge.

2.   Cationic - surfactants that ionize in solution
        with the long chain carrying a positive charge.

3.   Nonionic - surfactants that do not ionize in
        solution.

4.   Amphoteric - surfactants that ionize in
        solution with the long chain carrying either
        a positive or negative charge, depending on
        the pH of the solution.

Common soaps and detergents are anionic surfactants. The
detergents and many commercial wetting agents (e. g., the Igepon
series), are sulfonates. Generally, cationic surfactants are amines
or quaternary ammonium compounds (common germicidal agents).
There are a wide variety of nonionic and amphoteric surfactants. The

46

amphoteric surfactants contain both an anionic and cationic group and are cationic in acid solution and anionic in alkaline solution. Lecithin, an excellent surfactant for certain liquid crystal applications, is an amphoteric surfactant with a phosphate as the anionic group.

In water solution, the surfactant molecules orient with their polar group directed into the water and their hydrocarbon chain directed outward. Therefore, a cationic surfactant, with its positive long chain, will be strongly adsorbed on a surface carrying a negative charge, and an anionic surfactant will be strongly adsorbed on a surface carrying a positive charge. For this reason, surfactants are selected on the basis of the electrical nature of the surfaces in contact with the solution. If the surface characteristics are unknown, then surfactants from each of the four classes can be tried to determine the correct class.

D. EXPERIMENTAL TECHNIQUES

The uniformity studies involved assembling and testing a large number of liquid crystal cells, so it was necessary to establish critical tests that could be executed quickly and repeatably. We chose the following three tests for evaluating each trial cell:

1. Photographing the image plane of the cell with the cell placed between crossed polarizers. This test provided an immediate evaluation of whether or not single domain alignment was achieved and whether the molecular axes were aligned parallel or perpendicular to the substrates. A perpendicular aligned cell exhibits a dark image plane when placed between crossed polarizers and the image plane remains dark as the cell is rotated about the optical axis. A parallel aligned cell exhibits an image plane that goes from dark to light to dark at 45° intervals of rotation about the optical axis.

2. Photographing the image plane of the cell with the cell placed between polarizers oriented at an angle of about 45°. This test was a measure

of the cosmetic quality of the devices, i.e., it indicated the presence of defects in the substrates as well as the presence of contaminants such as dust. This test was primarily a test of substrate quality and of cleaning and assembly techniques.

3.   Photographing the Fourier transform plane with the cell placed between crossed polarizers. This test was very sensitive to any scratches or low frequency phase variations that caused depolarization of the transmitted coherent wavefront.

The first two tests were performed on an optical system with incoherent illumination to avoid any confusion with diffraction of coherent light by dust or defects in the optics. This system is illustrated in Fig. 16. The Fourier transform photographs were made on the coherent light optical system illustrated in Fig. 17. These systems are depicted and described below under the topic of experimental apparatus.

Each liquid crystal cell was tested with the following systematic procedure:

1.   Test for uniformity and optical quality as described above.

2.   If the tests showed a clean and uniformly aligned liquid crystal film and exhibited no noise or unwanted structure in the Fourier plane, the cell was tested for dynamic scattering under dc excitation, and if the cell was a light-activated device, it was tested in a coherent optical system for response time and memory effects. (Memory effects refers to effects that cause a faint outline of old images to remain on the cell.) These tests were performed by exciting the cell with an image, usually an Air Force Resolution Chart.

3.   If the initial tests indicated uniform alignment, but with excessive noise or structure in the Fourier plane, then the cells were disassembled and the individual electrodes were tested in the coherent optical system to determine if the cause of the unwanted Fourier plane scattering is due to flawed electrodes or if it is due to inadequate alignment of the liquid crystal.
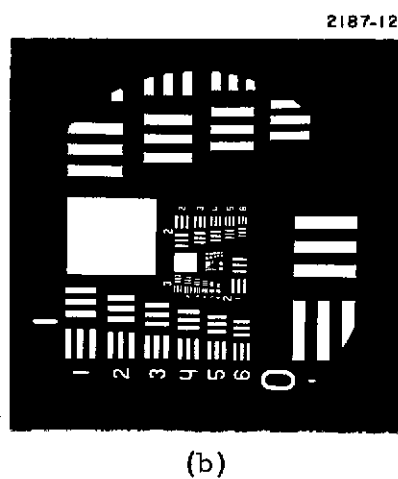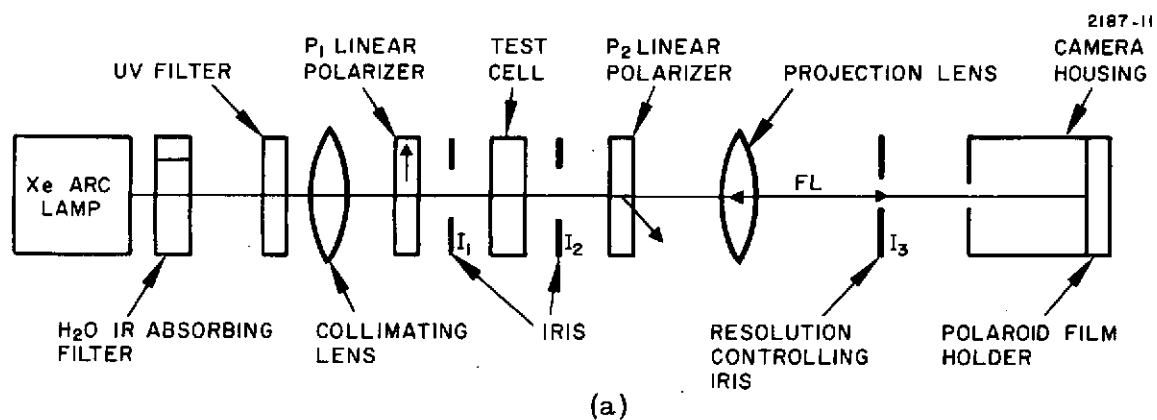
(a)

2187-12

(b)

Fig. 16.   Image Plane Optical System.

UV FILTER

IRIS

FRONT SURFACE
MIRROR

ZIRCONIUM
LAMP

DIVERGING
LENS 10 mm Fℓ

COLLIMATING
LENS 20 cm Fℓ

LIQUID CRYSTAL
TEST CELL

50%
BEAM
SPLITTER

632.8nm
IF FILTER

POLAROID
CAMERA HOUSING

3mW He-Ne
LASER

Fℓ

Fℓ

Fℓ

LINEAR
POLARIZER

6.8μ SPATIAL
FILTER

ND
FILTER

ADJUSTABLE
IRIS

FOURIER
LENS

LINEAR
POLARIZER
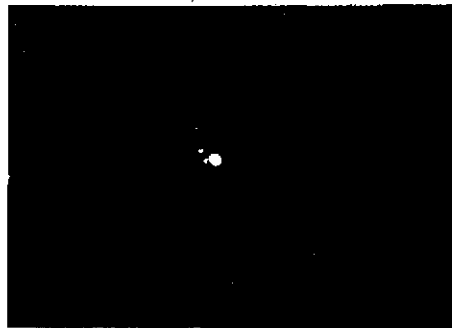
FILM
BACK

(a)

(b)
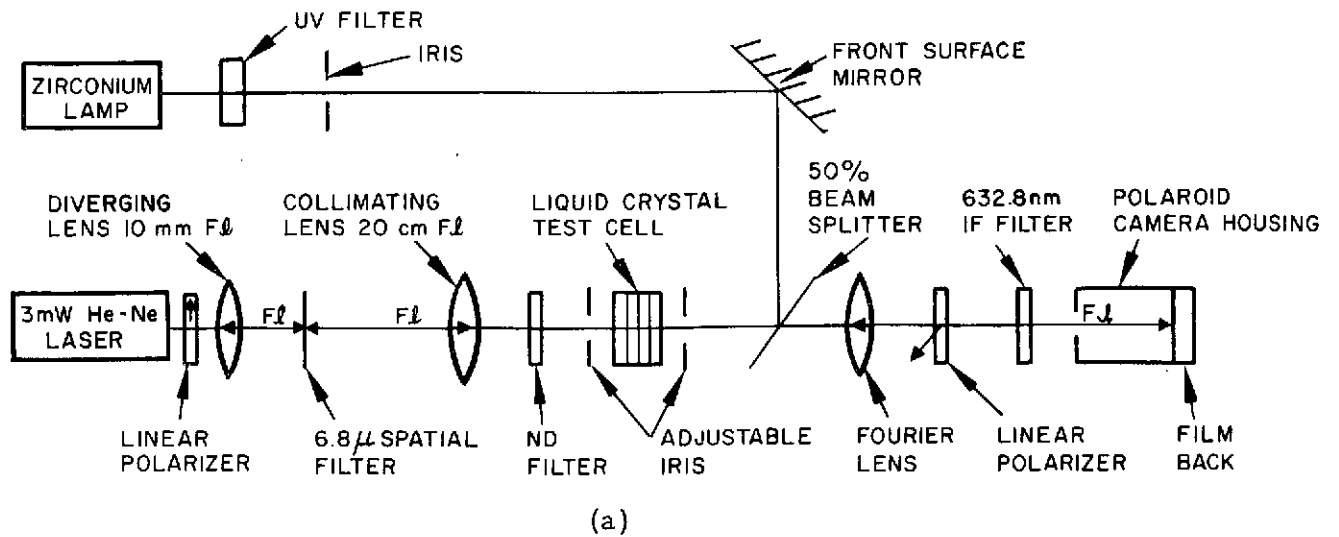
Fig. 17. Fourier Plane Optical System and Image.

50

E.   EXPERIMENTAL RESULTS

The experiments can be discussed best by dividing them into categories according to the particular liquid crystal and electrode materials used in the cell. The categories are as follows:

1.   MBBA liquid crystal with both transparent electrodes of In_2O_3. The bulk of the surfactant selection work was done on these cells. All four types of surfactants plus several miscellaneous techniques were tried.

2.   MBBA liquid crystals with one electrode of In_2O_3 and the other of CdS over In_2O_3. Rubbing experiments and surfactants were tested with these cells.

3.   Ester liquid crystals with both electrodes of In_2O_3.

4.   Ester liquid crystals with one electrode of In_2O_3 and the other of CdS over In_2O_3.

The results from the rubbing experiments are discussed first, then the surfactant experiments with both light-activated and non-light-activated MBBA liquid crystal cells, and finally the surfactant experiments with ester liquid crystal cells.

1.   Experimental Apparatus

During this phase of our investigations on photoactivated liquid crystal light valves, we attempted to monitor semi-quantitatively the amplitude and phase distortions introduced by domains and other inhomogeneities associated with the liquid crystal layer. Both amplitude and phase distortions were recorded on the optical arrangement shown in Fig. 16(a). This apparatus was used essentially to photograph on Polaroid^{TM} type 42, ASA speed 200, film a magnified image (3.5X) of the central activated region (1 x 1 cm) of a liquid crystal test cell. This procedure provided phase information when

linear polarizers P_1 and P_2 were crossed with respect to each other and it provided primarily amplitude information when the polarizers were oriented at $45°$. The limiting resolution of this system was controlled by iris I_3 and was set to a value in excess of 20 cycles/mm, as shown in Fig. 16(b). Coherent phase distortions were observed using the Fourier phase optical system depicted schematically in Fig. 17(a). The zirconium white light source was used to photoactivate CdS cells when it was desired to observe the Fourier transform characteristics of a photoactivated cell in the dynamic scattering mode (DSM). All information obtained via this technique was also recorded on Polaroid^{TM} type 42 film with an ASA 200 sensitivity rating. A major portion of the data recorded to date was recorded with exposure times of either 1 or 4 sec. The photograph shown in Fig. 17(b) is a 180-sec Fourier transform exposure of the optical system in the absence of a light valve or a liquid crystal cell. In this picture, two small spots are visible to the left of the central maximum; they result from multiple reflections off various optical components in the system. These imperfections limit the ultimate noise performance of the experimental apparatus, but since they occur in exposures which are 45 to 180 times longer than those associated with the data, adequate signal-to-noise ratios can be easily maintained. Neutral density filters were sometimes used and this must be accounted for when comparing exposure times.

2.   Data

The alignment technique employed in our initial studies was rubbing both the CdS and the In_2O_3 electrodes with a polyurethane swab before applying the liquid crystal. This technique promoted reasonably good parallel alignment as observed in the image plane. It was also effective (as observed in the image plane) for cells made with two In_2O_3 electrodes. Chatelaine[7] first described this method

in 1943 and since then it has been used by many others to promote homogeneous (parallel) alignment.[8,9] Although the above procedure produces a fairly well-aligned liquid crystal layer when viewed in the image plane, inspection of the Fourier plane data (Fig. 18) indicates that the cell is not perfectly homogeneous. In this photograph, two approximately horizontal lines can be seen superimposed on a bright diffuse background. These lines represent diffraction effects from a series of straight, parallel, and nonuniformly spaced inhomogeneities at first assumed to be scratches in the In_2O_3 and/or CdS electrodes resulting from the process of rubbing. This suspicion was abandoned after the cell was taken apart and each of the bare electrodes was observed in the Fourier transform plane. The Fourier plane photos of the electrodes did not exhibit either the line structure or the diffuse noise, indicating that neither electrode had been damaged and that the undesirable line diffraction pattern shown in Fig. 18 actually resulted from imperfections within the liquid crystal layer itself. The bright diffuse spot also seen in Fig. 18 is a consequence of random phase distortions that arise either because the bulk liquid crystal is not aligned by the boundary conditions imposed from the electrodes, or more likely because uniform boundary layers have not been established. Attempts to correct the diffraction spikes by using other rubbing materials such as lens tissue, cotton, etc., and other rubbing techniques such as Argon ion beam etching all failed. They all resulted in similar patterns to that shown in Fig. 18. Cells were also made with only one rubbed electrode, and this procedure again displayed an excessive amount of random noise superimposed upon a few (1 or 2) reasonably clean line diffraction patterns (see Fig. 19). In this photograph, we can see that the random noise is even more intense than that in Fig. 18. From the above results, we conclude that the often used Chatelaine rubbing technique was not an effective and reproducible method for achieving homogeneous alignment with sufficient uniformity for application to coherent optics systems.
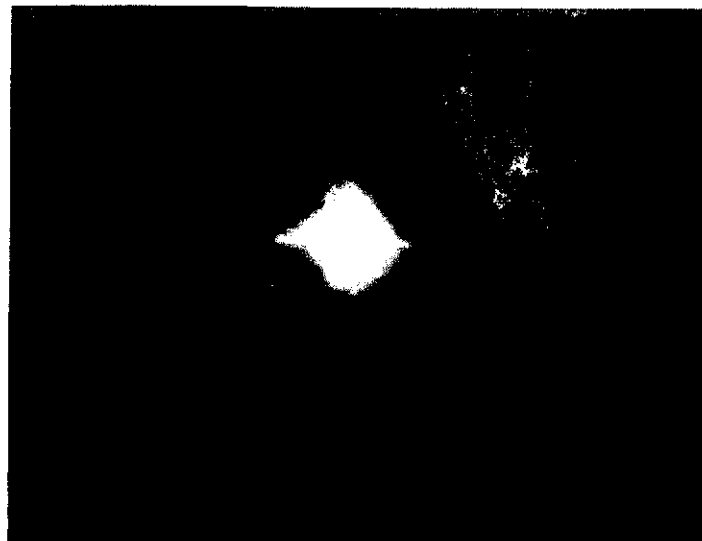
M9450

Fig. 18.
Cell: CdS/MBBA/In$_2$O$_3$. Both Elec-
trodes Rubbed with Polyurethane;
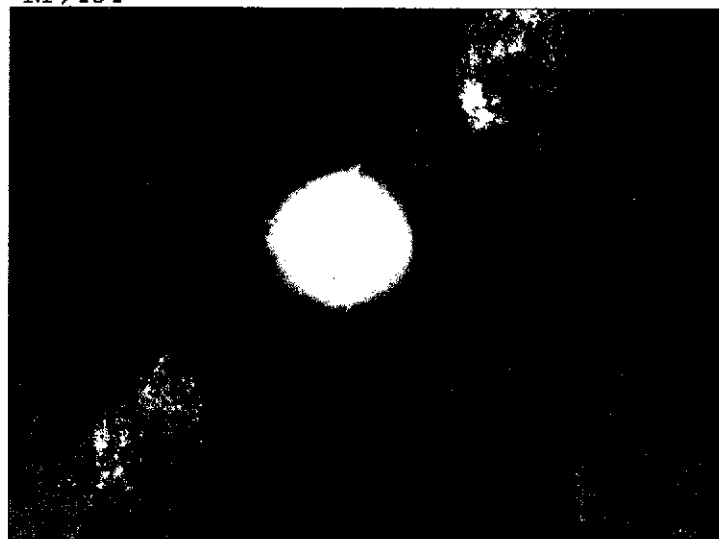Exposure 0.1 Sec.

M9451

Fig. 19.
Cell: CdS/MBBA/In$_2$O$_3$. Only In$_2$O$_3$ Elec-
trode was Rubbed with Polyurethane;
Exposure 0.1 Sec.

54

At this time, it was decided that a more fruitful approach would be to investigate procedures for promoting uniform homeotropic (perpendicular) alignment. The remainder of this section is concerned with efforts to achieve perpendicular alignment on CdS and In_2O_3 electrodes with two different liquid crystals, MBBA and an HRL proprietary DSM ester liquid crystal.

3.   MBBA

When one prepares an MBBA liquid crystal cell using only cleaned (as described in Section II) In_2O_3 electrodes, the MBBA does not align either homogeneously or homeotropically to the electrode surfaces. Instead, small and randomly oriented domains are formed (see Fig. 20(a)). This image plane pattern is associated with an excessively noisy Fourier plane as shown in Fig. 20(b).

The first and only attempt to align liquid crystals to electrode surfaces homeotropically, without employing surfactants, was via the acid etch technique.[10] These authors used a chromic acid etchant made with a 20:1 mixture by weight of H_2SO_4 to $K_2Cr_2O_7$. Our experience with this procedure indicates that it will not suffice for either In_2O_3 or CdS electrodes. Some In_2O_3 electrode cells made with this technique did show reasonably good homeotropic alignment, but the results were not reproducible (see Figs. 21(a) and (b). We attempted to use other etchants such as acetic acid, HCl, and NH_3OH in dilute concentrations with uniformly bad results. The technique of etching the electrode with an Argon ion beam also proved to be ineffective.

Our next approach to achieving homeotropic alignment involved the use of chemical surfactants, which through the mechanism described above, promote uniform homeotropic alignment at the electrode surfaces. Hass, Adams and Flannery[11] reported perpendicular alignment in the liquid crystal ABUTA by using the polymeric
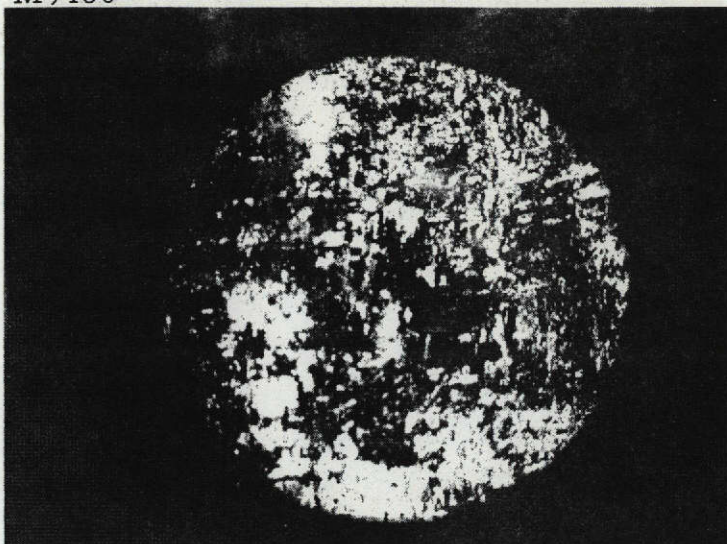
M9460

Fig. 20(a).
Image Plane.   Cell: In_2O_3/MBBA/In_2O_3.
No Attempt Made to Align MBBA; Exposure
0.2 Sec, $\perp$ Polarizers.

M9459

Fig. 20(b).
Fourier Plane. Cell: In_2O_3/MBBA/
In_2O_3. No Attempt Made to Align MBBA;
Exposure 1 Sec, $\perp$ Polarizers.

M9462
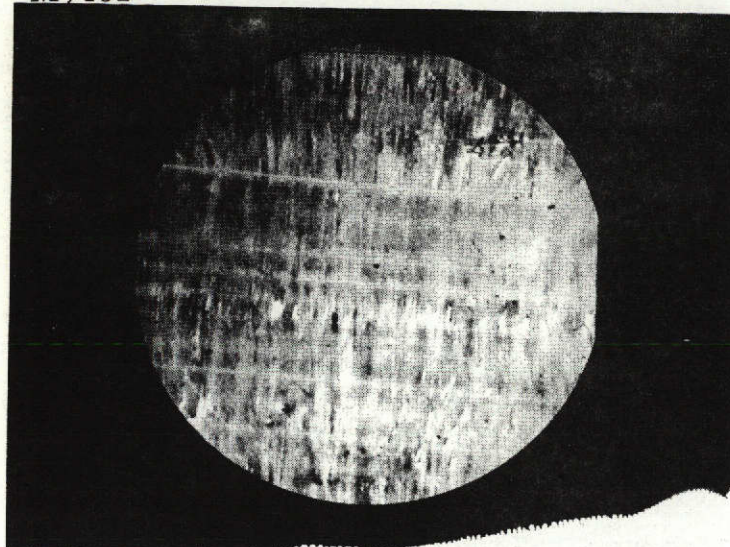

Fig. 21(a).
Image Plane. $In_2O_3/MBBA/In_2O_3$. Both
Electrodes Etched in Chromic Acid for
1 Min. at 100°C; Exposure, 1/60 Sec,
$\perp$ Polarizers.

M9461

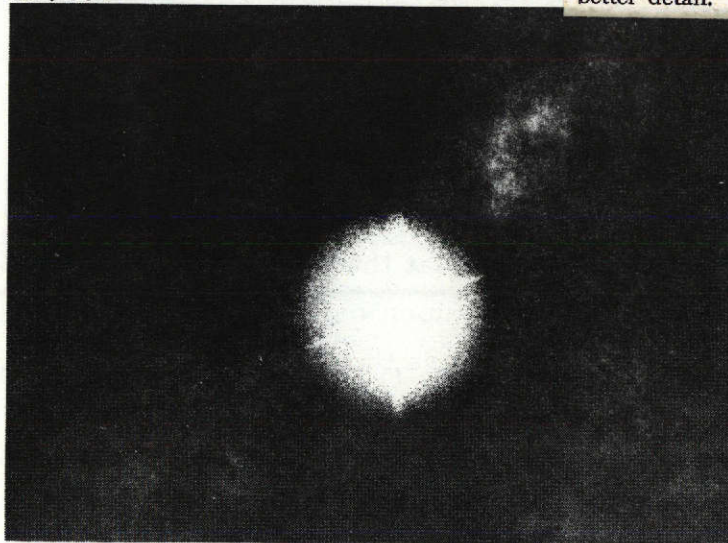
Fig. 21(b).
Fourier Plane. $In_2O_3/MBBA/In_2O_3$. Both
Electrodes Etched in Chromic Acid;
Exposure 1 Sec, $\perp$ Polarizers.

surfactant polamide resin, which is sold by General Mills under the trade name Versamid 100. Fairly good homeotropy was achieved as shown in Fig. 22(a), using a doping concentration of approximately 1% and chromic acid etched In_2O_3 electrodes. The degree to which the alignment was not free of inhomogeneities can be seen in the Fourier plane photographs, Fig. 22(b) and (c), which indicate the presence of parallel uniform imperfections. Note that Fig. 22(c) is a 30-sec exposure, which indicates that the noise level is really quite low. The performance of In_2O_3 electrode cells in the dynamic scattering mode (DSM) was not affected in any apparent way by the presence of polyamide dopant. Although this technique was effective with In_2O_3 electrodes, it did not promote homeotropic alignment with CdS electrodes.

Next we tried soybean lecithin, which belongs to the class of amphoteric surfactants.[12] This material could be applied with either of the three following methods:

a.   Rubbing onto the electrode surfaces with soft lens tissue

b.   Spinning onto the electrodes from dilute (< 1%) solutions of hexane, trichloroethylene, or toluene

c.   Doping the material into MBBA.

Our results with the spinning technique were rather inconsistent, which we attributed to the fact that the uniformity and homogeneity of a spun layer depends critically upon many parameters such as spinning speed, substrate temperature, and cleanliness. The most reproducible results were obtained with the doping technique. We normally used lecithin concentration of 1% in MBBA, but we also performed a series of tests to determine if this rather arbitrarily chosen doping level was excessive. The results of this are shown in Figs. 23 and 24 from which we conclude that the minimum concentration (for use with In_2O_3 electrodes) was approximately 0.1% by weight. In_2O_3 cells made with doped lecithin could not be operated with dc excitation because the lecithin forms a highly resistive

58

M9444
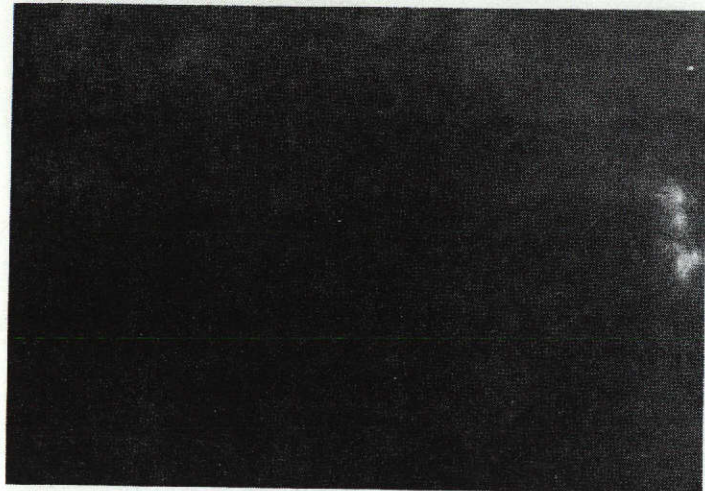
Fig. 22(a).
Image Plane.
$In_2O_3/MBBA/In_2O_3$ + 1%
Polyamide. Both Elec-
trode Etched in Chromic
Acid; Exposure, 4 Sec.,
⊥ Polarizers.

M9446

Fig. 22(b).
Fourier Plane.
Same Cell as Fig. (a),
Exposure, 1 Sec, ⊥
Polarizers.

M9447

Fig. 22(c).
Fourier Plane.
Same Cell as Fig.(b),
Exposure, 30 Sec, ⊥
Polarizers. This
Photograph was Taken
4 Days After That of
(b).

M9456

Fig. 23(a).
Image Plane. In_2O_3/MBBA + 1% Lecithin/
In_2O_3; Exposure, 4 sec, $\perp$ Polarizer.

M9457

Fig. 23(b).
Fourier Plane. Same Cell as Fig. 8(a);
Exposure, 30 Sec, $\perp$ Polarizers.

M9445

Fig. 24(a).
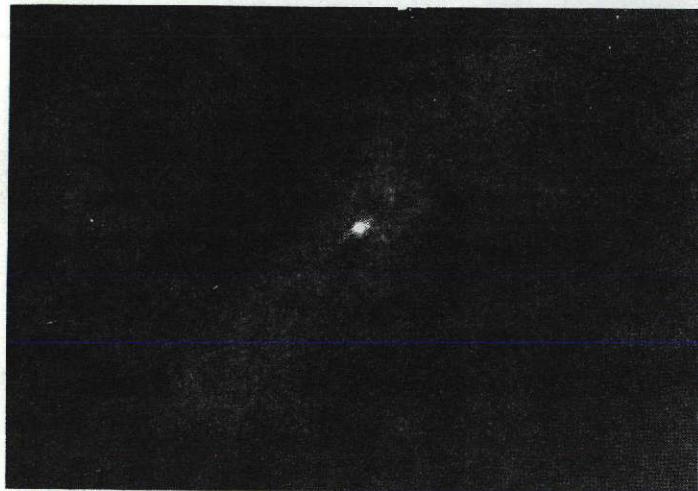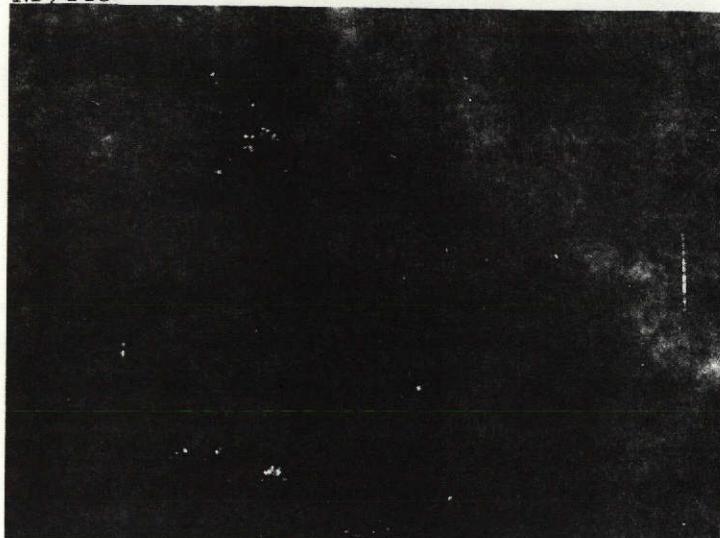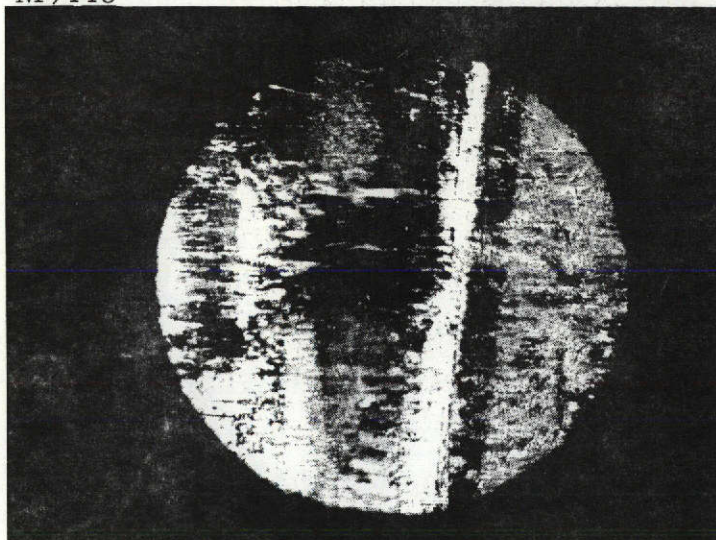Image Plane. $In_2O_3/$
$MBBA/In_2O_3$, 0.1% Leci-
thin; Exposure, 4 Sec,
$\perp$ Polarizers.

M9449

M9448

Fig. 24(c).
Image Plane. $In_2O_3/$
$MBBA/In_2O_3$, 0.001%
Lecithin; Exposure,
0.2 Sec, $\perp$ Polarizers.

layer between the electrode and bulk liquid crystal. This problem can be alleviated by employing an ac voltage (100 Hz) to excite the dynamic scattering. The lecithin dopant also can be used to align MBBA homeotropically on CdS, but with a similar problem associated with dc excitation. In this case an ac activating field was not an adequate solution because the capacitance associated with the depletion charge layer at the CdS/MBBA interface negated the effect of the blocking electrode when the CdS was not photoactivated. At this time, a series of anionic, cationic, and nonionic surfactants were tried with MBBA on both In_2O_3 and CdS cells. The results of these tests are summarized in Table II. From this data we conclude that there are at least six good methods for achieving homeotropic alignment on In_2O_3 electrodes with no degradation of dynamic scattering performance. Most of these techniques also are quite effective with CdS, except that in this case a residual image is permanently stored after photoactivation and dc excitation. This is shown in Fig. 25. Notice also that besides having a residual image, the homeotropic alignment is almost completely gone. That is, the homeotropic alignment is not stable when induced by these methods on CdS.

4.   DSM Ester

A limited number of attempts were made in an effort to align the DSM ester either homeotropically or homogeneously to the electrode surface. The ester was of interest to us because it has recently been demonstrated that this nematic material has significantly longer lifetime than MBBA in the dynamic scattering mode of operation. The difficulty associated with ester alignment is that many of the surfactants that proved to be successful in MBBA were not soluble enough in the ester to be effective. The results of these tests are summarized in Table III. We conclude from these data that there exist at least two good surfactants for the DSM esters for cells made with In_2O_3 electrodes. As in the case with MBBA, we are able to align the ester homeotropically to CdS electrodes, but upon photoactivation this alignment is destroyed and a residual image is formed.

TABLE II

Summary of Tests Performed with Different Surfactants Used to Achieve Homeotropic Alignment in MBBA

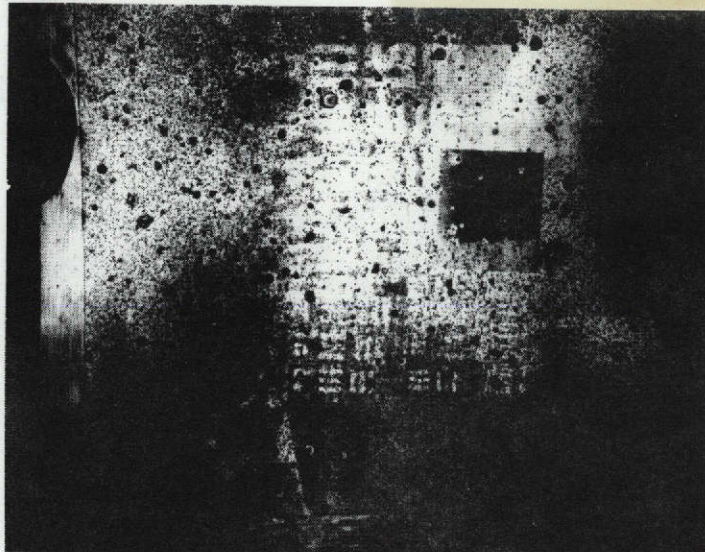|	Manufacturer Trade Name	Chemical Name	Type of Surfactant	Method of Application	In_2O_3 Electrodes	CdS Electrodes
1.	Versamid 100 General Mills	Polyamide Resin	polymeric	dopant < 1%	good ⊥ alignment good DSM	poor ⊥
2.	MCB	Soybean Lecithin	amphoteric	(1) dopant (2) spun (3) rub	good ⊥ no DSM	good ⊥ no DSM
3.	Union Carbide L-76 Silicone	not given	nonionic	0.99% dopant	not tested	very poor
4.	Atlas Chem. Tween-20	Polyoxyethylene Sorbitan Monolaurate	nonionic	dopant 0.19%	not tested	very poor
5.	IGEPAL CTA-639 GAF	Alkylphenoxypoly (ethyleneoxy) Ethanol	nonionic	dopant 0.24%		very poor
6.	GAF NEKAL WT-27	Sodium Dioctyl Sulfosuccinate	anionic	dopant 0.84%		very poor
7.		Potassium Decyl Xanthate	anionic	spun from MeOh solution	very poor	not tested
8.		Dibenzal · Benzidine	cationic	dopant 1%	very poor	not tested
9.	Aliquot H-226 General Mills	Dimethyl Di (Hydrogenated Tallow) Ammonium Chloride	cationic	dopant 0.5%	very good ⊥ good DSM	poor
10.	Eastman Kodak	n-Methyldioctadecyl Amine	cationic	dopant 0.5%	excellent ⊥ good DSM	excellent ⊥ good DSM residual stored image
11.	Varilight Non Orienting Coating Solution	Unknown	unknown	spun	excellent ⊥ good DSM	excellent ⊥ good DSM residual stored image
12.	Alconox Laboratory Detergent			spun on or electrode washed in it	excellent ⊥ good DSM	excellent ⊥ good DSM residual stored image

T888

63

M9458

Fig. 25.
Image Plane. CdS/MBBA/In$_2$O$_3$.
Alconex Solution in Deionized H$_2$O
Spun on Both Electrodes; Exposure,
0.001 Sec, Polarizers. This Photo-
graph was Taken after the Cell was
Photoactivated with an AF Test Pat-
tern Image.

64

TABLE III

Summary of Attempts at Homeotropic Alignment
in the DSM Ester

	Manufacturer Trade Name	Chemical Name	Type of Surfactant	Method of Application	In_2O_3 Electrodes	CdS Electrodes
1.	Witco Chem Emco CC-9	MeEt$_2$ Polyoxypropylene Ammonium Chloride	cationic	dopant 2.66%	not tested	very poor image plane
2.	General Mills Aliquot 4	Trimethyl Laurel Ammonium Chloride	cationic	dopant 3.6%	not tested	very poor image plane
3.	General Mills Aliquot 26	Trimethyl Tallow Ammonium Chloride	cationic	dopant 1.2%	not tested	very poor image plane
4.	Union Carbide L-79 Silicone	not given	nonionic	spun on from 50% solution DI H$_2$O	not tested	very poor image plane
5.	MCB	Soybean Lecithin	amphoteric	dopant 1%	excellent ⊥ alignment but poor DSM	not tested
6.	Varilight Non Orienting Coating Solution	Unknown	unknown	spun	not tested	excellent ⊥ good DSM residual image
7.	Eastman Kodak	Hexadecyltrimethyl Ammonium Stearate	cationic	dopant 0.1%	excellent ⊥ alignment good DSM very conductive	excellent ⊥ good DSM very conductive residual image

T889

65

SECTION IV

PHOTOCONDUCTOR STUDIES

A.   PHOTOCONDUCTOR FABRICATION CONSIDERATIONS

During the course of the contract many changes were imple-
mented to improve the CLV quality by altering the processing employed
in the production of the electrode photoconductor substrate. These
changes are discussed here.

1.   Selection of Transparent Conductive Coatings on Glass

The original coherent light valves were fabricated on antimony-
doped tin oxide coated glass substrates purchased from the Corning
Glass Co. Microscopec examination of these substrates revealed that
they had almost a continuous coverage of flaws consisting of small
particles (probably glass polishing compound) imbedded under the tin
oxide coating, pinholes through the coating, and "orange peel" irregular-
ities due to corrosion of the glass during the high temperature coating
process. In addition, the glass was warped so that uniform cell fabri-
cation was impossible. Thus, a search was initiated for other sources
of conductive coatings. In addition, inhouse fabrication was begun.
Three other vendors were found who offered coatings far superior to the
Corning glass tin oxide. These coatings still had flaws,[*] but by careful

---

[*] (1) Pittsburgh Plate Glass Co., Nesatron^{TM} coating: (Sputtered
     In_2O_3:Sn, post-baked in air) coating uniform; high transparency
     ($>85\%$ for $10^2 \Omega/\square$); flaws consisted of small metal particles
     (probably Indium) imbedded with random density in coating.

   (2) Optical Coating Labs Inc. (OCLI) transparent coating (probably
     sputtered $In2O3$:Sn) coating uniform, transparency somewhat less than
     Nesatron; flaws consisted of small pinholes in the conductive coating.

   (3) Varalight Corp., transparent coating spray deposited, Sn_2O_3:Sb
     some coating non-uniformity; less transparent than either Nesatron
     or OCLI, circular surface fractures and small imbedded particles.

inspection many high quality substrates could be selected from each large sheet of glass. To avoid any scratching or pitting during cutting, the coating was covered with tape or plastic that could later be stripped without damaging the transparent electrode material.

2. Improvements in CdS Film Deposition Techniques

Microscopic examination of the deposited CdS films indicated a high density of small CdS particles imbedded in the film. The particles were CdS powder that was ejected during evaporation from the open resistively heated boat and directed at the substrate. Several evaporation source configurations and source materials were evaluated for effectiveness in stopping this "spitting." It was found that the most successful combination was the use of a tantalum baffle box source (SM-10, RD Mathis Co.) together with polycrystalline CdS chips and quartz wool baffle. In addition the H_2S processing furnace was renovated with an all-Teflon gas flow system and in-line particle filter installed.

3. Dust Contamination

Dust-related flow in films is a serious problem in thin-film technology. It requires the most stringently controlled handling procedures. To control the dust problem, the following steps were implemented:

a. Final cleaning of substrates was done under a laminar flow hood.

b. Substrates were loaded into a closed substrate holder for transport to the vacuum deposition station.

c. Vacuum station was pumped down and a glow discharge was initiated with one holder still closed. This procedure avoids any dust from being deposited on the substrates during pump down and also allows dust in the system to be pinned by the discharge action.[13]

d. Substrates were removed from the vacuum system in a closed holder and loaded into the furnace tube in the laminar flow hood.

A comparison of substrates at a magnification of 50X at the beginning and end of the program is shown in Fig. 26.

## B. MODEL OF OPERATION OF CLV AND OPTIMIZATION OF SENSITIVITY

To optimize the sensitivity of the photoconductor, it is necessary to understand the operation of the device. Initial observations indicated that many differences existed between CdS and ZnS-activated CLV's. The observations on the CdS devices, which are reviewed below, indicated that both the solid state and electrochemical aspects of the photoconductor required study. Thus the approach taken was to model the device and improve its operation on the basis of conclusions drawn from the model.

1. Initial Observations

Before and at the beginning of the contract, several observations had been made regarding the operation of the CLV devices. They are summarized below:

1. The device operated only in one polarity, with the CdS biased positively with respect to the liquid crystal layer. In the reverse polarity, the photoconductor acted as low resistance to the liquid crystal and the entire cell was activated irrespective of light activation. This behavior is shown in Fig. 27, where the current-voltage and scattering-voltage characteristics are shown. The curves with CdS (-) and CdS (+) light activated do not show an exponential growth in current because of the high series load resistance of the liquid crystal that limits the current. Thus the slowly rising linear behavior is observed. From this asymmetric behavior it was inferred that a rectifying junction was formed at the CdS-liquid crystal interface. In addition, the effects of a superimposed high frequency ac voltage on the scattering properties were noted. As shown in Fig. 28, there is a definite increase in the scattering threshold as a function of rms ac voltage (see Section V for elaboration of this effect).

M9454
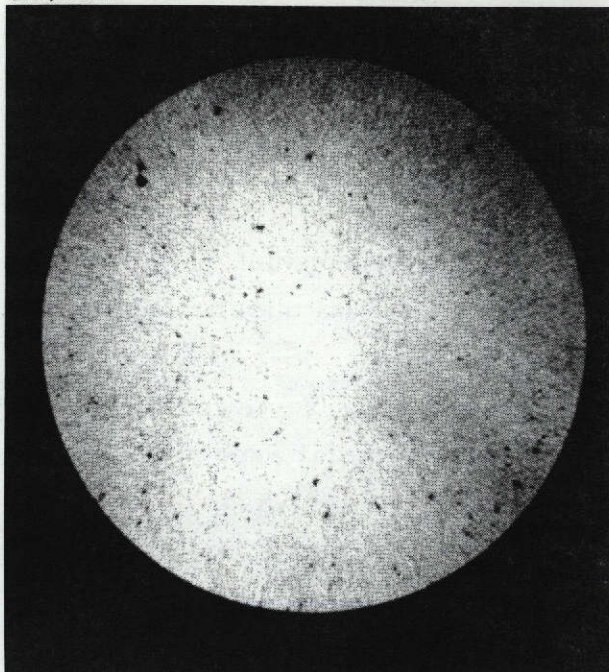
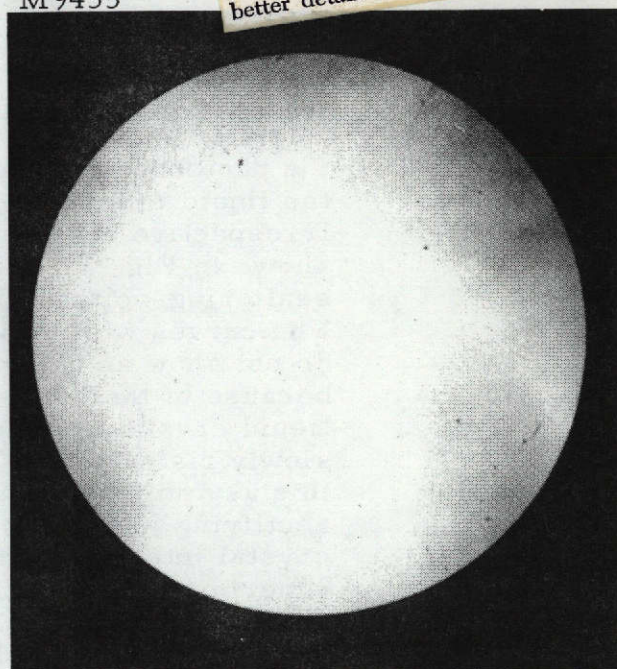(a) Film on Corning Tin Oxide Deposited from Open Boat with CdS Powder.

M9455

(b) Film on Sputtered Indium/Tin Oxide Coating Deposited from Baffled Source with CdS Crystal Chips.

Fig. 26. Comparison of CdS Films on Conductive Coatings at a Magnification of 50x.
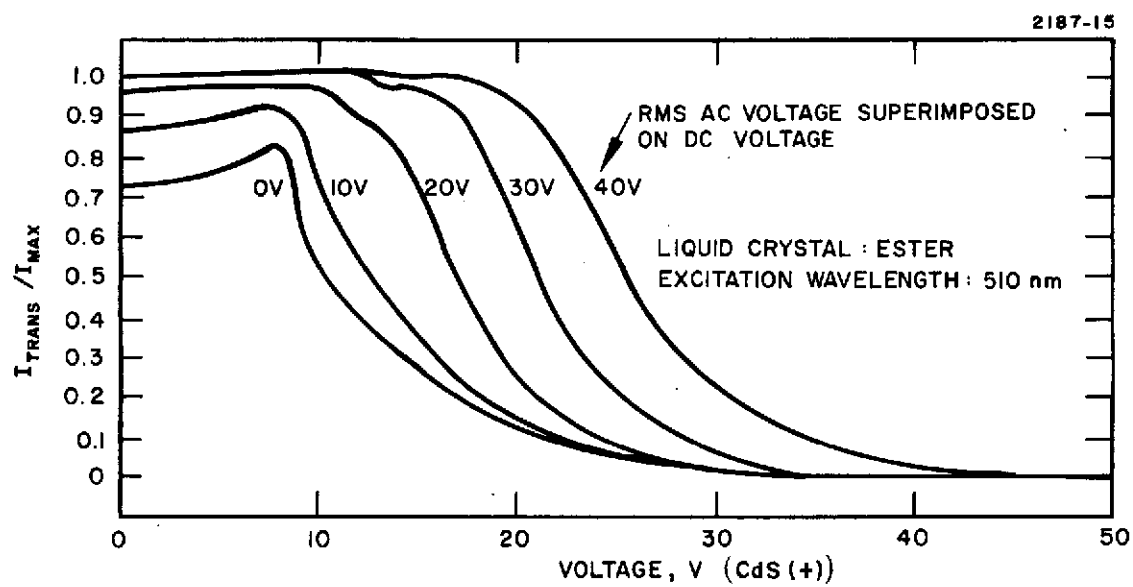
70

Fig. 27. Relative Scattering Versus Applied dc Voltage with ac Bias Voltage as a Parameter.
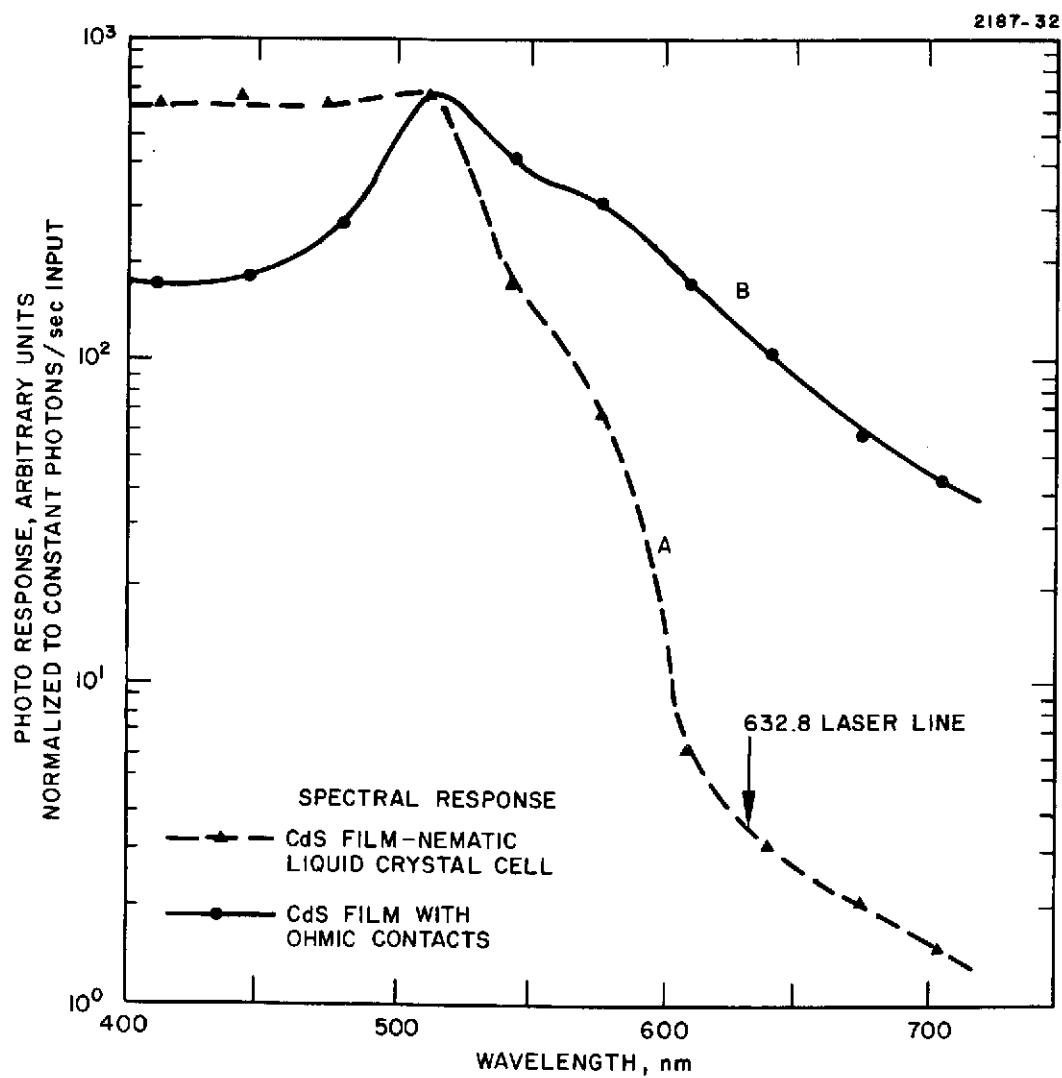
Fig. 28. Graph of CdS Spectral Response with and Without Liquid Crystal Present.

2.   The spectral response was high for photon
        energies greater than the band gap of CdS and
        dropped sharply in comparison to the broader
        response observed in a CdS film with metal
        contacts. This is shown in Fig. 29, which was
        part of the original proposal.

3.   There was a strong asymmetry in relative sensi-
        tivity for activation through the liquid crystal as
        compared to that through the back electrode of
        the photoconductor. The light to dark ratio was
        10-20:1 for activation through the liquid crystal
        but only ~2:1 for activation from the rear. This
        again was indicated from the formation of a high
        field region between the CdS and liquid crystal.

4.   The CdS electrode was etched in the photoactivated
        regions and a metallic deposit was observed in
        corresponding regions on the counterelectrode.
        Microprobe analysis indicated that the metallic
        deposit was cadmium metal. The depth of the
        etching on the CdS electrode was closely cor-
        related to the total charge that passed between
        the electrodes, which indicates that the dis-
        solution of the electrode was a major source of
        current carriers in the liquid crystal electrolyte.

2.   Model for CLV Operation

Following the work of Williams[14] and Gerischer,[15,16] a model
has been formulated to explain the operation of the CLV. The model
proposes a space charge layer formed in the CdS next to the liquid
crystal interface, which blocks current flow when the n-type CdS is
biased positively with respect to the liquid crystal.

The mechanism is modeled diagramatically in Fig. 30, which
shows band diagrams for the electrical configurations involved.
Increasing electron energy is plotted upward while distance (not to
scale) is plotted horizontally. In Fig. 30(a) the equilibrium situation
with no applied bias (V external = 0) is shown. Due to the condition
that Fermi energies be equal through the materials in contact a
rearrangement of charge takes place. The result is that a space charge
of positive ionized donors in the CdS is formed with a corresponding
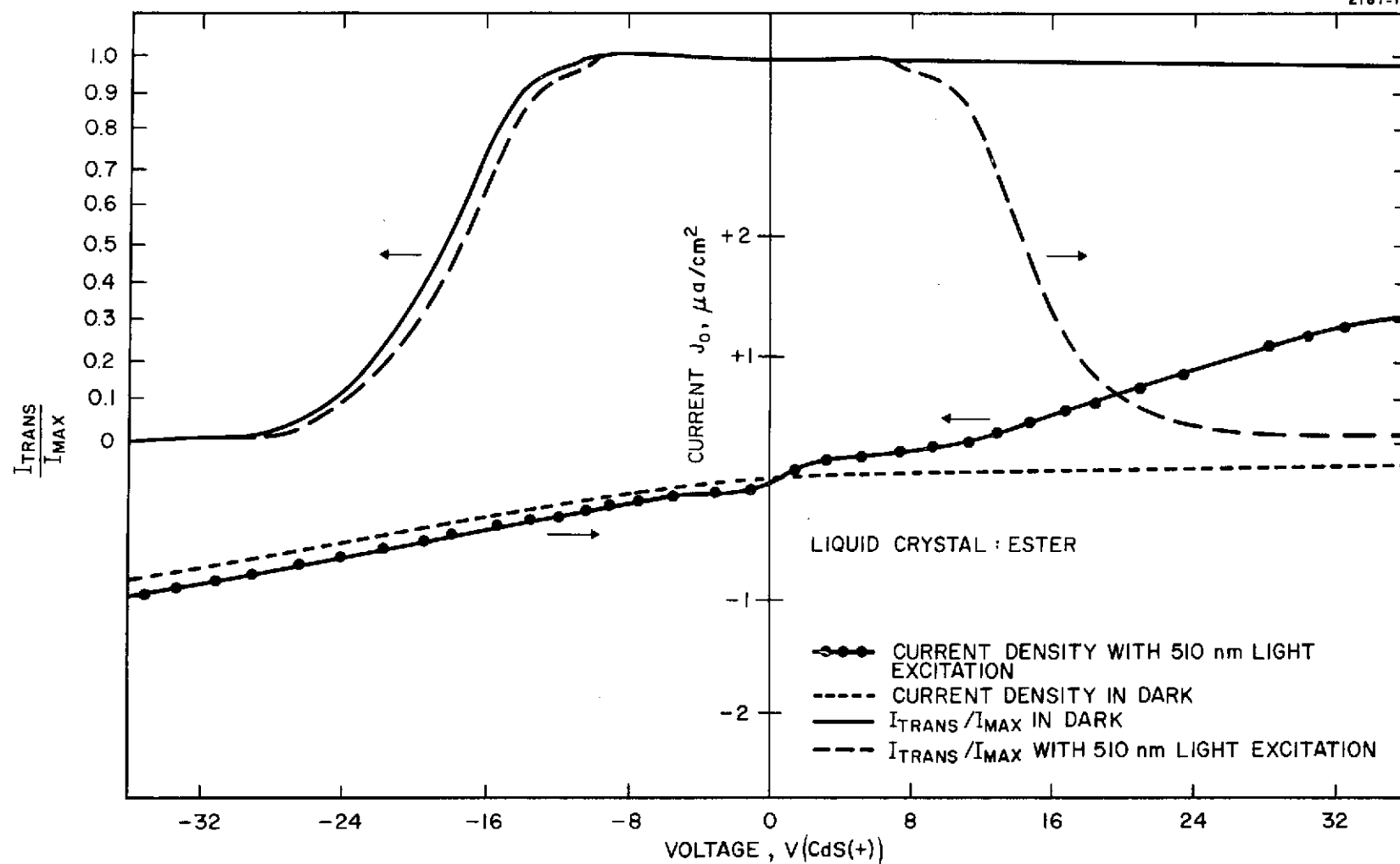
Fig. 29. Current and Relative Transmission Versus Applied dc Voltage.

(a)

IONS IN
SOLUTION

LIQUID CRYSTAL
(DILUTE
ELECTROLYTE)

ELECTRON
ENERGY

CdS

In$_2$O$_3$:Sn

EQUILIBRIUM $\left[V_{EXTERNAL} = 0\right]$

2187-18

(b)

IN DARK WITH $V_{EXTERNAL} = V_A$

2187-19

Cd^{++}

V_A

BAND
GAP LIGHT

(c)

BAND GAP LIGHT INCIDENT
ON INTERFACE WITH $V_{EXTERNAL} = V_A$
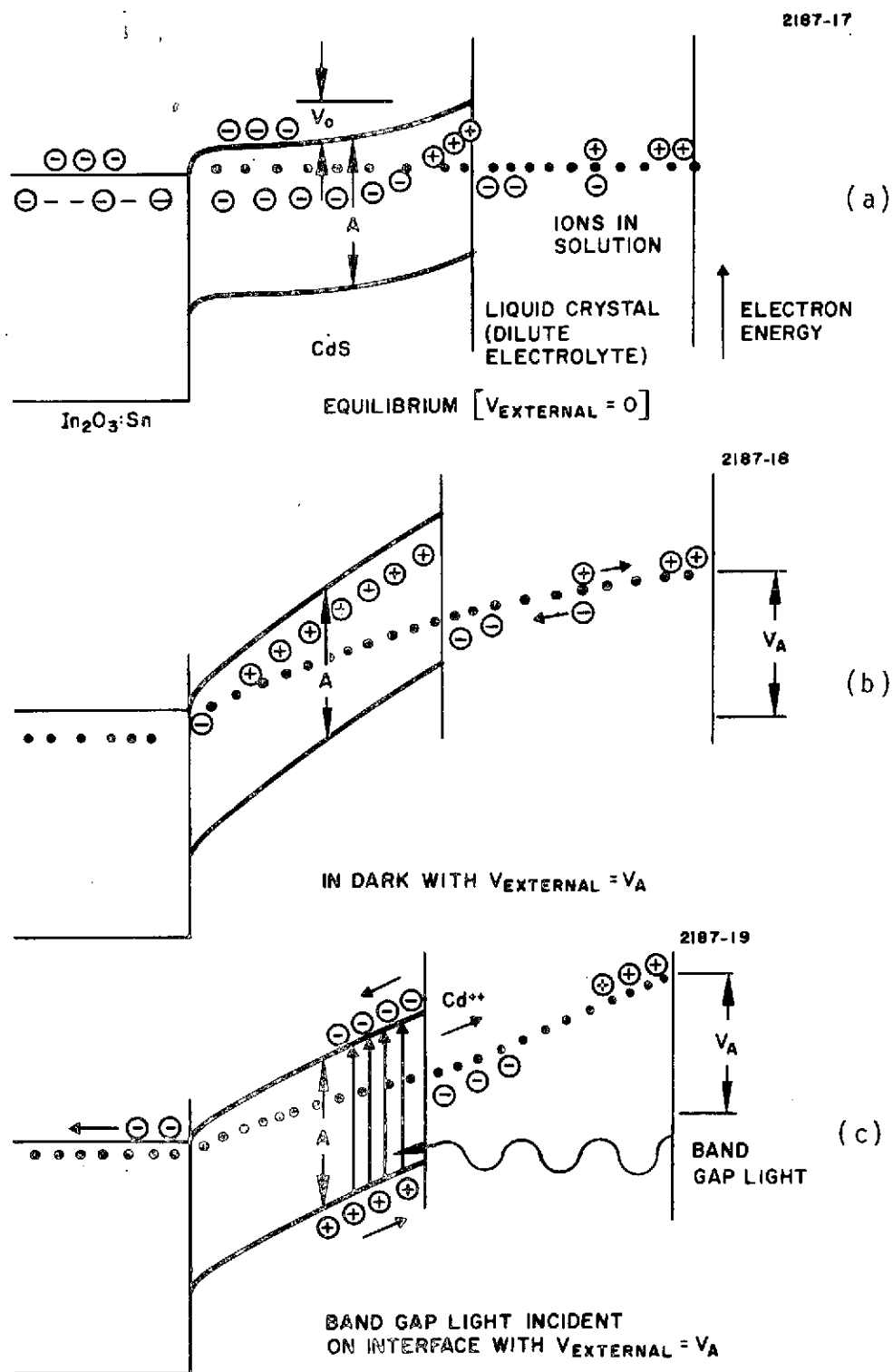
Fig. 30.   Bandgap Light Incident on Interface
with $V_{external} = V_A$.

polarization of ions in the liquid crystal. (In the electrolyte, both the narrow Helmholtz layer of atomic dimensions and the diffuse space charge layer contribute.) The explicit separation of effects of surface stat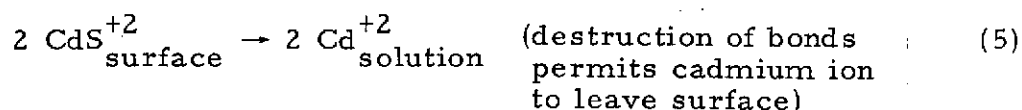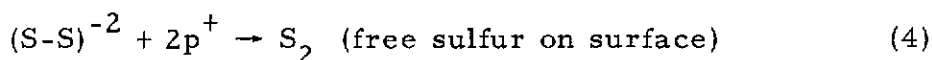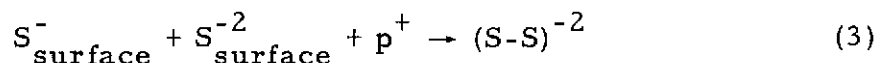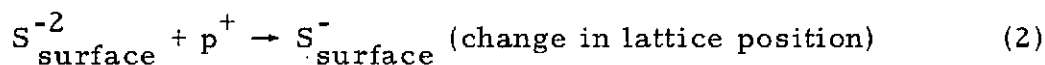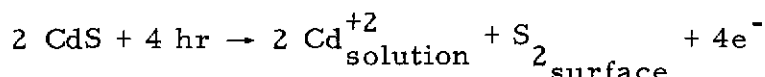es and absorbed ions is not shown. After equilibrium is reached, a contact surface potential on the CdS of magnitude V_o is reached. The In_2O_3:Sn, which is a highly n-doped wide bandgap semiconductor, makes a near-ohmic contact at the CdS back electrode and thus no space charge region is formed at that interface. In Fig. 30(b) an applied bias of magnitude V_a is applied with the CdS (+) with respect to the liquid crystal (anodic polarization). Because there still is no effective mechanism for charge transfer across the interface, the applied electric field sweeps out more carriers in the semiconductor creating a broader depletion region. In this configuration a small current can flow due to second-order electrochemical effects at the interface that are not considered here. This current constitutes the dark current observed in a non-light activated cell.

The configuration, shown in Fig. 30(c) is that under the condition of light excitation through the liquid crystal with the same external bias. Light with photon energy greater than the bandgap energy creats electron-hold pairs in the depletion region. Due to the high electric field in this region, the pairs are rapidly separated, with the recombination with the electrons flowing to the back contact, and the holes moving to the liquid crystal interface. The increased concentration of holes at the surface represent a large departure from the equilibrium and creates a mechanism for charge transfer at the interface. The specific mechanism that takes place depends on the energetics of the transfer process. Because ions of the proper energy to exchange charge are not available (this will be discussed in the liquid crystal chemistry section) the transfer takes place through dissolution of the CdS according to the reactions shown below.[15]
The equations that govern this process are:

$$CdS + 4 \, hr \rightarrow CdS + 4e^- + 4P^+ \tag{1}$$

$$S^{-2}_{surface} + p^+ \rightarrow S^-_{surface} \text{ (change in lattice position)} \tag{2}$$

$$S^-_{surface} + S^{-2}_{surface} + p^+ \rightarrow (S\text{-}S)^{-2} \tag{3}$$

$$(S\text{-}S)^{-2} + 2p^+ \rightarrow S_2 \text{ (free sulfur on surface)} \tag{4}$$

$$2 \, CdS^{+2}_{surface} \rightarrow 2 \, Cd^{+2}_{solution} \quad \begin{array}{l}\text{(destruction of bonds} \\ \text{permits cadmium ion} \\ \text{to leave surface)}\end{array} \tag{5}$$

Net
Equation (6):

$$2 \, CdS + 4 \, hr \rightarrow 2 \, Cd^{+2}_{solution} + S_{2\,surface} + 4e^- $$

In equation (2) the holes that are generated by light act to remove the chemical bonds of the surface sulfur ions, thereby creating S^- ions which can have a less energetically stable lattice position. Further interaction with holes creates bound sulfur-sulfer pairs, eq. (3), which are finally completely separated by additional holes, eq. (5), to create free sulfur on the CdS surface.[17] Finally the weakening of the bonds and movement of the sulfur atoms allows a Cd^{++} ion to leave its lattice position and go into solution. It also should be noted that the creation of adsorbed sulfur on the CdS surface creates surface states that affect the electrical behavior of the interface as they build up in concentration. Under reverse bias [CdS(-)] with respect to the liquid crystal electrons are easily injected into the CdS film from the back In_2O_3:Sn contact and tend to accumulate at the CdS-liquid crystal interface. At that point electrochemical reactions can occur that are analagous to those just described to effect a charge transfer. However, the easy injection of

electron/hole pairs that are generated by light have a high probability of radiative or non-radiative recombination
or non-radiative recombination.

The validity of this model has been established by the observations discussed above and by several additional measurements. One of the latter is the measurement of the instantaneous open-circuit photovoltage. This measurement is shown in Fig. 31. DeWald[18] has shown that the sign and magnitude of the fast-rising part of the photovoltage gives the magnitude and sign of the contact or surface potential (labelled V_o in Fig. 30(a). For an n-type semiconductor and a positive (or depleted) surface, the sign of the observed voltage should be negative. This is observed and an equilibrium value of V_o = +400 mV has been measured. This value along with donor concentration determines the extent of the space charge region in the CdS. While measurements have not been made of the donor concentration, preliminary indications are that for the applied biases used in operation depletion of the entire film can be achieved as shown in Fig. 30(b). This means that a high collection efficiency of light-generated carriers can be obtained over the complete region of absorption of the light. In fact, for absorption of light of energy greater than part of the band gaps (which light is completely absorbed in 0.2-0.3 of film. See Fig. 32 for the wavelength dependence of optical absorption) and incident on the interface so that hole transport is not a limiting factor, quantum efficiencies approaching unity can be achieved. This has been experimentally verified for a threshold photocurrent current measurement on a sensitive CLV. For an incident light power density of 0.4 $\mu W/cm^2$ (at 510 nm) a change in current $\Delta I = I_{light} - I_{dark}$ = 0.12 $\mu amp/cm^2$ was observed. The photon flux at this light power density is 9.7 x 10^{11} photons/cm^2, and the photoactivated current corresponds to a electron flow of 7.5 x 10^{11} electrons/cm^2 sec thus

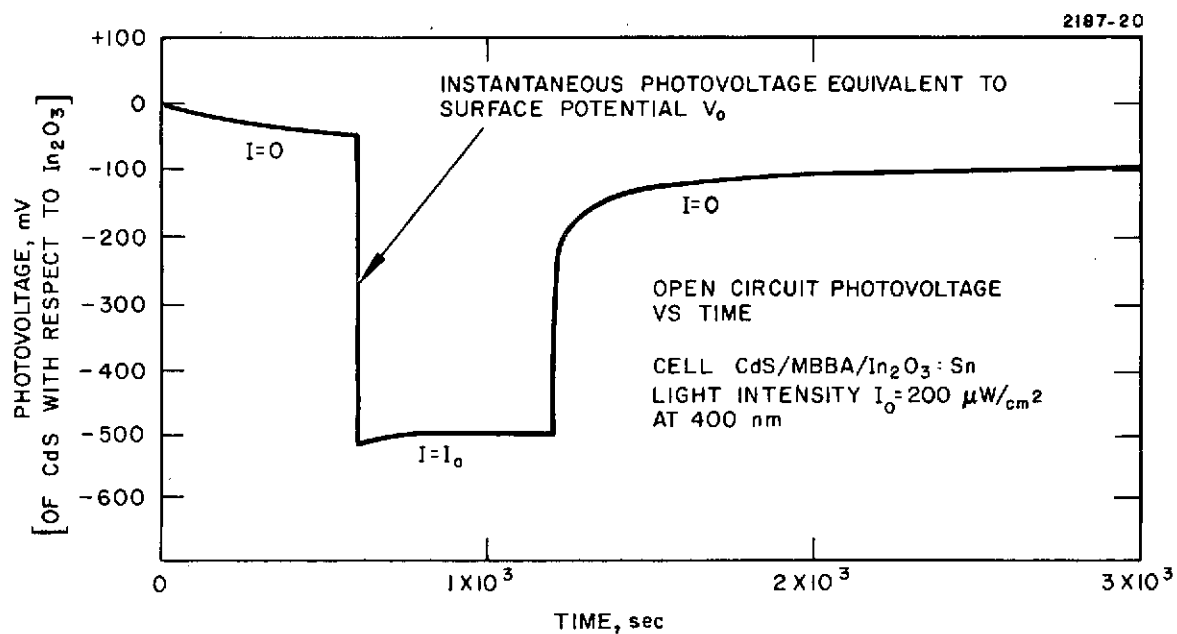$$\text{Quantum Efficiency} = \frac{\Delta I}{\Delta Q} = \frac{7.5 \times 10^{11}}{9.7 \times 10^{11}} = 0.77$$

2187-20
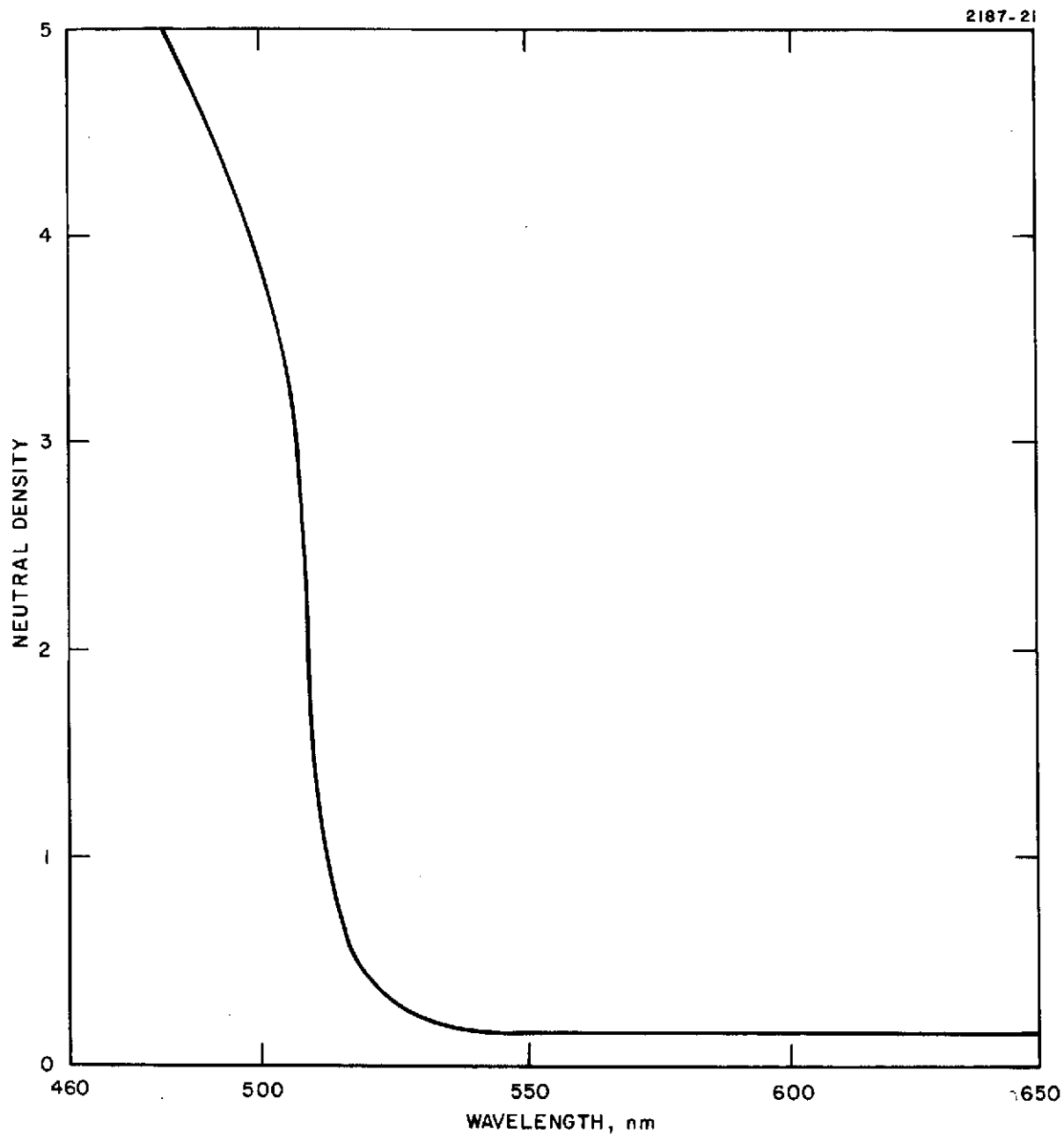
Fig. 31. Open Circuit Photo Voltage Versus Time.

Fig. 32. Optical Absorption of CdS Film on In_2O_3:Sn.
Thickness = 3 μm.

Allowing for measurement error and reflection losses, this number can be seen as approaching the value of unity, predicted by the model.

The loss in quantum efficiency from illumination through the back electrode of the photoconductor can be attributed to several effects. One is the lower mobility of the holes in CdS as compared to electrons. This becomes a limiting factor, because in the case of back illumination the hole must transit the entire film thickness to reach the liquid crystal interface. This effect can be significant as is emphasized by the fact that in CdS the ratio of electron-to-hole mobilities is on the order of 10^2. Another factor is surface electron-hole recombination at the In_2O_3:Sn-CdS interface. Due to reduced field strength in this region, much higher recombination through surface states can be expected than at the liquid crystal interface. Thus a model of the CLV has been established and confirmed in many respects. While this model gives direction for optimizing performance, more knowledge is necessary of the details of deep levels near the back contact which cause the observed residual red sensitivity, and also of the properties of surface states and structure at the liquid crystal interface which effect the important charge transfer mechanisms and control the liquid crystal alignment.

3.   Cell Optimization Considerations

Initial cell performance was limited by flaws and defects in the substrates and CdS films which require the deposition of thick layers. The early films on Corning tinoxide required a thin pre-layer of 500 Å ZnS on the substrate to provide renucleation sites for the adjacent CdS film. And further, to avoid shorting flaws which exhibited high liquid crystal scattering at low applied voltages, films of thicknesses up to 12 μ were used. These thick films effectively limited sensitivity by providing a long transit length for the photoexcited electrons which were generated close to the interface. Thus the most important approach to improved cell performance was to improve film quality in order to

reduce film thickness. This was also the prime factor in cell uniformity. Further improvement could be obtained, in terms of the model, by reducing donor impurities in the films thereby to improve the carrier mobilities and extend the depletion region. Another step is to optimize the post deposition thermal processing in H_2S to provide high film resistivities, and in particular to provide low excess surface cadmium concentration.

These considerations were implemented in the following manner. The film quality was improved, as was discussed in the film uniformity section by the use of a baffled evaporation source which eliminated CdS particle spitting and also by the use of improved cleaning and handling techniques. In addition, the electronic grade CdS powder previously used as deposition material was replaced by ultrahigh purity CdS crystal chips.[*] This material is generally state-of-the-art in purity and provides the best means of avoiding impurities in the films. Next, the post heat-treatment in H_2S was optimized with regard to temmperature and time. Excessively high temperature causes gross recrystallization (scattering in films) and interaction with the transparent conductor coating that causes film shorting. Low temperature gives a slow reaction rate which gives high nonstoichiometry for reasonable process times. The schedule reached was for 30 min processing in flowing H_2S at $475^{\circ}C$. This provided saturation for the complete conversion of the films. See Fig. 32 for sharpness of absorption edge and low residual absorption beyond the edge. The value of ND 0.14 beyond the absorption edge is primarily due to the reflection losses at the substrate interfaces. Thus with the implementation of the process changes and improvements, high quality films of thickness is small as 2-3 μ could be used for the CLV application. This, along with the improvement in liquid crystal characteristics (see liquid crystal chemistry section) lead to the improvements in sensitivity (approximately a factor of 10) realized over the course of the contract.

---

[*]Eagle Picher Co., ultra high purity grade CdS crystal chips.

There are still some problems in overall reproducibility from cell to cell. We attribute these problems primarily to the importance of the interface in the electrical behavior. Stringent controls must be exercised over the ambient and impurities the film surface sees before cell fabrication. Other problems relate to the difficulty of correlating good liquid crystal alignment with CdS film surface microstructure. However, it appears that many of these problems are solvable as more knowledge of the device is gained.

SECTION V

LIQUID CRYSTAL SCATTERING STUDY

A. INTRODUCTION AND SUMMARY

The light activated, dynamic scattering liquid crystal cell used as a coherent light valve (CLV) was found to have improved contrast ratio when a high frequency ac voltage was applied in series with the standard dc voltage that activates the cell. The effect of the ac on the light scattering properties of the light activated cell was opposite to the observed effects on the cell when not light activated and on other cells having no light activation capability. A description of the experiments that led to these conclusions and an analytical explanation of the observed effects are given in this section.

Three types of measurements were made on the cell with various dc and ac bias voltages and both with light activation and without light activation. These included: (1) scattered light intensity as a function of angle, (2) transmitted light intensity as a function of dc voltage, and (3) microscopic observations of domain structures in the cell. The scattered and transmitted light data show that the superimposed ac field reduces scattering when the cell is not light activated and increases scattering when the cell is light activated. Both of these effects serve to enhance the contrast ratio of the device. The visual data show four separately identifiable regimes of liquid crystal domains. The dc voltage thresholds of these regimes are increased by the addition of ac fields.

B. EXPERIMENTAL SETUP

The liquid crystal cell is of a photoconducting design as described above. It consists of an ester base liquid crystal with nematic range of 15 to 52°C and a cadmium sulfide photoconducting layer sandwiched between glass plates overcoated with transparent

In_2O_3 electrodes. The liquid crystal layer was 6 μm thick and no attempt was made to align the liquid crystal. The cell was biased with dc voltages from 0 to 40 V applied in series with ac voltages from 0 to 40 V rms at 10 kHz; positive dc was applied to the electrode on the CdS side of the sandwich. The ac impedance of the cadmium sulfide photoconductor was considerably lower than the ac impedance of the liquid crystal. Thus, the cell could not be light activated with only the ac field applied.

The apparatus employed for the scattering measurements is shown in Fig. 33. A Spectra Physics Model 123 HeNe laser beam, which is linearly polarized, was projected through the liquid crystal onto a silicon photo diode detector. A 50 $\mu W/cm^2$ light source with center frequency at 5100 Å and bandwidth of 300 Å was used to light-activate the cell. The detector output was amplified with a five-decade logarithmic amplifier and recorded on an x-y plotter as a function of the scattering angle or dc bias voltage.

The spectral response of the cadmium sulfide-liquid crystal sandwich was approximately uniform at wavelengths of 5000 Å or less (See Fig. 29, above). Above 5000 Å, the photo response fell rapidly and was down by a factor of about 170 at the laser light wavelength of 6328 Å. The 5100 Å activating light described above completely turned on the cell, whereas the laser light only slightly activated the cell. Thus, the laser served as a light source for monitoring the scattering without activating the cell.

When the apparatus was first assembled, it was found that some of the green activating light was scattered into the detector. This light was reduced to a level that gave no output on the logarithmic amplifier. The light level was reduced by placing the red filter shown in Fig. 33 between the cell and the detector.

The rotating arm of the setup (see Fig. 33) that holds the lens, red filter, analyzer, and detector is attached to a turntable (like those used on a machine shop mill) that is positioned under the cell. The turntable's crank was removed and a Bodine type NSH 12R speed reducing motor was connected directly to the shaft that rotates the
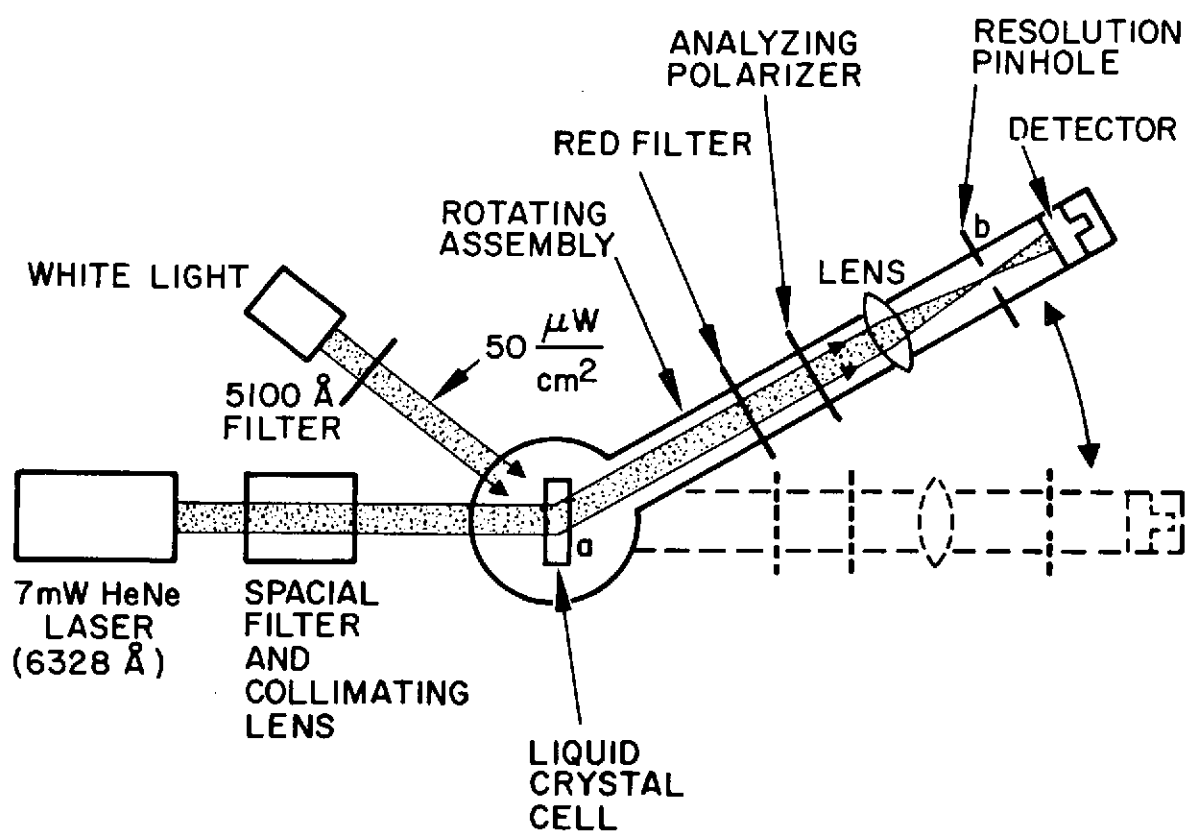
ANALYZING
POLARIZER

RESOLUTION
PINHOLE

RED FILTER

DETECTOR

ROTATING
ASSEMBLY

LENS

WHITE LIGHT

$50 \dfrac{\mu W}{cm^2}$

b

5100 Å
FILTER

7mW HeNe
LASER
(6328 Å)

SPACIAL
FILTER
AND
COLLIMATING
LENS

a

LIQUID
CRYSTAL
CELL

Fig. 33. Apparatus for Measuring Scattering Properties
of Liquid Crystal Materials.

table. At full speed, the motor drives the table about $0.5^{\circ}/sec$. A variable speed controller is employed with the motor. High speed was used except when sweeping through the angles about 0°. In this range a slow speed is used to allow time for the plotter to trace the 0° scattered light peak more precisely. A gear is mounted on the motor shaft and is connected by a belt to a gear on a 10 turn pot. This pot is biased and provides a voltage proportional to scattering angle, which we use to drive the x coordinate of the plotter.

The resolution of the optical system is varied by changing the size of the pinhole (Fig. 33(b) in front of the detector. The maximum spatial frequency l passed by a pinhole of radius R placed at the focal point of a lens with focal length f given by $l \cong R/\lambda f$ for the relatively small spatial frequencies of interest here. (The resolution of the system and its relationship to this formula are discussed in detail at the beginning of V-D.) We used four pinholes corresponding to 2.9, 10, 20, and 30 cycles/mm resolution at the surface of the cell (a in Fig. 34). An analyzing polarizer was inserted between the liquid crystal and the detector and oriented parallel or perpendicular to the polarization of the laser light for polarized scattering measurements.

We now turn to a detailed description of the performance (Fig. 34) and operation of the detector and logarithmic amplifier. The circuit employed (Fig. 35) is quite simple; it consists of a Philbrick logarithmic amplifier module, No. 4350, connected to a United Detector Technology PIN 5 detector. (Note that the case of the detector is connected to the logarithmic amplifier input and the signal lead of the detector is grounded. If a Philbrick No. 4351 module had been used, this crossed connection would be eliminated.) No preamplifier is needed between the detector and logarithmic amplifier if the detector is biased around 22-1/2 V: The specifications of these two components are well-matched. In fact, the log amplifier saturates (the output goes to -2 to 13 V) at currents about one order of magnitude lower than that put out by the detector when uniformly illuminated by light that just begins to burn the surface of the detector.
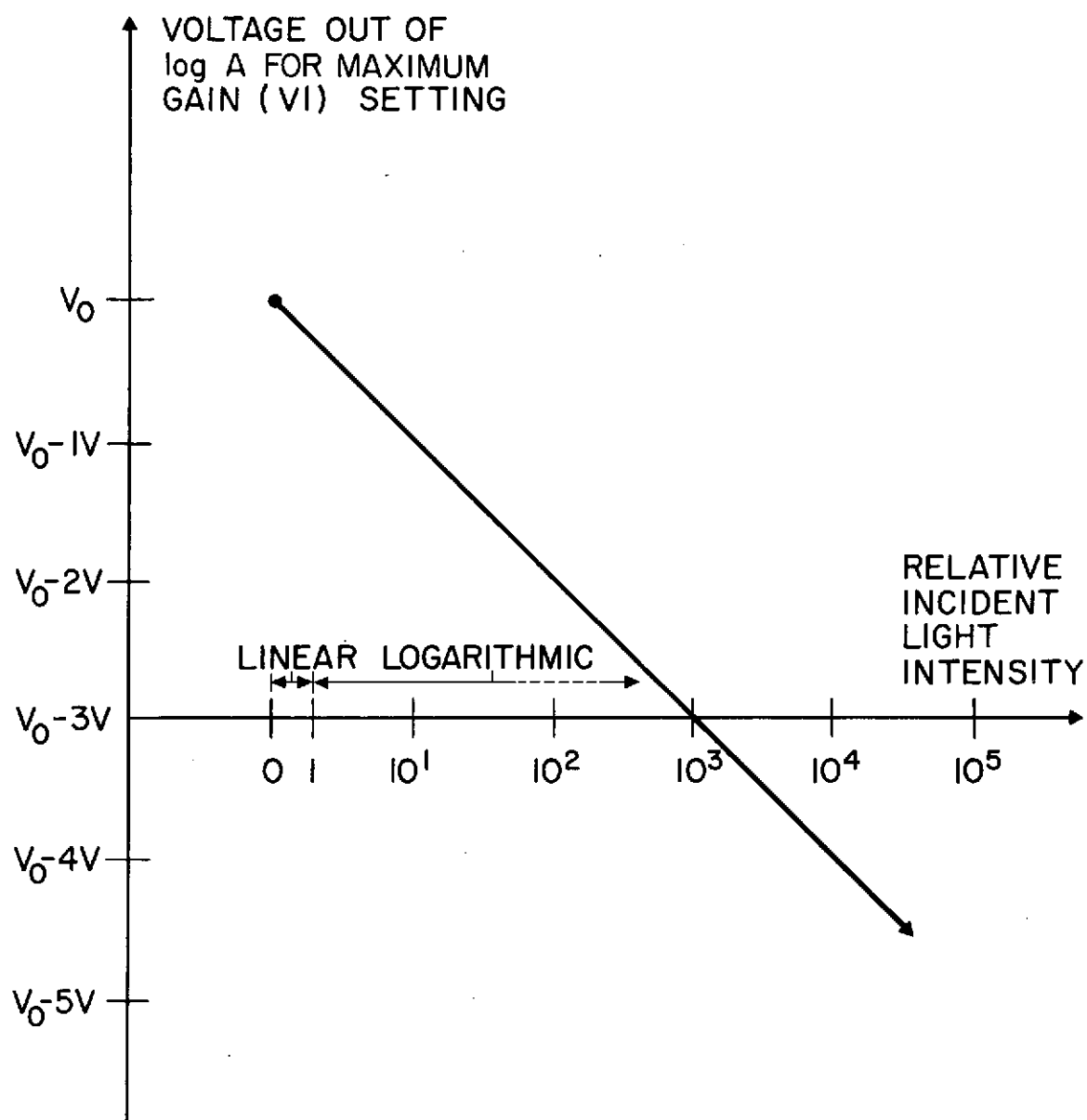
Fig. 34. Description of Performance and Operation of Detector and Logarithmic Amplifier.
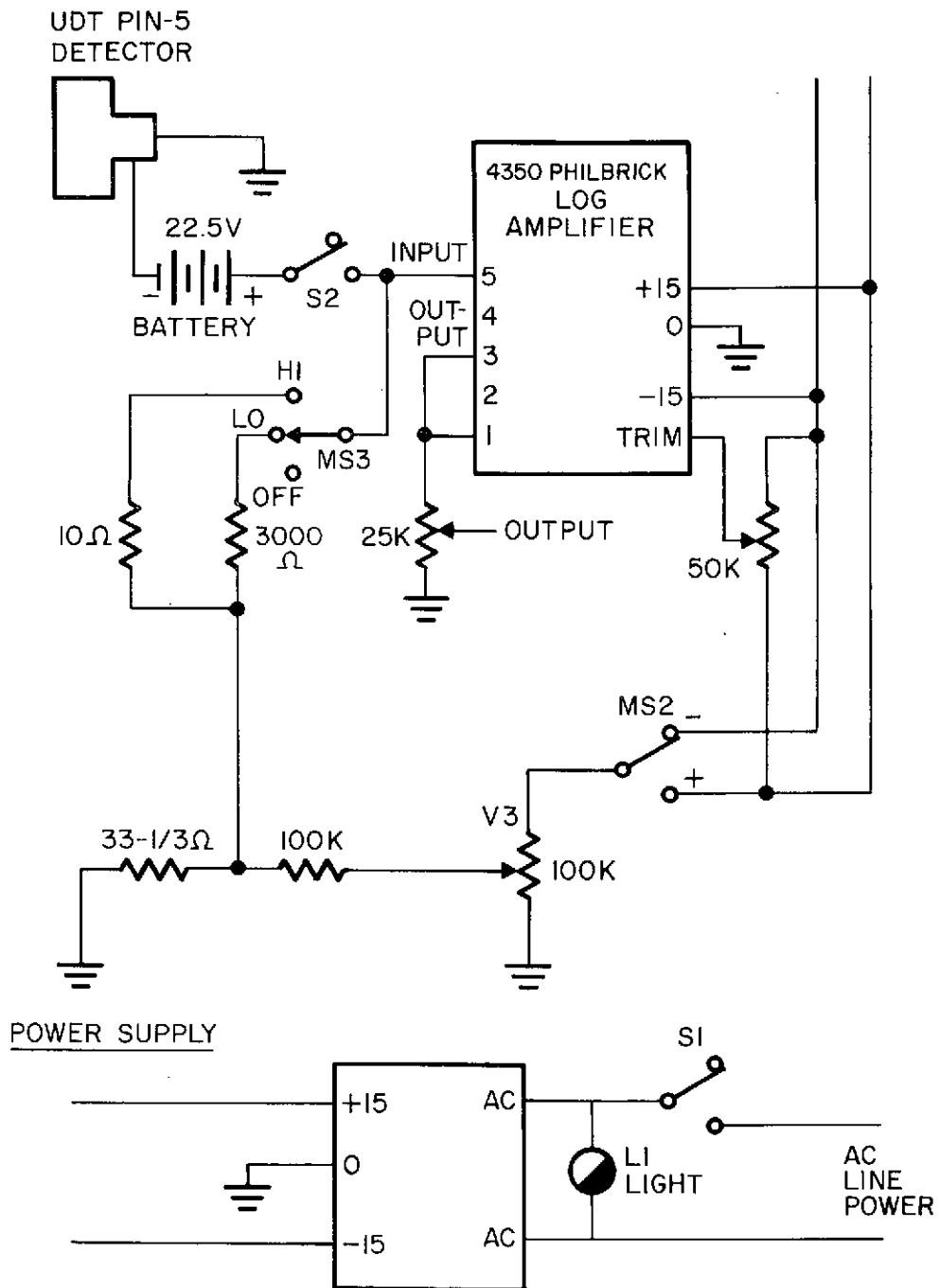
DETECTOR/LOG AMPLIFIER

UDT PIN-5
DETECTOR

4350 PHILBRICK
LOG
AMPLIFIER

22.5V

INPUT

OUT-
PUT

S2

BATTERY

+15

O

−15

TRIM

HI

LO

MS3

OFF

10 Ω

3000 Ω

25K

OUTPUT

50K

MS2

+

33-1/3Ω

100K

V3

100K

POWER SUPPLY

+15

O

−15

AC

AC

SI

L1
LIGHT

AC
LINE
POWER

Fig. 35.   Detector and Amplifier Circuit Design.

To eliminate noise, the detector was mounted inside the amplifier chassis, close to the logarithmic amplifier module. The chassis is mounted on the end of the rotating arm. The surface of the detector has an approximate area of 1 cm^2 and is placed 6.5 cm inside the chassis from a hole in the side of the chassis from a hole in the side of the chassis. The geometry of the scattering apparatus is such that the light scattered from the cell is focused onto a pinhole (discussed above) mounted over the hole in the side of the chassis, so that it struck the detector after re-expanding to a beam approximately 8 mm in diameter.

The detector puts out a dark current I plus a current proportional to light intensity. A variable current source is built into the chassis to subtract out the dark current from the total detector current before the signal enters the logarithmic amplifier. The detector/logarithmic amplifier combination performs very well, providing as much as 5 decades of range. But at low input light levels there is a problem of output voltage drift, probably caused by changes in component resistances and detector dark current with temperature. The closer the subtracted current is to the detector's dark current, the better the small signal response the detector/amplifier provides (the greater V_o in Fig. 34), but the greater is the sensitivity of the output voltage to drift in I_o for small inputs or in the subtracting current source. Using the labels in Fig. 35, optimum performance was obtained when MS2 was set on "−", MS3 on LOW, and V3 was set at 30 to 50 K. Turning up V3 caused the logarithmic amplifier to saturate (output to go positive to +2 to +4 V). V3 has to be turned down 2 to 5 K to remove the saturation. It should be turned up close to this saturation for high small-signal sensitivity. After warmup, it was found that the drift can be compensated by turning up V3 now and then, so that a constant voltage (V_o in Fig. 34) corresponding to zero input light is maintained.

C.   SCATTERING DATA

To understand the performance of a liquid crystal light valve, the scattering from the cell when illuminated with a collimated beam and biased with a range of dc and ac voltages was examined. Plots of the logarithm of the relative scattered light intensity as a function of angle were recorded for all combinations of the following: (1) light activation off and on, (2) analyzing polarizer absent and analyzing polarizer oriented parallel and perpendicular to the polarization of the incident laser light, (3) 0, 10, 20, and 30 V dc bias, (4) 0 and 40 V rms at V 10 kHz ac bias. The scattering was measured with a pinhole of the sharpest angular resolution pinhole (one corresponding to 2.9 cycle/mm band pass). These 48 curves are presented in the twelve figures in Appendix A. In this section we discuss an expanded version of four of the curves (Figs. 36(a) and (b)) to illustrate the general effect of ac voltage on scattering, and to identify several peculiar features of these plots.

The data shows clearly that ac voltage decreases scattering in a nonlight activated cell (see Fig. 36(a)) and increases scattering in a light activated cell (see Fig. 36(b)). Both effects serve to enhance the contrast of the cell. In effect the ac voltage sharpens the threshold curve of the liquid crystal.

Cells containing the same liquid crystal and no CdS layer have been examined to study the effects of ac. They show the known effect, observable in MBBA and other liquid crystals, that high frequency ac reduces the scattering as if it were decreasing the dc voltage that is applied to the cell. We found that for ac voltages up to 60 rms V at 10 kHz, the cell would not scatter appreciably until the dc voltage became somewhat larger than the rms ac voltage. A simple theoretical explanation can be given. When (and only when) the rms ac voltage exceeds the dc voltage, the instantaneous voltage across the cell goes both positive and negative. At sufficiently high frequency, this oscillating field shakes up the ions in the liquid crystal sufficiently to break up scattering domains, thereby inhibiting the scattering effect.
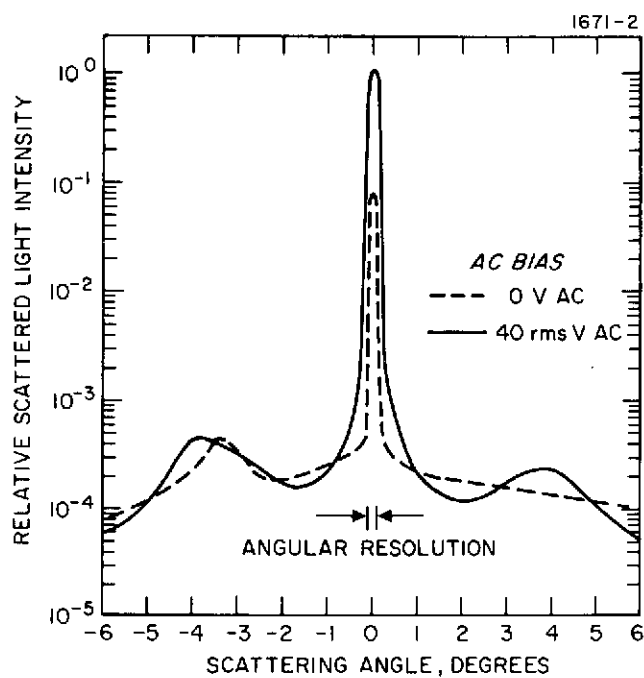
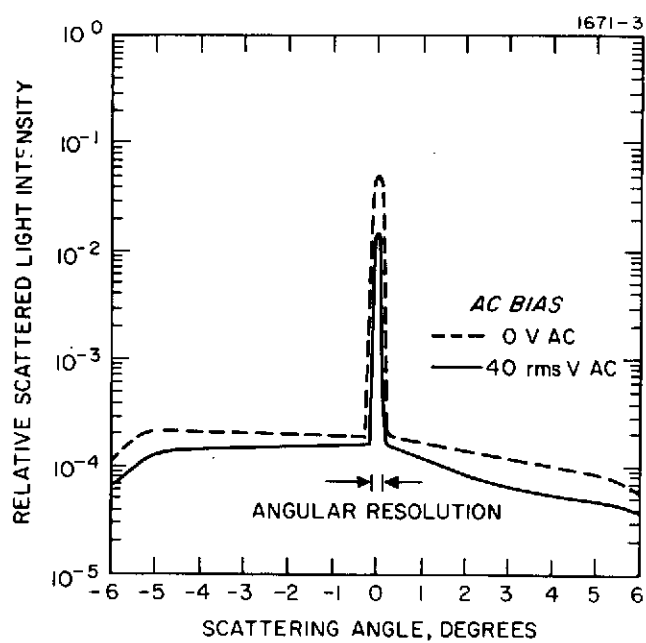(a) Unilluminated

(b) Illuminated

Fig. 36. Scattering Diagrams for Photoactivated Liquid Crystal Light Valve.

93

There are two layers in a light activated cell that share the dc voltage across the cell — the CdS layer and the liquid crystal film. When the cell is not light activated, most of the dc voltage drop falls across the CdS. Due to its capacitance CdS even in the dark, has low high-frequency ac impedance relative to the liquid crystal, so the liquid crystal sees the full ac with a small portion of the dc component added as bias. According to the model discussed in the paragraph above, we would expect the ac to suppress the small amount of scattering produced by the relatively small dc voltage drop across the liquid crystal; and indeed, this is observed. In contrast, when the cell is light activated, most of the dc voltage drop is across the liquid crystal. For low dc voltages, we again expect the ac voltage to suppress scattering according to the argument just presented. This can be readily observed if one examines the forward scattering peaks at 0°, in the curves shown in Appendix A. These forward scattering peaks have heights equal to the difference between the total incident light minus the light scattered outside of the angular passband of the optical system at 0°.

At 0, 10, and 20 V dc, the superimposed ac voltage increases the height of the forward scattering peaks, thereby indicating that scattering has been reduced. For dc voltages roughly equal to the rms ac voltage, the dc plus ac voltage across the cell almost always has one polarity. On the cell without CdS, no suppression of scattering by the superimposed ac voltage was observed (as discussed above). The data in Appendix A and Fig. 36 show that under this condition the ac voltage decreases the height of the forward scattering peaks, thereby indicating that scattering has been enhanced. This enhancement is never observed in the absence of the CdS layer. It is caused by an electrochemical interaction between the CdS and liquid crystal layers (See Section IV).

The scattering curves show side peaks (see, for instance, Fig 36(a) that look like the first side lobes of a diffraction pattern.

Assuming the domains in liquid crystal causing these secondary maxima, we can use the scattering data to calculate the size of the scattering domains. For diffraction around small domains having a linear dimension D, we find that two rays from opposite edges of a domain constructively interfer when

$$D \sin \theta = n\lambda.$$

In our case, θ is small, $n = 1$, and $\lambda = 0.63$ μm. We obtain

$$D \text{ (in } \mu) = 36/\theta \text{ (in degrees)}.$$

The graphs in Appendix A give scattering angles for the lobes. We list the data and corresponding computed linear dimensions of the scattering domains in Table IV. Domains of roughly these sizes are actually observed in the cell. We discuss them further in V-E which is concerned with microscopic observation of the cell; but before we leave this topic, we have another comment to make regarding the size of the domains. A likely candidate mechanism for these effects is Williams domains. The visual appearance of Williams domain bears this out. The observed width for Williams domains reported in the literature[18] is slightly less than the thickness of the liquid crystal layer in the cell in which they appear. In our case that would be approximately 5 μm. This number is considerably smaller than the lengths D that we calculate (Table IV) and the thickness of the domains that we observe. Perhaps, here again, we are witnessing anomolous effects associated with the CdS liquid crystal interaction.

We wish to comment on two other features that we observed in these graphs: (1) Side lobes are observed even when the cell is not light activated (Fig. 36(a)). We attribute this to the slight light activation caused by the laser light used to monitor the scattering. (2) A number of the curves show considerable asymmetry. This appears to be due to alignment asymmetry because when we turned the cell around, the asymmetry reversed. We examined the cell between

TABLE IV

Domain Sizes Observed in The Cell in Various States of Activation

DC Bias, Volts	10 kHz ac Bias, rms Volts	Light Activation	Angle to Sidelobes, Degrees	Length Calculated From Side Lobe Angle: D = 36/θ, Microns	Regime (See Section E, Table III)	Observed Domain Size From Visual Data (Section E), Microns
0	0	No	——	——	1	——
10			1.8	20	2	15-30
20			3.1	11.6	4	10
30			3.1	11.6	4	10
0	40	No	——	——	1	——
10			——	——	2	15-30
20			——	——	2	15-30
30			3.6	10	2 or 4	15-30
0	0	Yes	——	——	1	——
10			2.5	14.4	4	10
20			3.8	9.5	4	10
30			4.2	8.6	4	10
0	40	Yes	——	——	1	——
10			1	36	2	15-30
20			4	9	4	10
30			4.5	8	4	10

T956

cross polarizers and found it to be aligned primarily with the director nearly perpendicular to the electrodes. If the director were to be rotated slightly away from perpendicular in a horizontal plane with preference either to the right or left, the observed asymmetry would be produced. Since we observed such rotation in the alignment of the cell, we attribute the observed asymmetry to this cause.

D.   CONTRAST RATIO DATA

1.   Liquid Crystal Effects on Resolution and Contrast Ratio

The light-activated liquid crystal light valve was used in the following experimental arrangement: The apparatus was set up as shown in Fig. 33. A transparency of a resolution chart, for example was put in the beam of the non-coherent activating light and a lens was used to focus the image from the slide onto the light valve. Only the illuminated parts of the light valve scatter the read-out laser light. This scattered light, that has passed through the liquid crystal, can be blocked by a lens and aperture and only unscattered light can be directed to the screen to give an image of the transparency.

The projected image can be characterized by resolution and contrast ratio (ratio between light intensity of dark and light sections of the image). A tradeoff exists between these two variables due to the liquid crystal properties. Activating light intensity and dc and ac bias all affect the actual resolution and contrast ratios observed.

2.   Optical System Effects on Resolution and Contrast Ratio

Assume that the light valve has ideal resolution, and consider the effects on resolution associated with the choice of optical system. We now may restrict the resolution of the optical system to any value that we choose less than the maximum possible value. A high-resolution optical system gathers light over a large angular bandpass

about the forward direction, whereas a low-resolution system gathers light over a small bandpass. Here again, we find there is a tradeoff between resolution and contrast ratio. In this case the resolution variation is due to the varying angular passband of the optical system. The contrast ratio varies inversely to the size of the angular passband of the system. Hence, the higher the resolution, the lower the contrast.

Let us now calculate the resolution of our optical system in terms of the size of the blocking aperture (as mentioned in Section II). Assume the cell modulates the incident laser read-out light with a sine wave of transmittance variation. A perpendicularly incident plane wave of light incident on the cell (a in Fig. 33) produces three plane waves that leave the cell at angles $0°$ and $\pm\,\theta$. Where θ is determined by the spatial frequency of the plane wave, let the amplitude of the incident plane wave be A, and the amplitude of the three scattered plane waves be A'. Then

$$A = e^{2\pi i x/\lambda}$$

$$A' = (A\sin(2\pi y\ell) + B)\,e^{2\pi i x/\lambda}$$

$$= \frac{A}{2i}\,(e^{2\pi(x/\lambda + y\ell)} - e^{2\pi i(x/\lambda - y\ell)}) + B e^{2\pi i x/\lambda}$$

where λ is the wavelength of the light and ℓ is the spatial frequency of the sine wave on the cell's surface.

$$\lambda\ell = \tan\theta \cong \theta$$

(for small angles i.e., large spatial wavelengths). Thus, an optical system with angular passband θ can resolve down to spatial frequency $\ell = \theta/\lambda$. Let these three beams be focused by a lens of focal length f on a plane (b in Fig. 33). Three image points result; one on the axis of the optical system and two others at $y' = \pm\,d/2$ where

$$f\theta = \frac{d}{2}$$

or

$$d = 2f\theta = 2\lambda \ell f.$$

In the case of our experiment,

$$f = 94 \text{ mm},$$

$$\lambda = 6.328 \times 10^{-4} \text{mm},$$

so that

$$d(\text{in mm}) = 0.119 \times \ell \text{ (cycles/mm)}.$$

This gives the pinhole sizes that correspond to the resolutions listed in paragraph 2, above: 0.34 mm (0.0135 in.) for 2.9 cycles/mm, 1.19 mm (0.0469 in.) for 10 cycles/mm, 2.38 mm (0.0938 in.) for 20 cycles/mm, and 3.57 mm (0.1407 in.) for 30 cycles/mm.

The scattering data were taken with the 0.34 mm pinhole, which corresponds to an angular passband of $\theta = d/2f \cong 0.1^{\circ}$. (This finite passband causes the observed finite widths of the forward scattering peaks shown in Fig. 36 and in the Appendix A figures.) To obtain the data for the larger angular passbands (higher resolutions) we used the larger pinholes.

A more detailed definition of the contrast ratio is the following. The contrast ratio of a light activated cell (light valve) at given dc and ac driving voltages is the ratio of the light intensity forward scattered within the angular passband of the pinhole by the non-light-activated cell to the intensity forward scattered within the same angular passband by the light-activated cell. We obtained contrast ratios by making the two measurements identified in this definition and dividing the intensities so obtained.

3.   Data and Analysis

The logarithm of intensity of laser forward scattered by the cell was measured and recorded as a function of applied dc voltage for all combinations of the following: (1) the angular passbands corresponding to the four pinholes listed above, (2) the presence or absence of light activation, (3) analyzing polarizer absent or analyzing polarizer present and oriented parallel or perpendicular to the incident laser light's polarization, and (4) 0 or 40 V rms, 10 kHz ac voltage. These combinations result in 48 curves which are given in the twelve figures collected in Appendix B. The ratio of the heights of these curves at a given dc voltage give the associated contrast ratios. Table V gives the contrast ratios obtained from these data at 30, 36.5, and 40 V dc. We first discuss the effects of polarization and ac on contrast ratio, and then return to the question of resolution.

Generally, the best contrast ratios are obtained at 36.5 V dc with parallel analyzing polarizer. We would expect, theoretically, that the best contrast ratio would be obtained with a parallel analyzer because when the cell is activated the incident light is multiply scattered and is thereby depolarized. A parallel analyzer further reduces the intensity of light that has passed through scattering sections of the cell without reducing the intensity from nonscattering sections of the cell.

The effect of the ac field on the contrast ratio is evident from the data. It improves the contrast ratio for dc voltages above 27 V dc sometimes enormously, as in the case of 36.5 V dc, parallel polarizers, at 2.9 cycles/mm resolution. It improves contrast ratio by decreasing forward scattering in the light-activated cell and increasing forward scattering in the non-light-activated cell. In the set-up described at the beginning of this section, the quality of the projected image is not really improved when the ac is turned on. Fig. 37 displays two photographs that show this improvement.

Now examine the effect of varying the resolution of the optical system. From Table V, we see the tradeoff discussed above, viz.,

100

TABLE V

Summary of Contrast Ratios Computed From Measurements
of Forward Scattered Light Intensity Versus dc Bias Voltage

Resolution (cycles/mm)	Analyzer Polarization	Contrast Ratio					
		30 Vdc		36.5 Vdc		40 Vdc	
		0	40	0	40	0	40 rms V 10 kHz ac
2.9	Parallel	1.3	22	0.7	100	0.7	24
10		0.9	28	1.0	60	0.9	31
20		1.2	29	0.8	30	0.8	10
30		1.2	21	0.9	15	0.8	7
2.9	Perpendicular	2.5	13	3.0	7	3.0	5
10		2.4	20	2.6	8	2.5	6
20		2.3	15	2.5	7	2.5	4.8
30		2.3	2.2	2.1	2.1	2.1	2.1
2.9	No Analyzer	1.5	25	1.0	14	1.0	6
10		1.8	24	1.1	22	1.0	12
20		1.8	19	1.2	16	1.1	10
30		1.9	18	1.2	16	1.2	8

T890
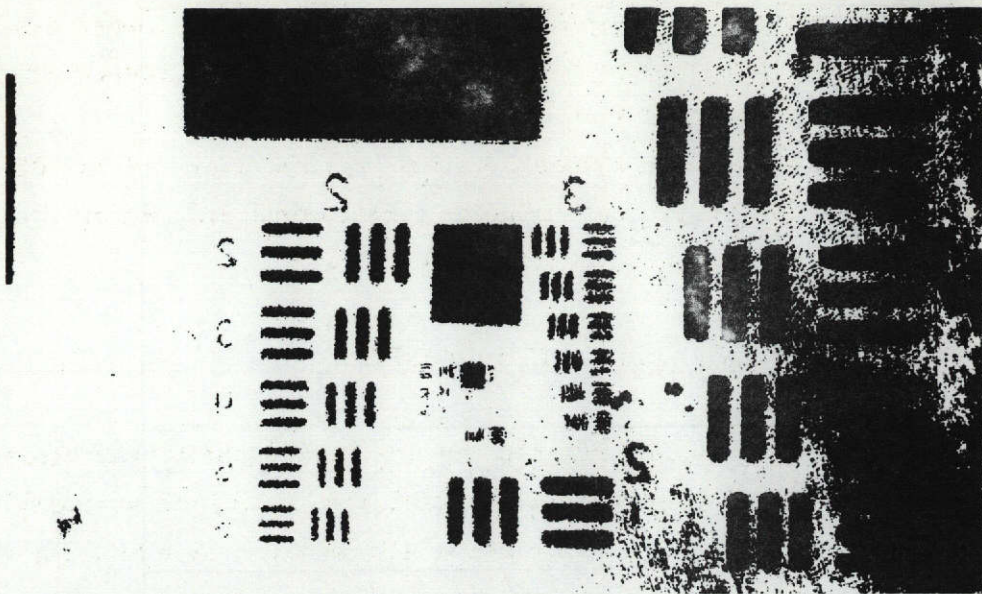
40 V rms 10 kHz AC
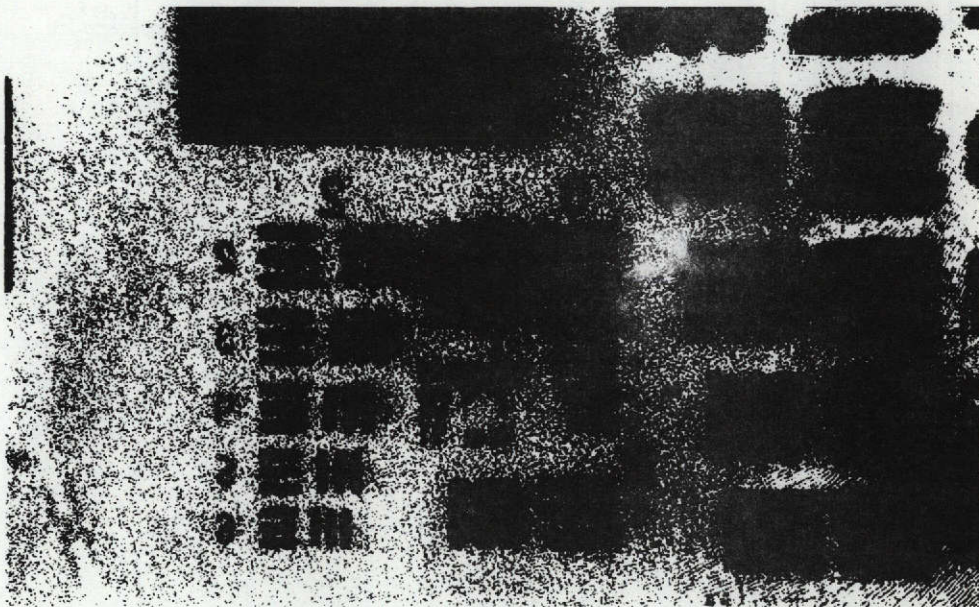
NO AC

Fig. 37. Projected Images From Light-Activated
Cell at 30 Vdc.

generally more contrast corresponds to less resolution. There are some exceptions, and there are a number of cases where the contrast ratio remains fairly constant despite changing resolutions.

The range of contrast ratios obtained varies from 1:1 to 100:1. Clearly detailed data of this sort is necessary to optimize an optical system for use with the liquid crystal light valve.

E.   VISUAL OBSERVATIONS ON THE CELL

In an effort to gain insight into the scattering characteristics of the CdS liquid crystal light valve, the cell was examined visually. It was placed between crossed polarizers, illuminated by white light intensities below and above the threshold for light activation, and observed in a microscope at 100 x magnification. Four major regimes of domain structure in the liquid crystal were observed as the dc voltage increased from 0 to 40 V. The addition of the ac field in series with the dc neither introduced nor eliminated any of these major regimes; it simply caused an increase in the dc threshold voltages at which each regime appeared.

The regimes in order of increasing threshold voltage are: (1) relatively uniform structure (the Frederick z transition[19] was observed within this voltage range), (2) Williams domains,[20] observed to be 15 to 30 μm wide in our cell, (3) breakup of Williams domains into small circular spots about 10 μm in diameter (the spots are spatially stable and are more numerous at high light-activation levels), and (4) jumbled and rapidly moving domain patterns. The turbulence characteristics of dynamic scattering. Scattering begins to be noticeable at voltages for which the cell is in regime (3) and is strongest in regime (4).

Table VI gives the dc threshold voltages at which these regimes appear. Figure 38 shows photographs of the cell in each of these regimes.

TABLE VI

DC Threshold Voltages for the Visually Observed Regimes in the Light Activated Liquid Crystal Cell

AC Bias, rms Volts	Light Activation	Regime Number	DC Threshold, Volts
0	No	1 2 4	0 7-8 11-13
40	No	1 2 4	0 8-10 28-40
0	Yes	1 2 3 4	0 3 7 8-9
40	Yes	1 2 3 4	0 5 15 16-17

T957

1671-11
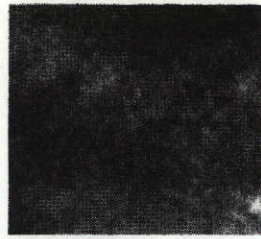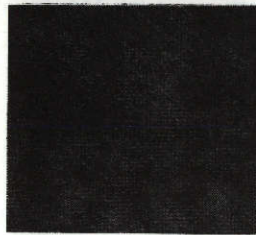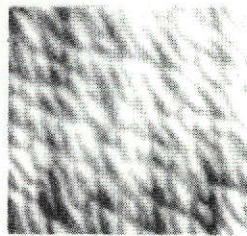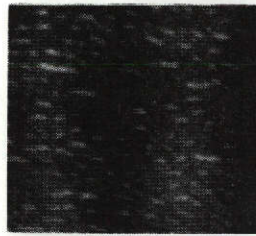
REGIME 1

REGIME 2

REGIME 3
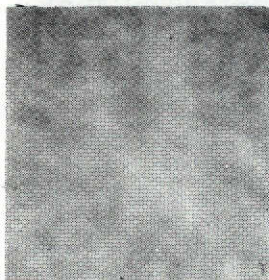
REGIME 4

Fig. 38. Direct Current Threshold Voltages.

When the observed sizes of the domains and the thresholds for their appearance are compared with the linear dimensions calculated from the side lobes measured from the scattering curves, we obtain consistent agreement (see the last two columns of Table IV). We appear to be seeing domains that are larger, given the liquid crystal's thickness, than those reported elsewhere. More elaborate correlation data between visually observed domain sizes and angular positions of scattering lobes on the scattering data could not be obtained, unfortunately, because of deterioration of the cell at the end of the experiment.

F.   THEORETICAL DISCUSSION OF THE IMPROVEMENT OF CONTRACT BY SUPERIMPOSING ON THE DC VOLTAGE HIGH FREQUENCY AC VOLTAGE

A simple equivalent circuit for the dc light valve is shown in Fig. 39. The diode represents the junction effect between the CdS layer and the liquid crystal (LC); the resistor R_D is the leakage resistance of the junction, and the R_L is the resistance of the LC. The effect of applying light to the cell is to decrease the value of R_D. Such an equivalent circuit can be drawn for each resolution element of the cell. Let us concern ourselves with two such elements, one unilluminated, and therefore having high leakage resistance R_D, and the other illuminated and thus having lower leakage resistance, let's say γ_D. In the case where only a dc voltage is applied to the cell, the first element will yield a current equal to

$$I_{1\,av} = \frac{V}{R_D + R_L} \quad .$$

The second element yields a current equal to

$$I_{2\,av} = \frac{V}{\gamma_D + R_L}$$

106
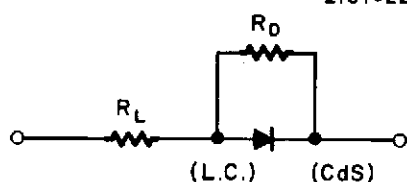
Fig. 39.
Dc Light Valve Equivalent
Circuit.

Assume for simplicity that the scattering is proportional to the current, then the contrast ratio will be[*]

$$C_{dc} = \frac{I_{2\ av}}{I_{1\ av}} = \frac{R_D + R_L}{\gamma_D + R_L}$$

Now let us see what happens when we superimpose an ac voltage on the dc. In this case, the voltage across the cell as a function of time is as shown in Fig. 40.
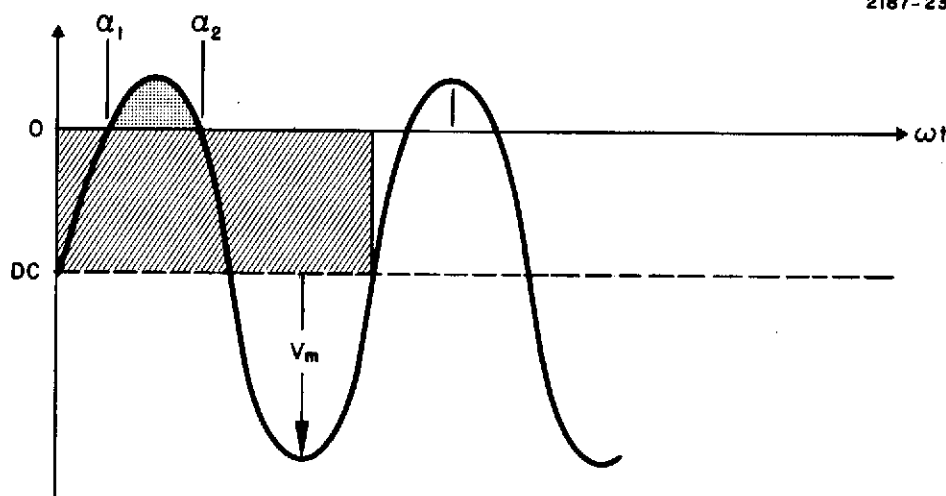

Fig. 40. Voltage Across Cell as a Function of
Time.

Assuming that the high frequency voltage alone does not cause the LC to scatter, we can calculate the new average currents in both elements. In the unilluminated element, the average current will be

---

[*]This assumption does not alter the logic of the argument. It merely simplifies the calculation.

$$I'_{1\,av} = \frac{1}{2\pi(R_L + R_D)} \int_0^{\alpha_1} (V_m \sin \omega t - V)\, d(\omega t)$$

$$+ \frac{1}{2\pi R_L} \int_{\alpha_1}^{\alpha_2} (V_m \sin \omega t - V)\, d(\omega t)$$

$$+ \frac{1}{2\pi(R_D + R_L)} \int_{\alpha_a}^{2\pi} (V_m \sin \omega t - V)\, d(\omega t)$$

or

$$I'_{1\,av} = \frac{1}{2\pi(R_L + R_D)} \int_0^{2\pi} (V_m \sin \omega t - V)\, d(\omega t) -$$

$$- \frac{1}{2\pi(R_L + R_D)} \int_{\alpha_1}^{\alpha_2} (V_m \sin \omega t - V)\, d(\omega t)$$

$$+ \frac{1}{2\pi R_L} \int_{\alpha_1}^{\alpha_2} (V_m \sin \omega t - V)\, d\omega t$$

Calculating the first integral and summing the second and third, we obtain

$$I'_{1\,av} = -\frac{V}{R_L + R_D} + \left(\frac{1}{R_L} - \frac{1}{R_L + R_D} \right) \frac{1}{2\pi} \int_{\alpha_1}^{\alpha_2} (V_m \sin \omega t - V)\, d(\omega t)$$

Defining

$$\frac{1}{2\pi V} \int_{\alpha_1}^{\alpha_2} (V_m \sin \omega t - V)\, d(\omega t) \equiv I,$$

we can write

$$I'_1 \text{ av} = V\left(-\frac{1}{R_L + R_D} + \frac{R_D}{R_L(R_L + R_D)}I\right)$$

"I" has a simple physical interpretation; it is the ratio of the average forward voltage (the black area in Fig. 40) to the average voltage (the dashed area in Fig. 40) applied to the cell.

In the same fashion, for the illuminated element we have

$$I'_2 \text{ av} = V\left(-\frac{1}{R_L + \gamma_D} + \frac{\gamma_D}{R_L(R_L + \gamma_D)}I\right)$$

and the contrast ratio under the previous assumption is

$$C_{ac} = \frac{I'_2 \text{ av}}{I'_1 \text{ av}} = \frac{\dfrac{1}{R_L + \gamma_D} - \dfrac{\gamma_D}{R_L(R_L + \gamma_D)}I}{\dfrac{1}{R_L + R_D} - \dfrac{R_D}{R_L(R_L + R_D)}I}$$

which can be reduced to

$$C_{ac} = \frac{R_L + R_D}{R_L + \gamma_D}\;\frac{R_L - \gamma_D I}{R_L - R_D I}$$

The ratio of the contrast in the "ac + dc" to that in the "dc" close case is

$$r = \frac{C_{ac}}{C_{dc}} = \frac{R_L - \gamma_D I}{R_L - R_D I}$$

The ratio of the contrasts as function of I is drawn in Fig. 41.

In the region $0 < I < R_L/R_D$, $r > 1$, which means that the contrast is improved by superimposing ac on the dc voltage. When I is too high, the average current changes its sign and in this case there is a net forward current in the diode. The whole cell writes up and the contrast decreases.

In the case when there exists a junction between the counter-electrode and the liquid crystal, the dc equivalent circuit is described in Fig. 42. In this case, the influence of ac depends on the relative value of R_C. If it is high, the ac doesn't improve the contrast. This condition could arise (we have seen evidence for the diode between liquid crystal and transparent electrode), and therefore should be investigated more systematically.

2187-24
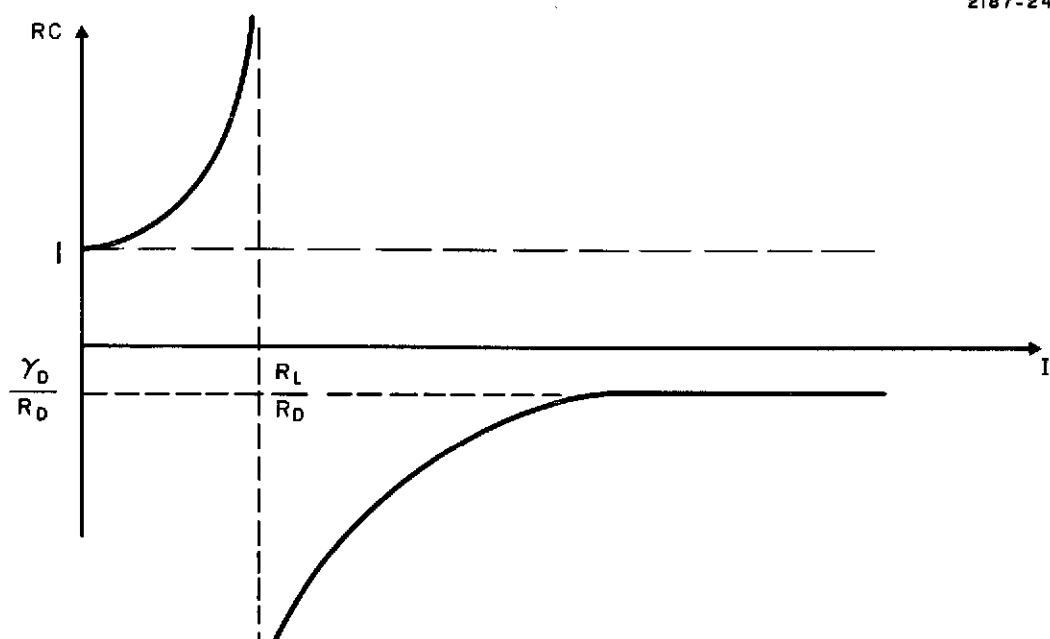
Fig. 41. Ratio of Contrasts as Function of I.

2187-25
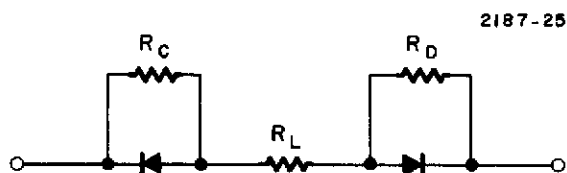
Fig. 42. DC Equivalent Circuit Where Junction Between the Counterelectrode and Liquid Crystal Exists.

110

SECTION VI

LIFETIME STUDIES

A.   INTRODUCTION

In general, the failure mechanisms that limit lifetime in liquid crystal dc devices are due to five different factors:

1.   Generation of gas bubbles within the active cell area

2.   Darkening of the cells conduction electrodes

3.   Deterioration of the liquid crystal

4.   Formation of an insulating polymer film

5.   Surface alignment changes at the electrode interface with the liquid crystal

These factors apply irrespective of the type of device that is considered. They are caused largely by electrochemical phenomena associated with the flow of current in the liquid crystal.

The rate of gas bubble generation is sensitive to the nature of the electrodes and the dopants used. For example, with MBBA between an aluminum electrode and an indium oxide electrode, we observe void formation a few minutes after a dc field is applied; whereas, replacing the aluminum with a gold opposing electrode under the same operating conditions, we find that no gas bubbles are generated after hundreds of operational hours. Using ionic dopants, a liquid crystal cell has virtually no dc lifetime, but on the other hand, if a non-ionic dopant is used the device can last hundreds of hours in the presence of a dc field. The darkening of electrodes with MBBA between transparent electrodes usually is directly correlated with the resistivity of the Nesatron electrode and with the surface defects of the electrode material. In general the deterioration of liquid crystals can be accounted for by at least four factors: first, the liquid crystal used, e.g., Schiff base versus ester;

second, the amount of charge (number of coulombs) that pass through the cell; third, the design of the cell package, e.g., sealed versus non-sealed device; fourth, the exposure to ultraviolet light which causes photochemical effects. The formation of a polymer film can be generated by both photochemical and electrochemical effects. The polymer can cause insulting effects as well as changes in the surface alignment of the liquid crystal.

All the above phenomena are also applicable to our light valves. The ordering of importance for a given device is dependent on the photoconductor, the liquid crystal, and the dopants used in that device. For example, in the case of the rate of the formation of polymer, a zinc sulfide light valve is degraded considerably faster than a cadmium sulfide liquid crystal cell. In a CdS light valve, bubble formation occurs much faster if MBBA is used, than if an ester liquid crystal is used. Darkening of the electrodes, at present, is dependent on the conductivity of the liquid crystal and on the defects on the CdS film. It also appears to depend on the type of dopant used to conduct the current in the liquid crystal.

To assess the nature of the failure mechanisms, a number of diagnostic experiments were carried out. The first CdS light valves were fabricated with Schiff base liquid crystals so that most of our lifetime experiments were carried out with MBBA. Failure in the CdS cell took two concurrent forms: gas generation and electrode darkening (see Fig. 43). The rate of failure was roughly proportional to current flowing in the cell. Though we observed generation of gas bubbles in CdS light valves, we were unable to simulate the experiment under either direct observation with a microscope or an indirect observation with a specially constructed cell (see below). These experiments were carried out because we wanted to know which electrode generated the gas and then we wanted to find out the nature of the gas that was generated. Investigation of the electrode darkening by microchemical analysis revealed the presence of reduced cadmium and also indicated the presence of reduced indium from the indium oxide conductive coatings. Along with the darkening of the electrodes and the formation of gas
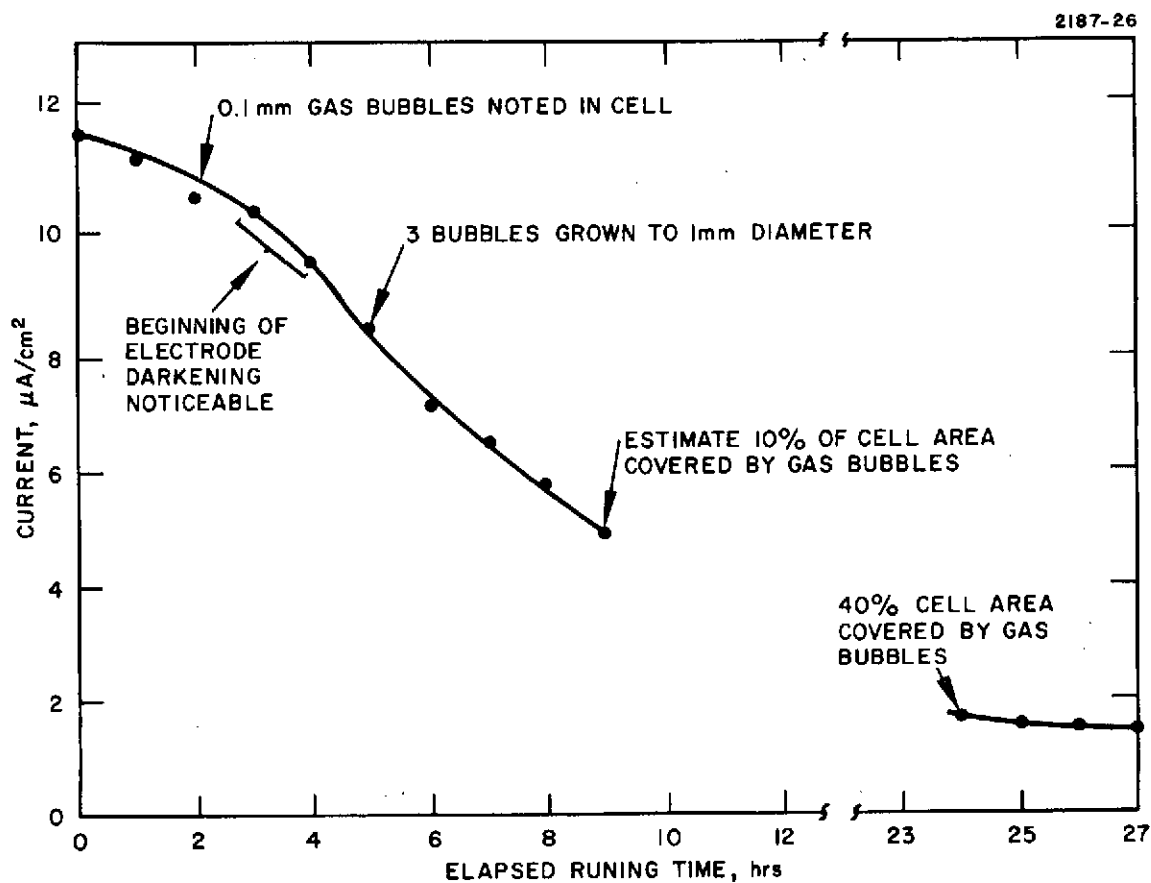
Fig. 43. Cell Current as a Function of Cell Operating Time — 12μ CdS Photoconductor, 30 Vdc (plus Polarity to CdS), 12.5μ Thick Cell, Impurity Doped MBBA 85μ Watts/cm^2 at 5100 Å Writing Illumination.

113

bubbles, we also observed considerable erosion of the CdS photoconductor (1000 $\overset{\circ}{A}$ in 1 hr of continuous operation).

Measurements such as those shown in Fig. 43 indicated a reduction in cell current with time. This could be accounted for due to two causes: (1) the generation of gas bubbles, thus reducing the exposed area available for conduction, (2) the buildup of an insulating film by electrochemical reaction. The second cause is suggested by the observed darkening, which appears to be due to the transport of reduced cadmium during operation, indicating the possibility of a buildup of atomic sulphur on the eroded cadmium sulfide surface.

These experiments indicate the conduction phenomena in these liquid crystals involves irreversible, or at least partially irreversible electrochemical reactions, that involve a charge-carrying atomic component of the photoconductor. In other words, the action of the liquid crystal on the photoconductor, at least in part, is to dissociate the CdS leaving the sulfur behind and transporting the cadmium across the cell. The indication was that these reactions are partially reversible because if they were not, the cells would have degraded even more rapidly than they did. Most probably the conduction phenomena in the cells involved these charge-carrying photoconductor species as well as other impurity charge-carrying species already present in the liquid crystal. The differences in degradation rate seen with different electrode materials further supports the idea of partial reversibility, in that materials such as indium oxide showed a lower degradation rate than compounds of higher electropotential such as zinc sulfide.

We attempted to analyze the cause of the darkening of the Nesatron counterelectrode in a CdS light valve using both microchemical analysis and polarographic (electrochemical) analysis. Microchemical analysis showed the presence of reduced cadmium on the counterelectrode; it also showed the presence of reduced indium. However, the result was looked upon as indicative rather than conclusive because the observations were within the limits of uncertainty of the analysis. We tried the polarographic analytical method; however, we were unable

to resolve the cadmium half-potential from the indium half-potential (see below) despite some earlier polarographic experiments that, again, indicated the presence of cadmium. Hence, we are unable to give unequivocal direct evidence of the transport of cadmium across the liquid crystal. However, we were able to gather indirect evidence of this failure mechanism by using silver electrodes. If a silver electrode is used as the anode in place of the CdS, silver ion transport through the liquid crystal to the cathode is detectable as the deposition of a silver mirror on the counterelectrode. Again, we regard this evidence only to be indicative rather than conclusive since it is observed for silver, not cadmium. Finally, we observed low molecular weight polymer formation, at least at the anode. This deposition behaves as a blocking layer for the dc light valve. Furthermore, at least in part, this mechanism is responsible for the residual image formation and in part for the photochemical deterioration of the light valve (see below).

On the assumption that the operational lifetime was strongly affected by the nature of the dopants, we performed several experiments to measure the effect of different dopants on device lifetime. The main goal of the experiments was to control the electrochemical reactions in the liquid crystal and at the electrodes by using redox dopants so that undesirable electrochemical reactions that directly lead to deterioration of the cell could be suppressed. Using impure MBBA, rather than a doped pure liquid crystal, we observed that the current decreased drastically with time (Fig. 43) so that the measured operational lifetime was short — at best, several hours. However, using pure MBBA, doped with a HRL-proprietary dopant system, (cobalt (II) and (III) tetraphenyl porphyrin complexes, the current remained relatively constant (Fig. 44) and the operational lifetime was enormously increased. The initial increase in current, seen in Fig. 44, appears to indicate that the electrochemical reaction is only partially controlled by the dopants. However, a CdS liquid crystal light valve with pure MBBA and this dopant system continued to show dc DSM photo response for a total of 170 hr continuous operation before complete failure. This
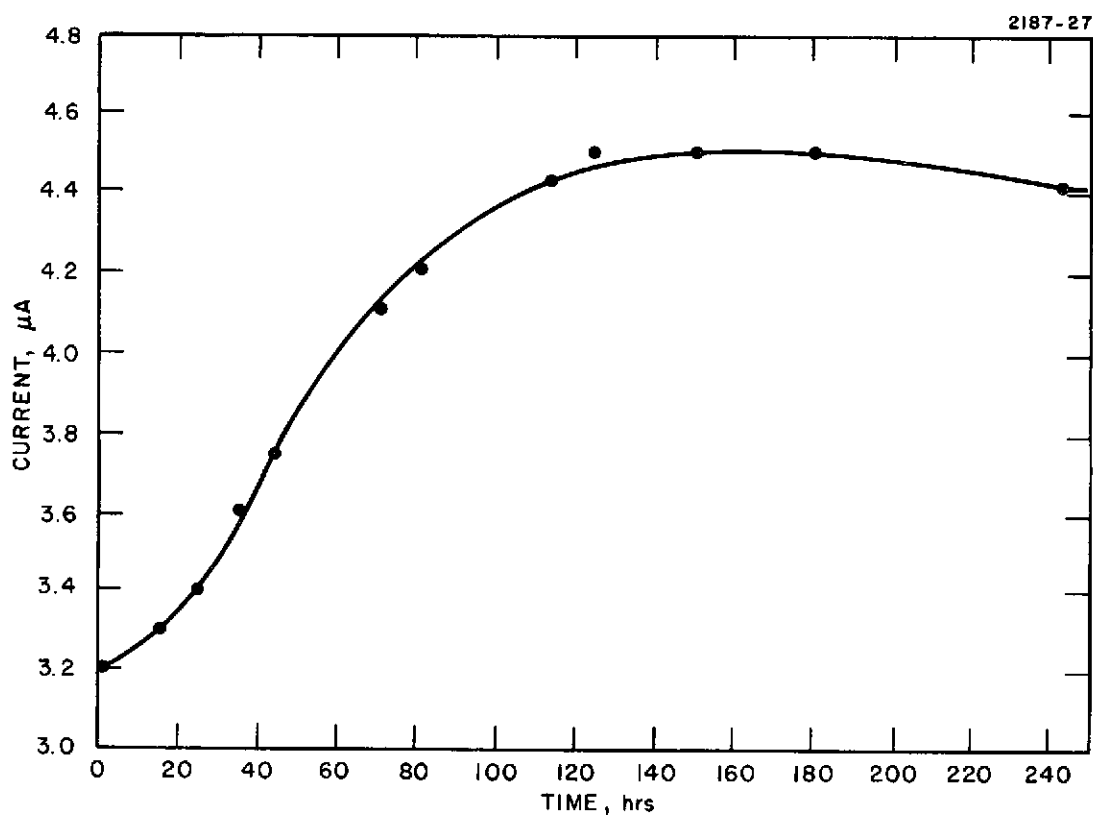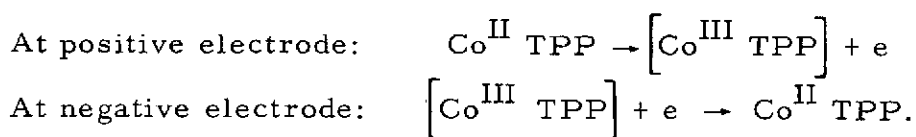
Fig. 44.   Lifetime Test — MBBA Metal Dye Complex
Dopant.

116

is more than an order of magnitude improvement compared to the use of impure MBBA without this dopant in a CdS light valve. The failure mechanism in this case was the staining of the electrodes in the unexposed area as shown in Fig. 45, rather than the formation of bubbles which did not occur until more than 200 hr of operation.

The improvement in lifetime can be explained by the following results obtained in the course of our parallel IR&D program: we found that the use of a proprietary dopant system, consisting of cobalt (II)-tetraphenylporphyrin and cobalt (III) tetraphenylporphyrin tetrafluoroborate, led to improved performance of the Schiff base liquid crystal. Studies of these complexes in dimethylsulfoxide solutions showed that these complexes were oxidized and reduced in a reversible manner with a redox potential at 0.15 V versus saturated calamel electrode (SCE).

$$\left[Co^{III} TPP\right] + e^- \rightleftharpoons Co^{II} TPP$$
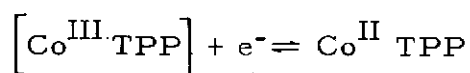
If the dopants behave similarly in the liquid crystal, a much more complicated host, the redox reaction of these complexes should occur at a much lower potential than the decomposition potential of the liquid crystal. Therefore, it is reasonable to assume that an equimolar mixture of the cobalt (II) and cobalt (III) complexes would carry nearly all the current in the dc-type electro-optic device:

At positive electrode: $Co^{II} TPP \rightarrow \left[Co^{III} TPP\right] + e$

At negative electrode: $\left[Co^{III} TPP\right] + e \rightarrow Co^{II} TPP.$

We believe control of electrochemical reactions is the most effective means for improving the lifetime of these devices. This is not only because the electrochemical reaction deteriorates the liquid crystal material, but also because the electrochemical products cause deterioration of the electrodes and disturb the liquid crystal surface alignment. All these undesirable effects may be due to reactive organic radicals that are generated during the electrochemical reaction.

2484-1

SPACER

SPACER

M9452

ELECTRODE STAIN

UNEXPOSED
SECTION

SMALL BUBBLES

EXPOSED
SECTION

This page is reproduced at the
back of the report by a different
reproduction method to provide
better detail.

ELECTRODE DETERIORATION
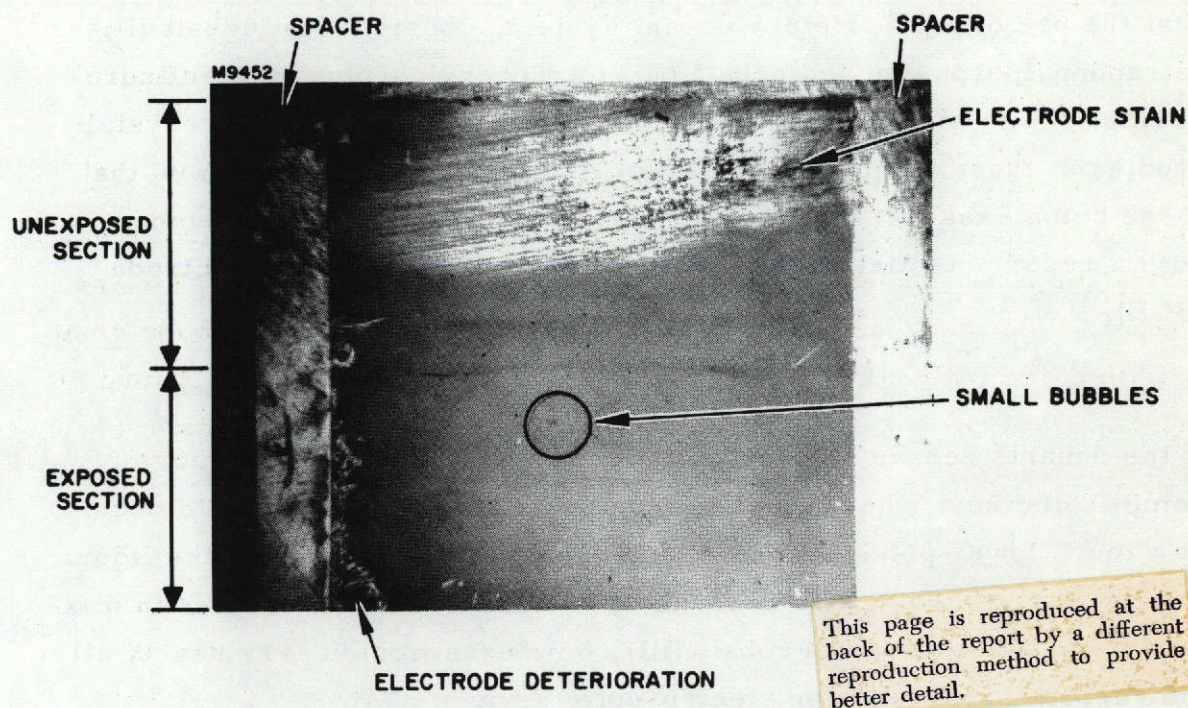
Fig. 45.   Polarized Picture of CdS/Doped MBBA/In$_2$O$_3$ Cell
After 245 Hrs of Operation: 13 μm Thick Cell,
0.1% Cobalt Complex Dopants, 20 Vdc, 63 μW/cm^2
Intensity During Exposure.

Therefore our approach to improve the lifetime is to minimize the generation of reactive intermediate products during electrochemical reaction by doping the liquid crystal with reversible redox dopants whose electropotentials are sufficiently low (compared with the other constituents of the device) that the dopant dominates the electrochemistry of the cell.

B. EXPERIMENTAL TECHNIQUES AND RESULTS

1. Observation of Gas Bubble Formation

Because void formations were one of the major failure mechanisms of the photoactivated CdS cell, we attempted to observe the gas formation directly; however, the attempt was unsuccessful. We were unable to observe whether the gas formation was at the CdS anode or at indium oxide cathode, or both. A quantitative analysis of the nature of the gas involved was also unsuccessful. Two such experiments are described below.

a. Direct Observation Under Microscope

The cell construction is shown diagrammatically in Fig. 46. We attempted to observe gas generation with the aid of a microscope. The liquid crystal used was impure MBBA; it was held between the electrodes by surface tension. At 250 V, electrohydrodynamic instability was observed; however, no bubble generation was observed even after several hours of operation. Presumably, it was because either the formed bubbles escaped into the air too fast to be observed, or the field was not strong enough to create electrochemical generation of gases.

b. Indirect Observation

A cell was constructed as shown in Fig. 47. The liquid crystal used was MBBA saturated with squarylium dye III. A potential of 1000 Vdc was applied to the cell for a period of 3 months.

MICROSCOPE

LIQUID CRYSTAL

CdS

In$_2$O$_3$

I mm

1.5 mm

GLASS PLATE
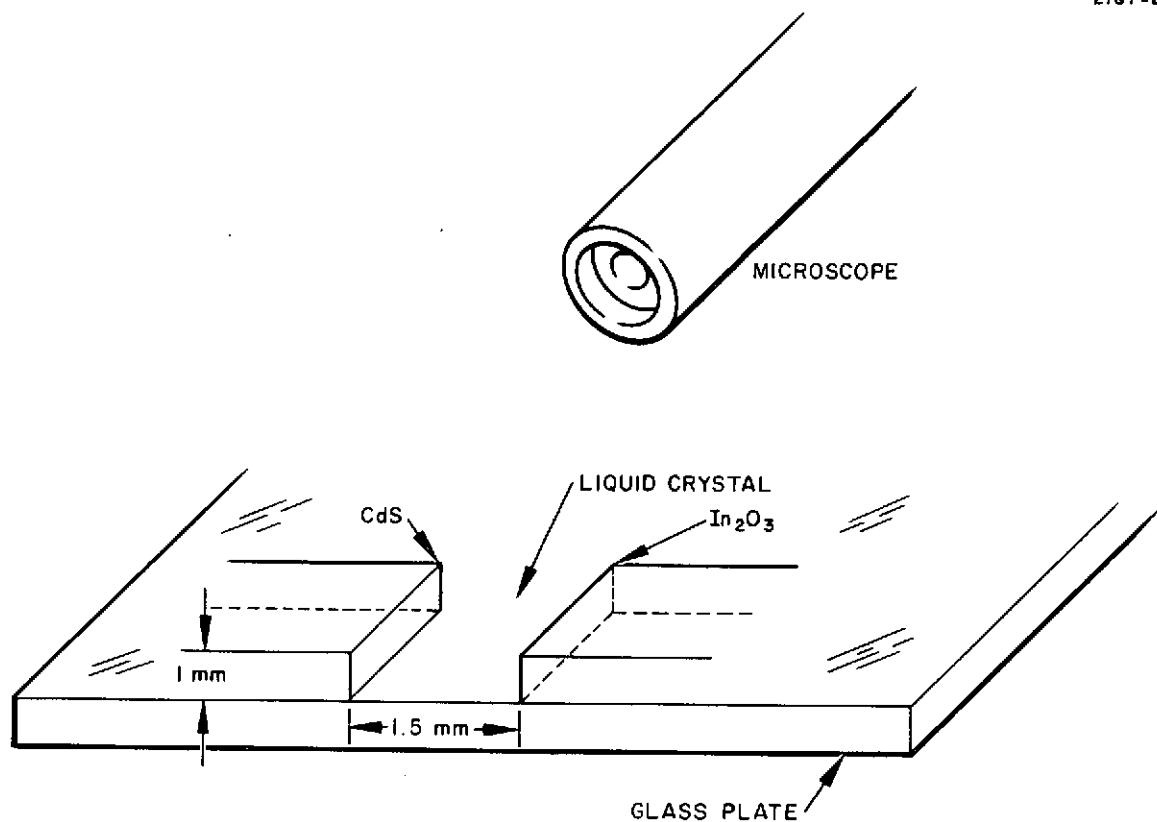
Fig. 46.   Schematic of Cell Construction for Direct
Observations of Bubble Generation.

In$_2$O$_3$

CdS

GLASS

GLASS

LIQUID CRYSTAL

6 mm

8 mm
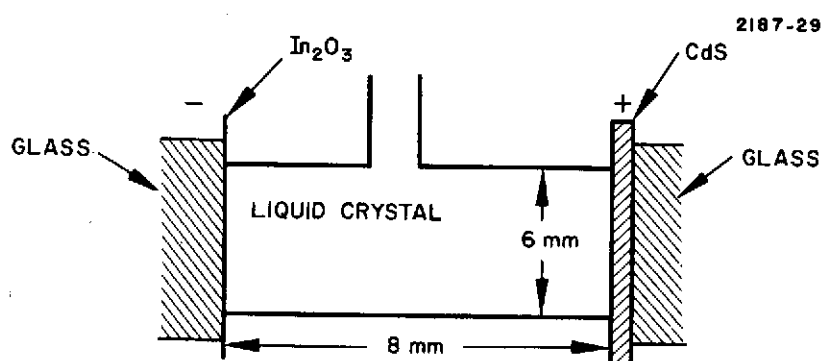
Fig. 47.   Schematic of Cell Construction
for Indirect Observation of
Bubble Generation.

Unfortunately, no gas bubble formation at the cathode or the anode was observed during this experiment.

2.   Life Test

a.   Life Test of CdS Cell Using MBBA Doped With Cobalt Organometallic Complex

A liquid crystal light valve was constructed using MBBA doped with 0.1% of cobalt organometallic complex. The cell itself was a sandwich of indium oxide and cadmium sulfide. The liquid crystal film was 12.7 μ thick and was 0.75 x 0.75 in. square.

A special setup was made for performing the dc life test. The cell was separated 5-3/4 in. from a diffused light source by a black cardboard tube that had an aperture on the cell side. A white light source of 62.8 $\mu W/cm^2$ was used as the illuminating source. The test was performed so the light entered the cell through the liquid crystal before activating the cadmium sulfide. Half the aperture of the cell was masked to prevent any light from activating that side. This was done in an attempt to provide a control on the experiment; the unillumi-nated side experienced no dynamic scattering (in theory) during the experiment. Unfortunately, during the experiment, the turbulence of the dynamic scattering that occurred on the exposed side may have caused a flow of new unexposed liquid crystal from the unexposed side to replenish the exposed side. This may have helped increase the life-time of this cell. Figure 46 shows the cell after the life test had been completed on the cell. The picture was taken with the light valve placed between crosspolarizers. Deterioration effects are shown in the corner of the exposed section. The darkening or staining of the electrodes that occurred in the unexposed area did not completely in-hibit the DSM when it was exposed. Figure 44 shows the variation of the current with time. The current characteristics are impressive. This result was obtained just prior to the termination of this contract, hence the experiment was not pursued further to determine if the result

was caused by the design of the cell or if it was intrinsic to the liquid crystal/dopant system used.

        b.   Life Test of CdS Cell Using MBBA Doped With Platinum Organometallic Complex

The life test setup used in this experiment was the same as was used for the cobalt organometallic complex experiment just described. The MBBA was doped with 0.02% of a platinum complex. The area of the cell was 1 cm^2. This cell was run for about 100 hr. The failure of this cell was due first to the staining of the electrode and then to the decomposition of MBBA to an isotopic liquid.

3.   Polarographic Analysis of Cadmium

A Nesatron chip of area 0.36 cm^2 and an unknown Nesatron chip of area 0.46 cm^2 were used. Each of the chips was digested with 0.5 ml of 0.1 $\underline{M}$ acetic acid in a 5 ml beaker. The acid was heated until the coating on the unknown chip was partially dissolved. The final solution was mixed with 2.5 ml of 1 $\underline{M}$ potassium chloride, 2.5 ml of 0.1% gelatin and was adjusted to pH 7 with diluted potassium hydroxide solution. Finally, the total solution was transferred to a 25-ml volumetric flask and it was diluted to the mark with water.

The E_p of these two samples was compared with the blank and with standard samples of indium, cadmium, and indium-cadmium mixtures. The results are summarized in Table VII. We were unable to conclude from the data whether the unknown chip contained any cadmium. Furthermore, we even were unable to separate the cadmium and indium using dimethylformamide as solvent. These data are summarized in Table VIII.

4.   Direct Observation of Metal Ion Transport

We were unable to obtain convincing evidence concerning the transport of ions across the electrodes of photoactivated CdS cells by conventional chemical analysis. Therefore, we resolved our problem

122

TABLE VII

Polarographic Analysis of Cadmium and Indium in Water Solutions

Sample	E_p	i_p
Blank	-0.50 V	0.02 μA
10^7 $\underline{M}$ Cd^2	-0.57 V	0.11 μA
	-0.57 V	0.12 μA
10^{-7} $\underline{M}$ Cd^2 $+10^{-6}$ $\underline{M}$ In^{+3}	-0.50 V	0.12 μA
9×10^{-6} $\underline{M}$ In^{+3}	-0.57 V	0.02 μA
9×10^{-6} $\underline{M}$ In^{+3} 1×10^{-7} $\underline{M}$ Cd^{+2}	-0.54 V	0.135 μA
Unknown Chip	-0.55 V	0.018 μA
	-0.37 V	0.010 μA
In_2O_3 Chip	-0.56 V	0.095 μA
(Nesatron)	-0.38 V	0.010 μA

T891

TABLE VIII

Polarographic Analysis of Cadmium and Indium In Dimethylformamide

Sample	E_p vs SCE
In^{+3}	-0.56 V
Cd^{+3}	-0.6 V
$In^{+3} + Cd^{+2}$	0.57 V*
*No separation of indium and cadmium peaks.	

T892

by the use of other metal electrodes. A liquid crystal cell 12.5 μ thick and 1 cm^2 in area was made up with MBBA doped with squarylium dye III. The anode was formed of evaporated silver and the cathode was Nesatron glass. A dc voltage of 40 V was applied to the cell. Within 20 minutes the cathode was significantly darkened. We then dismantled the cell and found no evidence of any deterioration of the liquid crystal; however, we observed that the silver electrode was etched, and that the cathode was coated with a reflective silver metal surface. We accept this as strong evidence in support of the possibility that metal ions can be transported across an organic liquid.

5. Direct Observation of Polymer Formation on the CdS Electrode

The construction of the cell used in this experiment is shown in Fig. 48. Impure MBBA was used in the cell. On one half, the cell had a CdS-CdS electrode combination. On the other half, it had a CdS-In$_2$O$_3$ electrode pair. A dc voltage of 150 V was applied to the cell. After 4 hr of DSM operation in room light the anodes were examined. Both anodes were coated with a polymer layer which could be rubbed away with a piece of Kimwipe, or washed away with acetone. Due to the minute quantity generated, it was not possible to analyze the polymer at the time of the experiments. It appeared that the polymer was of low molecular weight. One possibility could be the dimeric or trimeric form of the liquid crystal.

2187-30
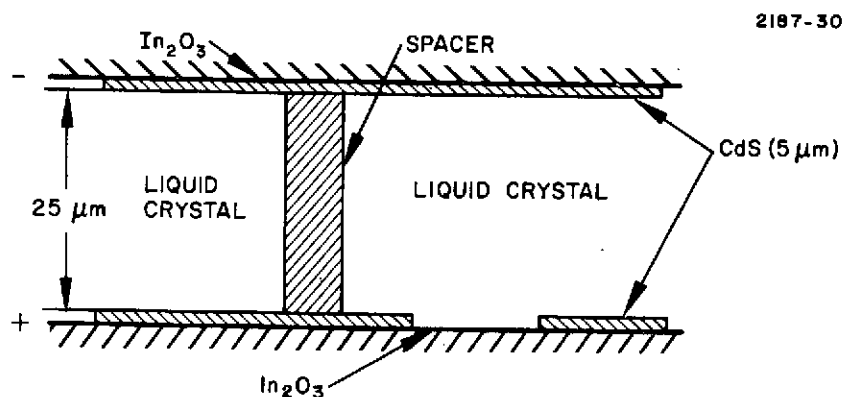
Fig. 48. Schematic of Dual Electrode Pair Cell
For Observation of Effect of Electrode
Asymmetry on Lifetime.

APPENDIX A

SCATTERING CURVES

Scattering curves are given in Figs. 49 through 60.
The optical system has resolution of 0.1^O (the 0.43 mm pin-
hole used) throughout. If analyzing polarization is used,
PARALLEL or PERP appears in the figure. If 40 rms V,10 kHz
ac is used, AC appears in the figure. If the cell is light-
activated, LIGHT appears in the figure.

Fig. 49.

Fig. 50.

126
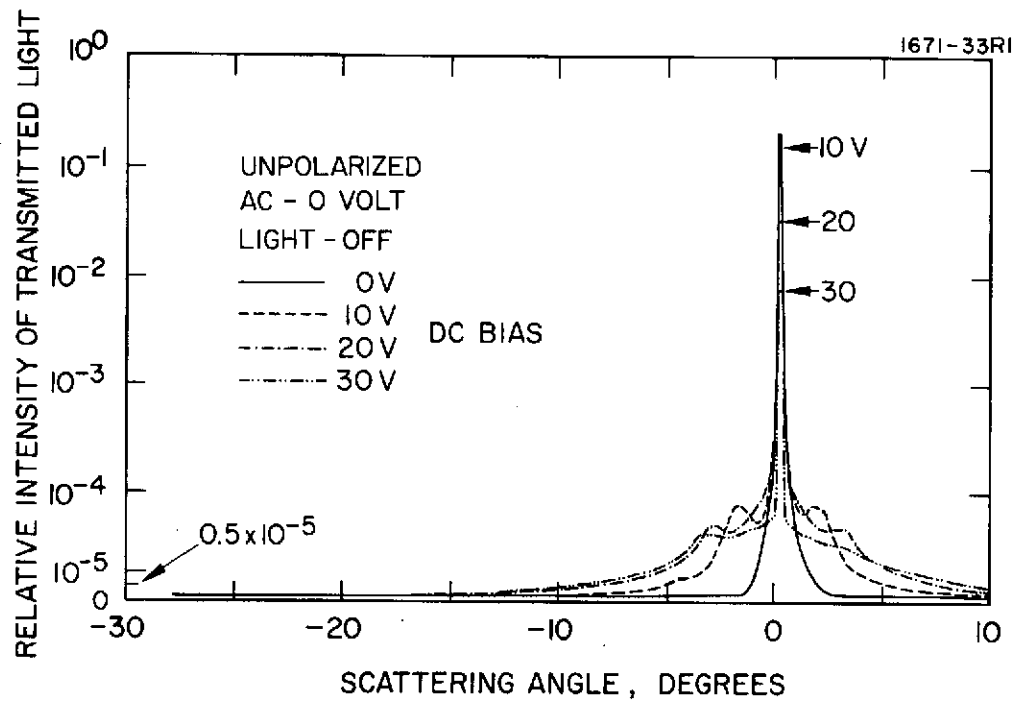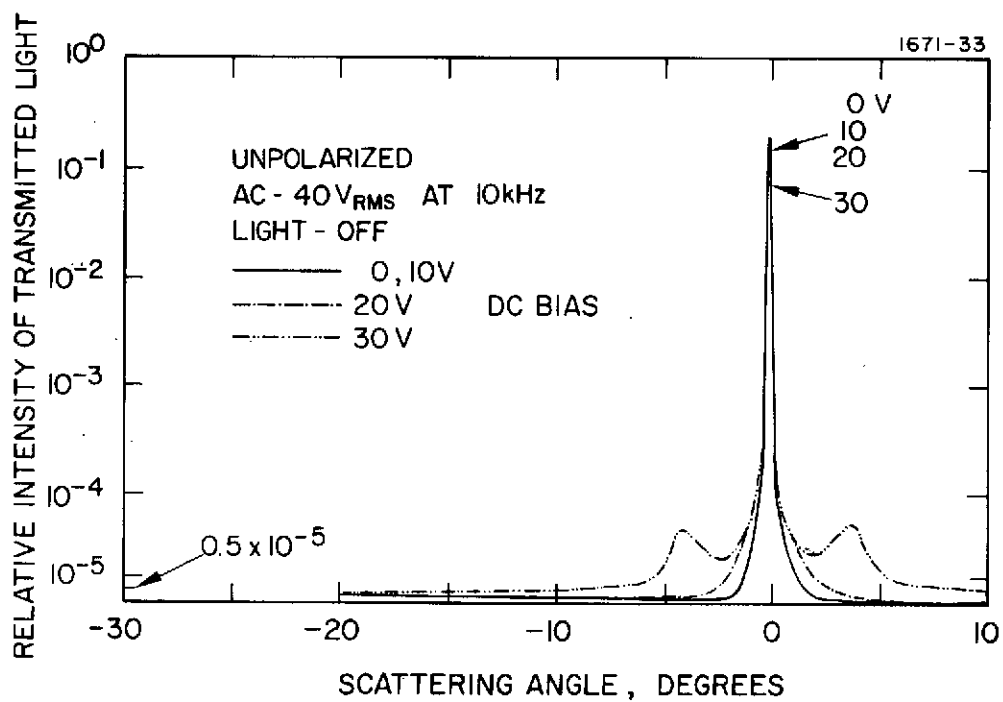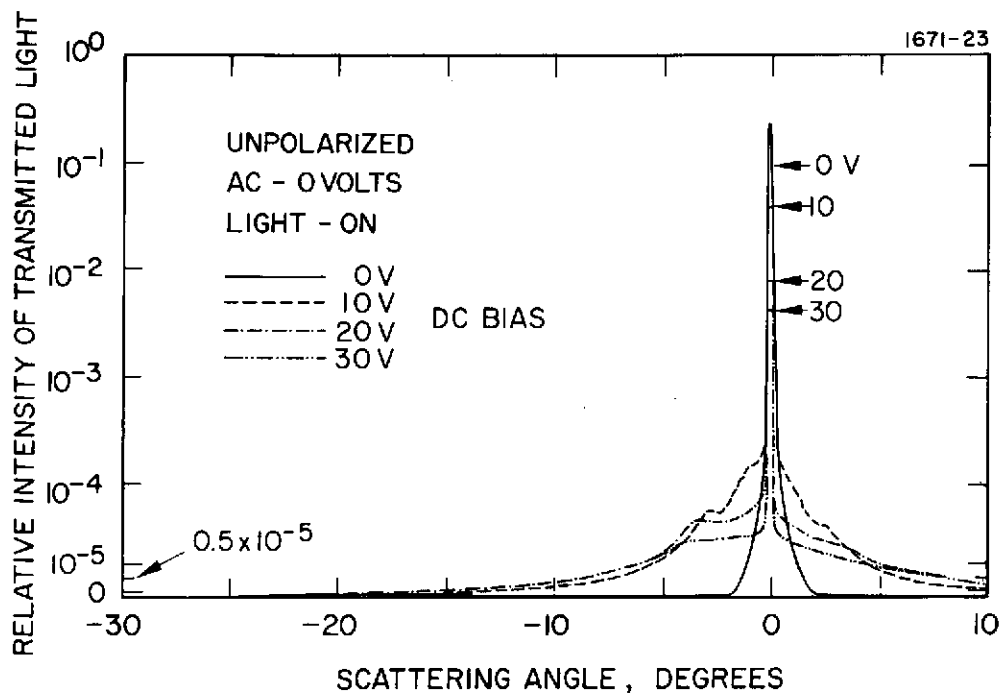
Fig. 51.

Fig. 52.

Fig. 53.

Fig. 54.

128
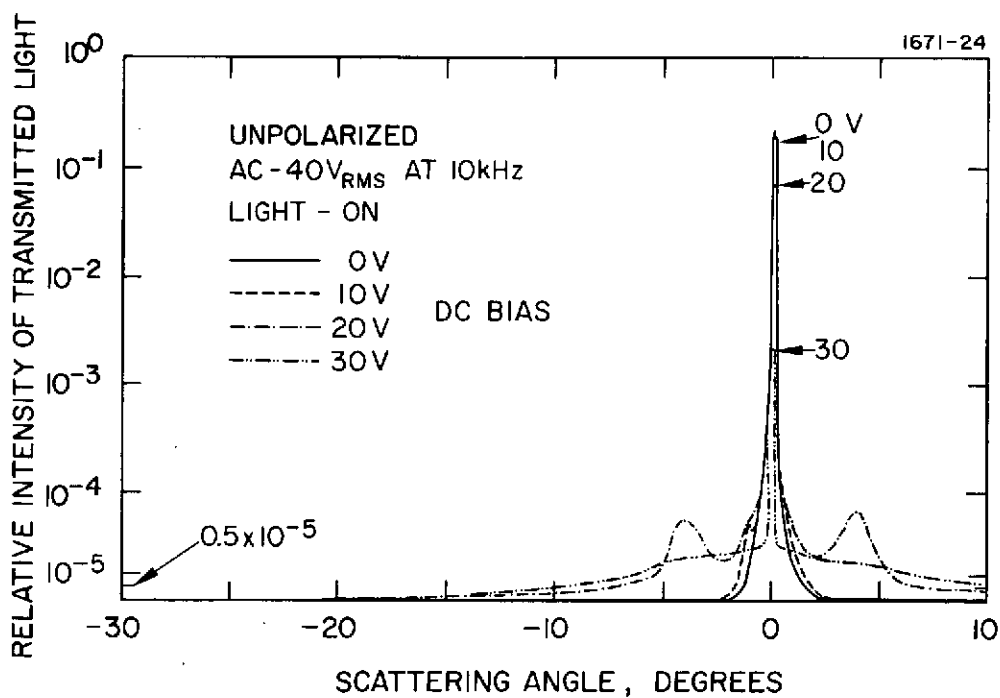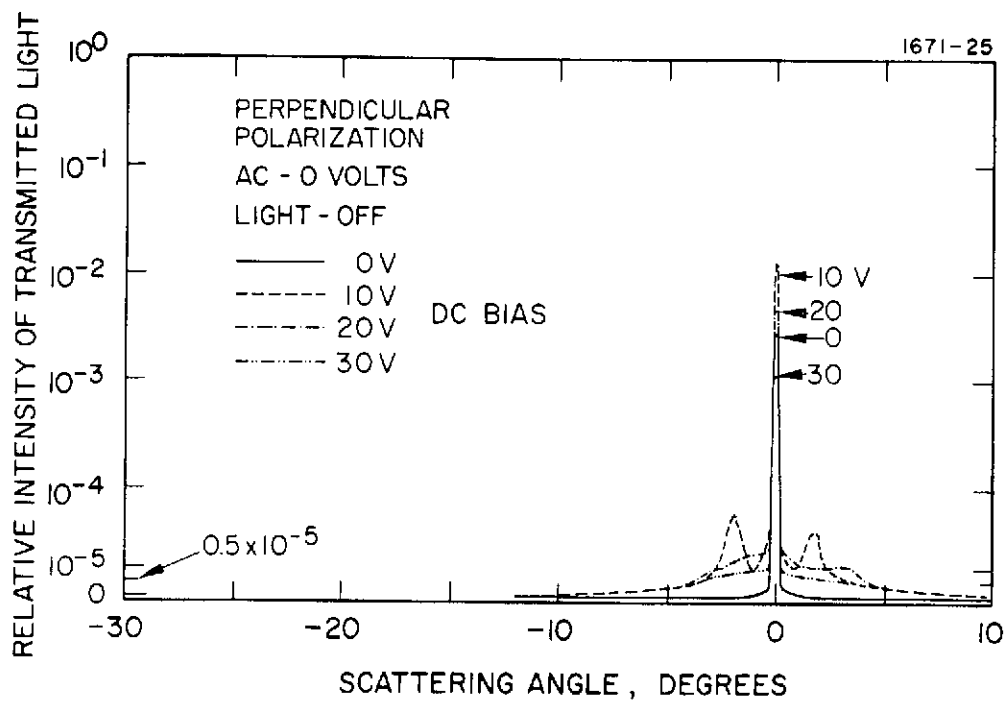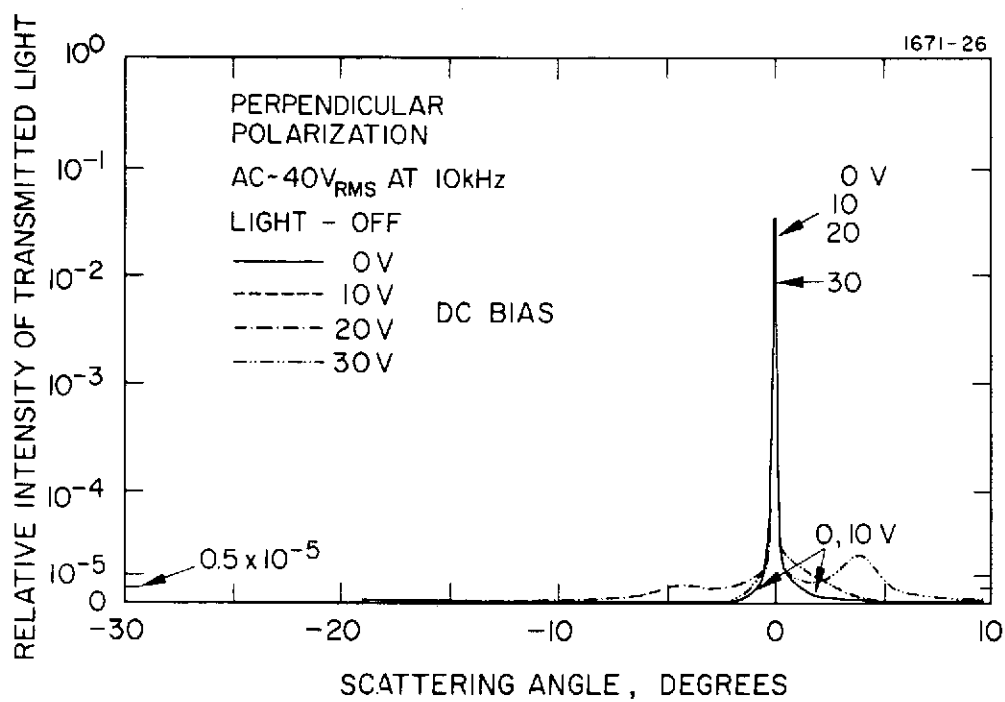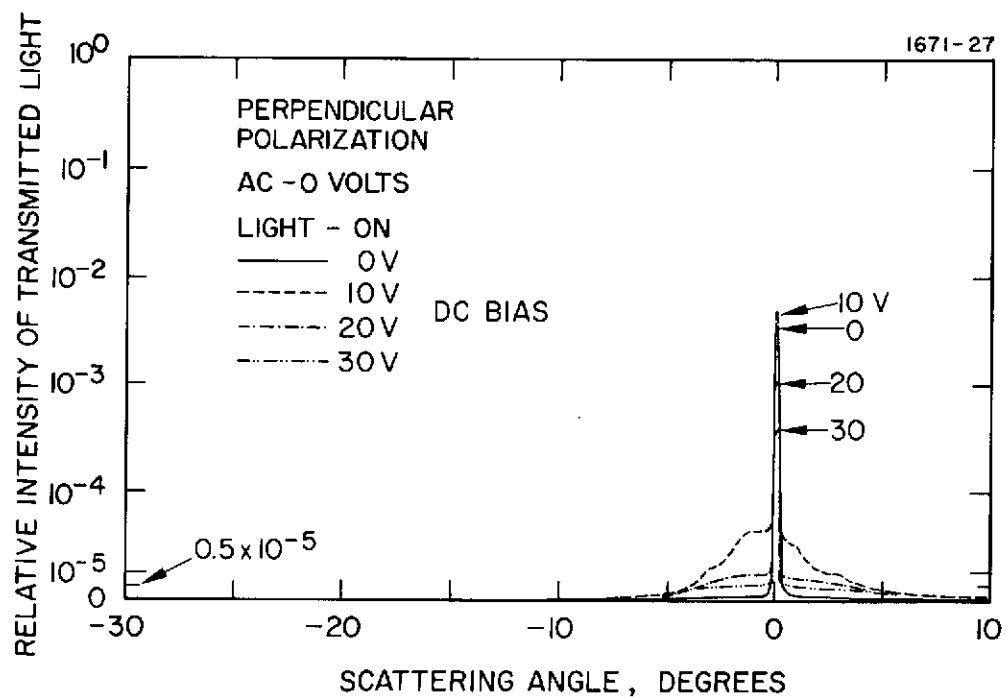
Fig. 55.

Fig. 56.

Fig. 57.

Fig. 58.

130
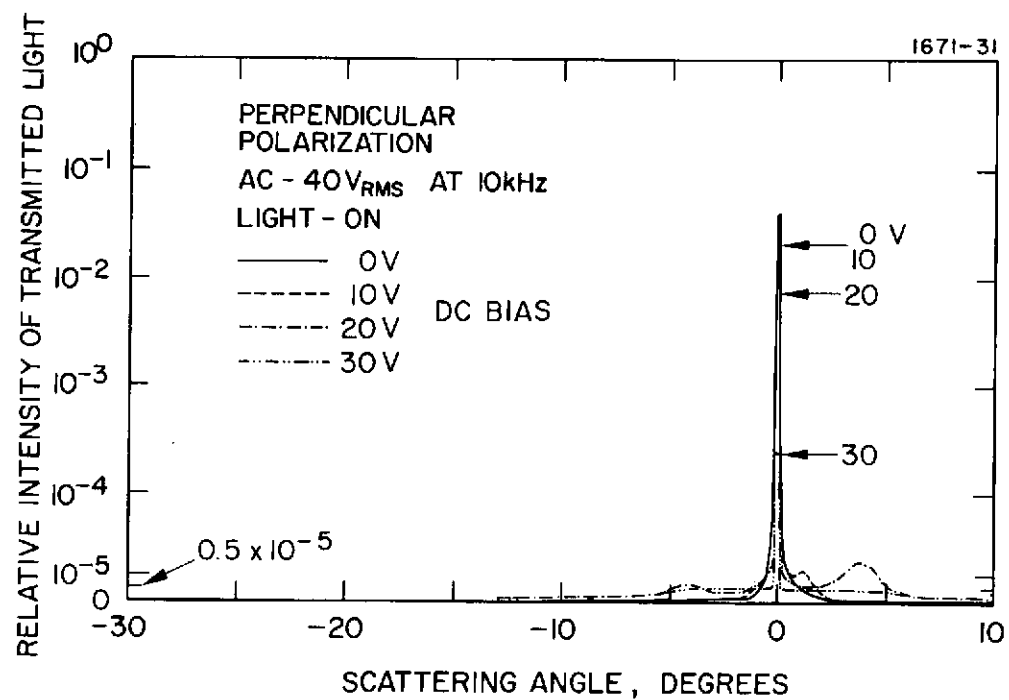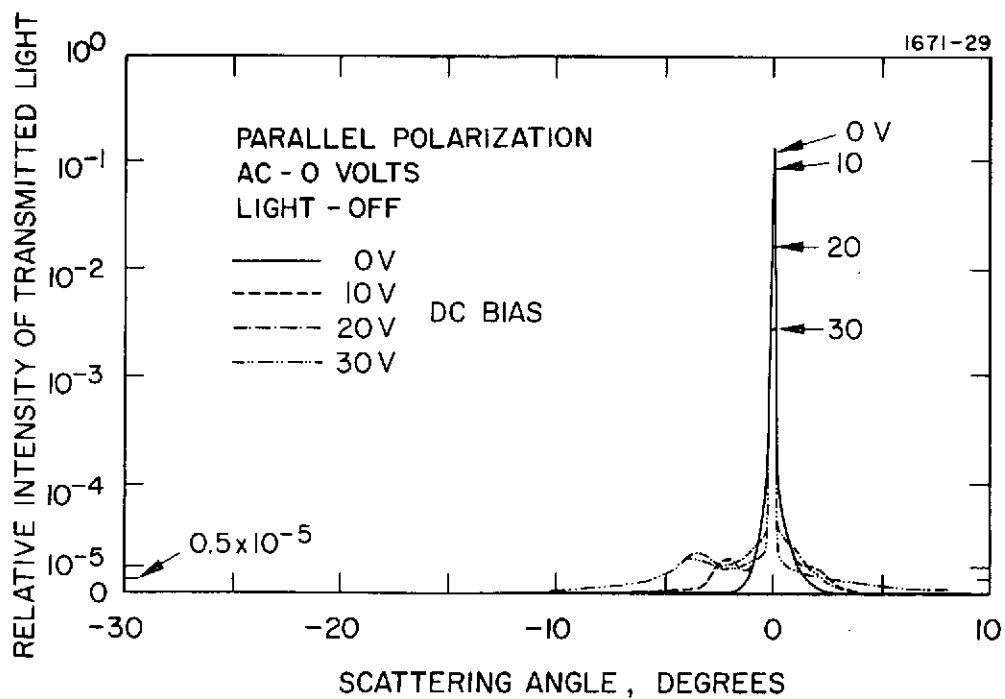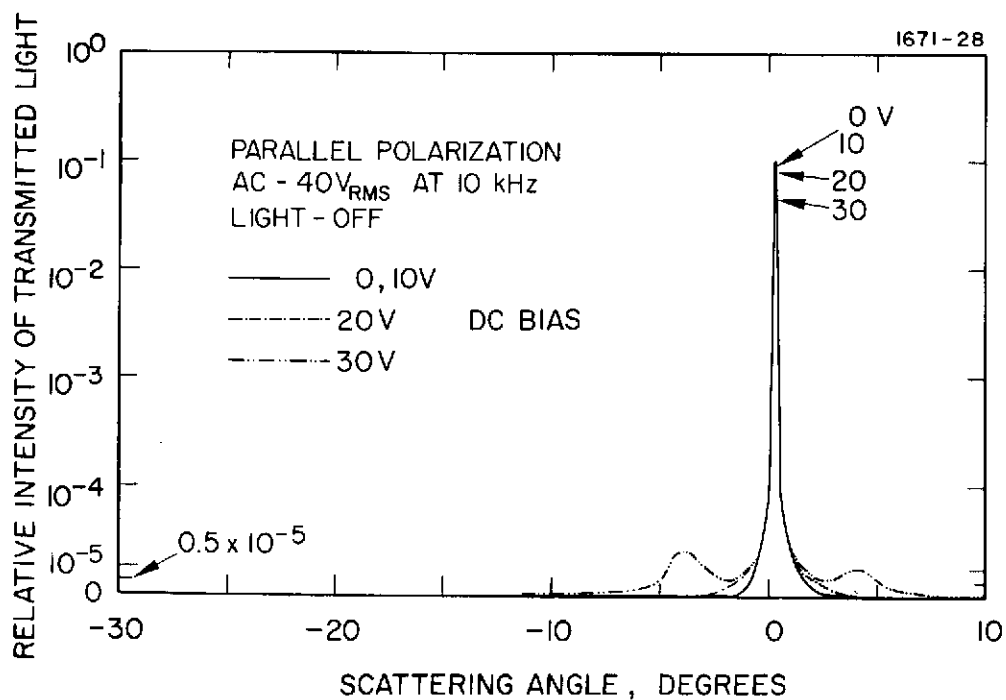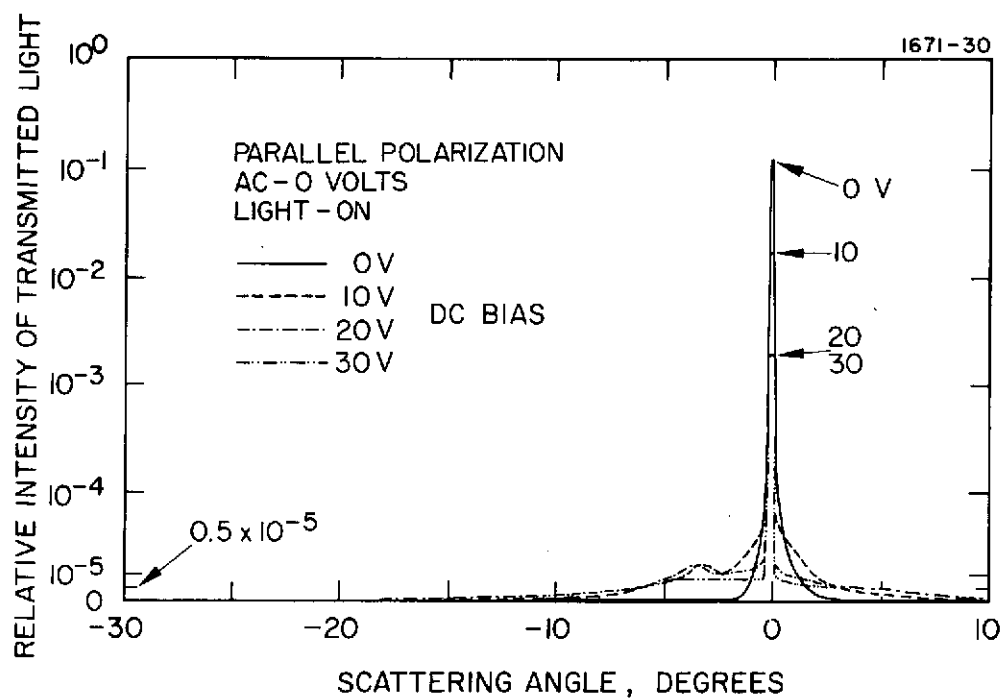
Fig. 59.
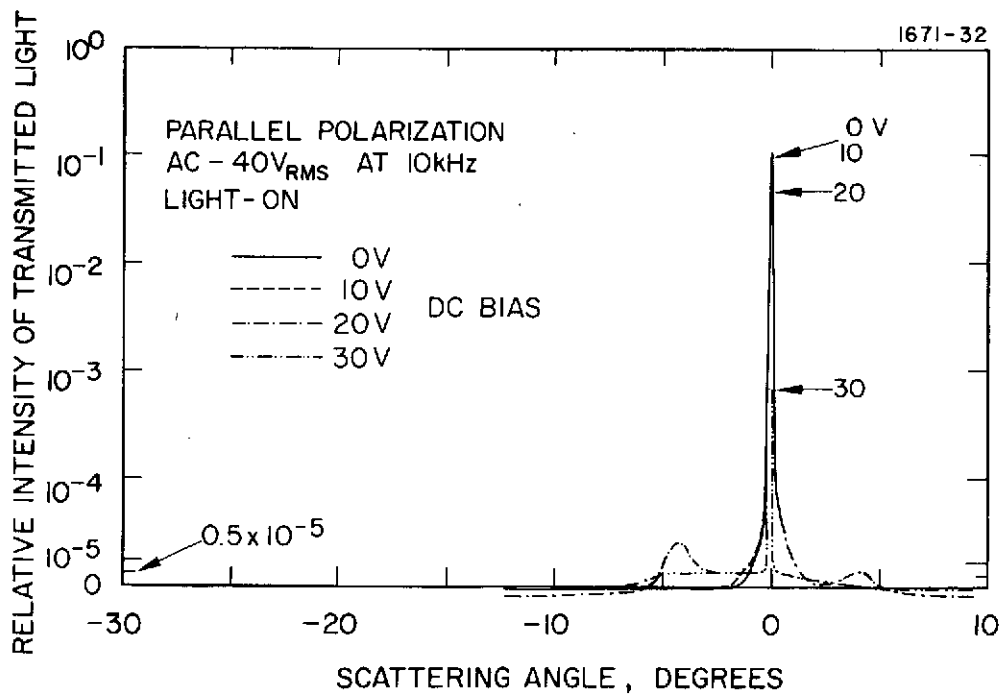
Fig. 60.

APPENDIX B

CURVES OF TRANSMITTED LIGHT INTENSITY
AS FUNCTION OF DC BIAS

Curves of transmitted light intensity as a function of dc bias voltage are given in Figs. 61 through 72. The maximum spatial frequency in cycles/mm at the surface of the liquid crystal that the optical system can resolve is noted. Analyzing polarization, if any, is noted by PARALLEL or PERP in the figures. Curves for the light-activated cell are marked LIGHT.

Preceding page blank
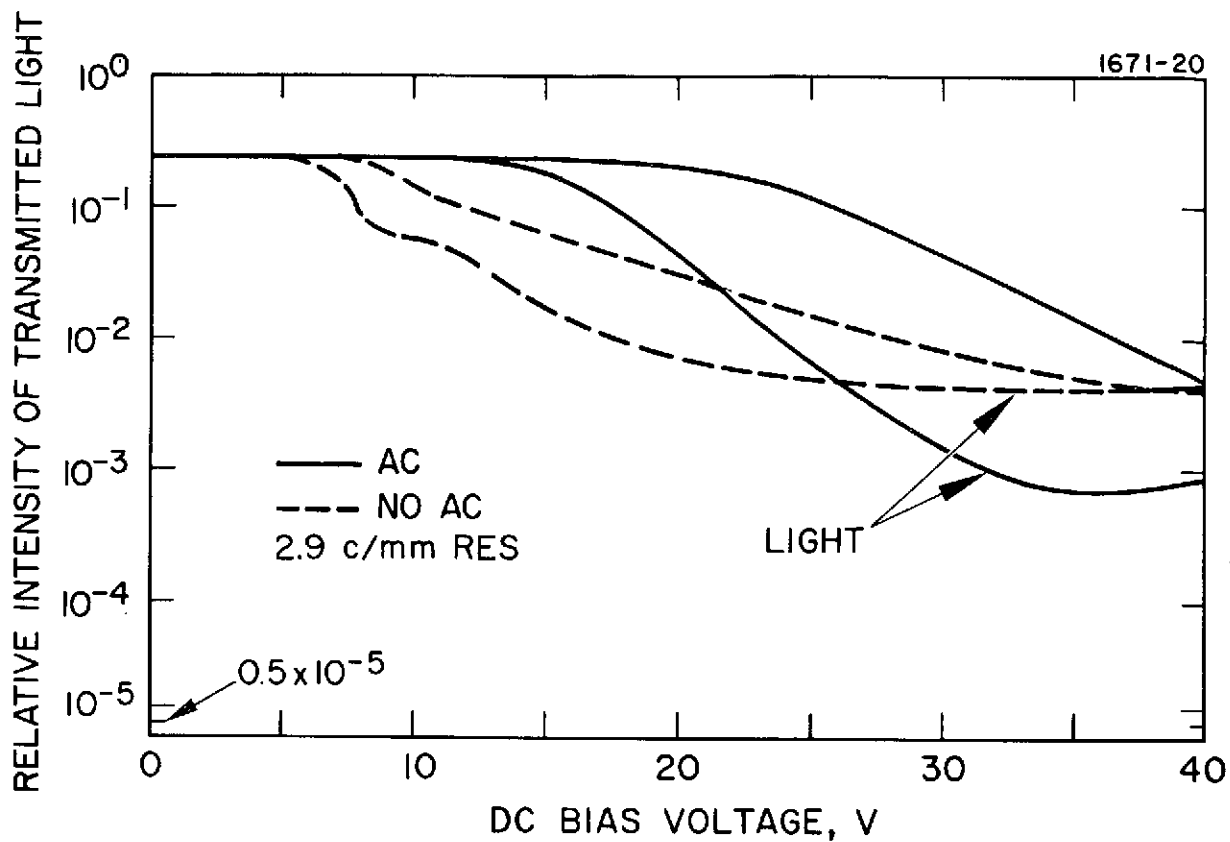
Fig. 61.

Fig. 62.

Fig. 63.

Fig. 64.

135

Fig. 65.

Fig. 66.

Fig. 67.

Fig. 68.
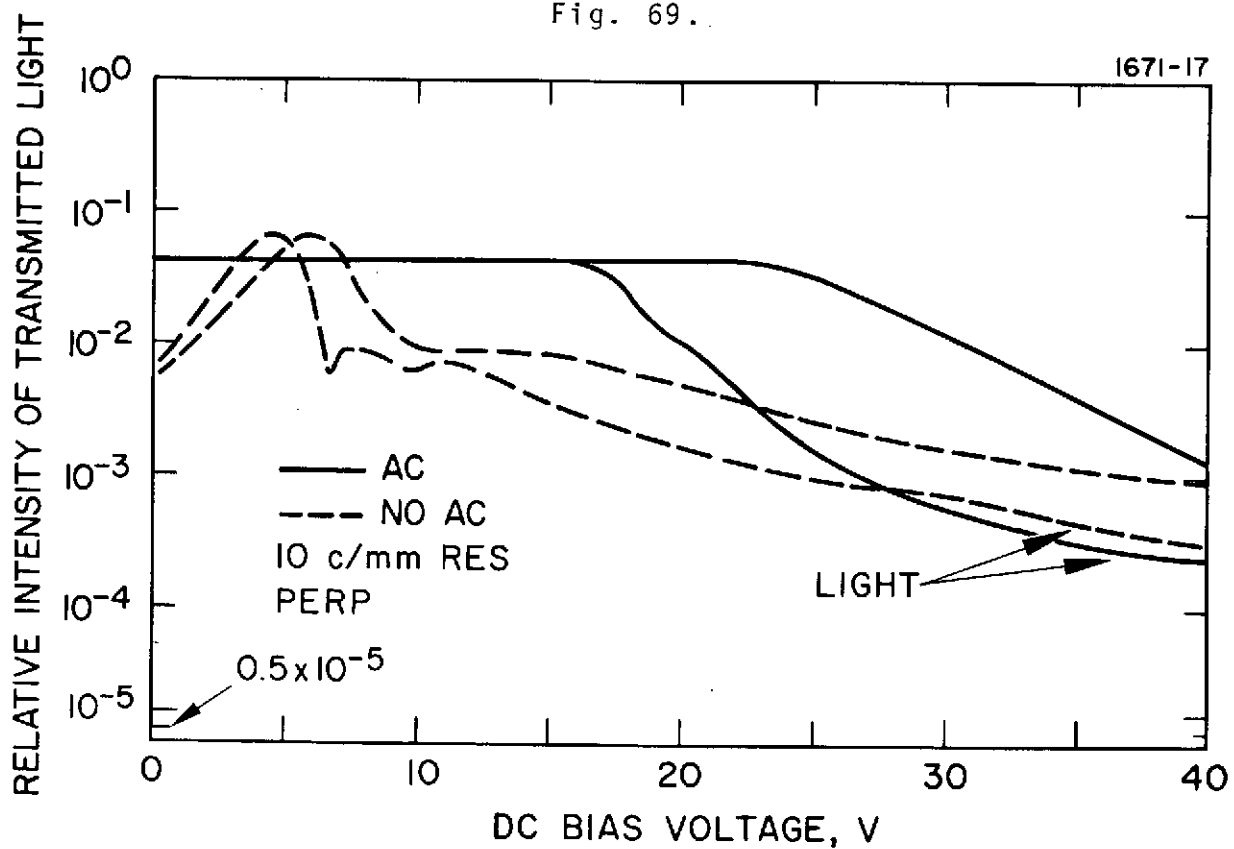
137

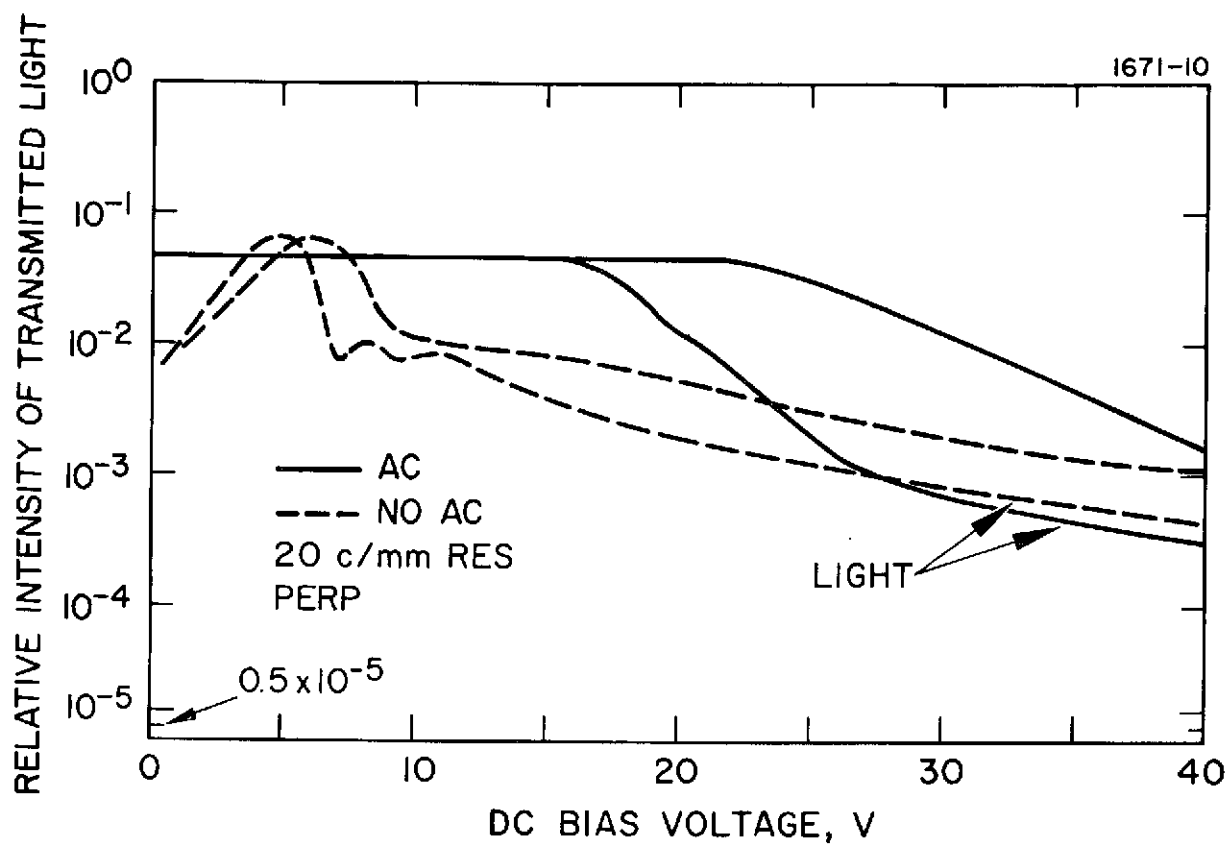Fig. 69.

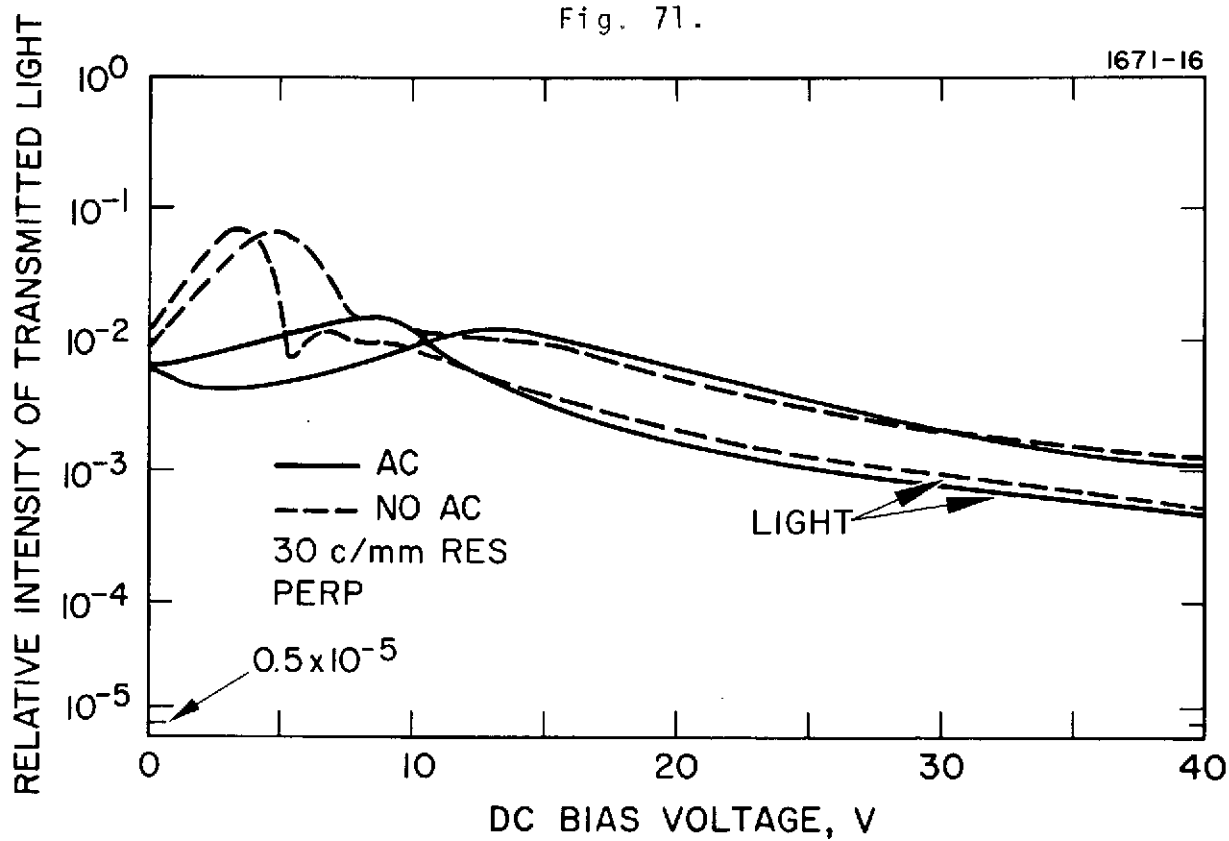138

Fig. 70.

Fig. 71.

Fig. 72.

Preceding page blank
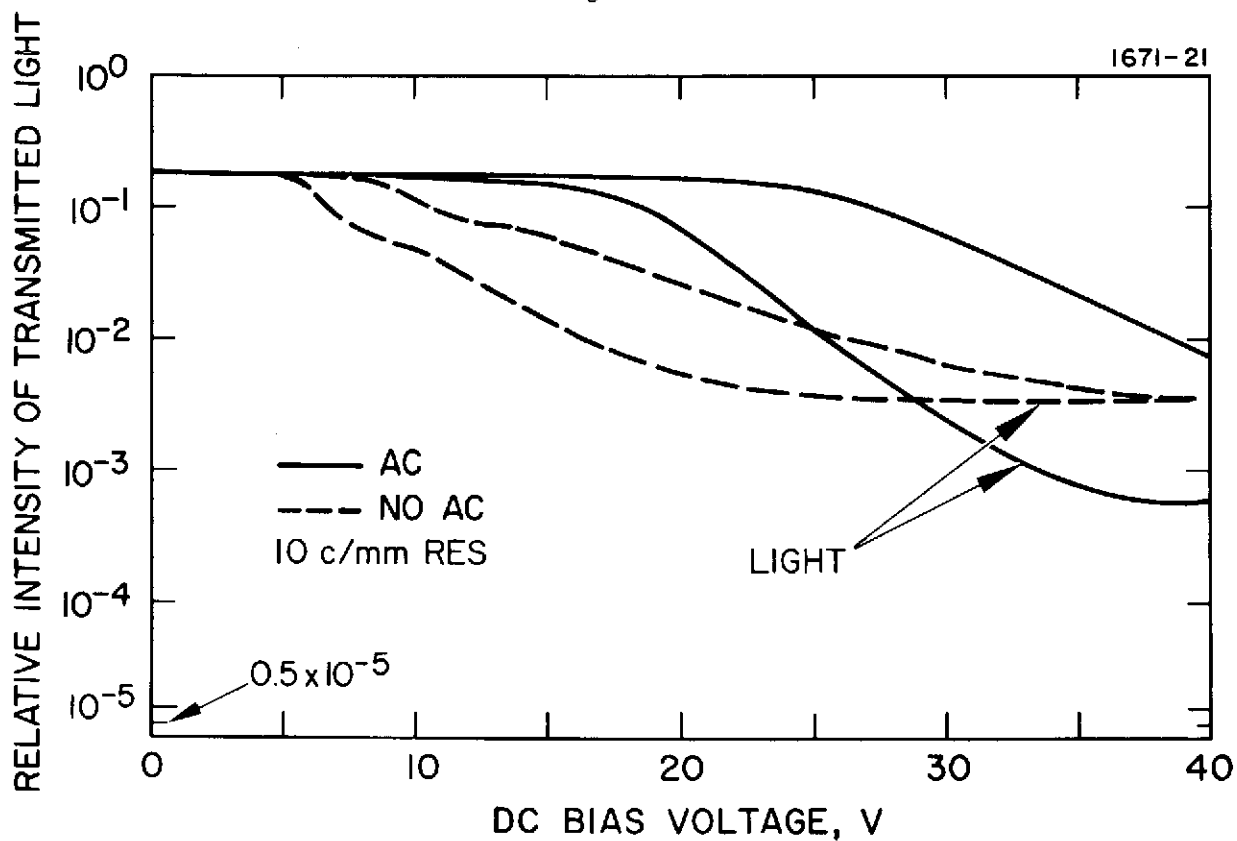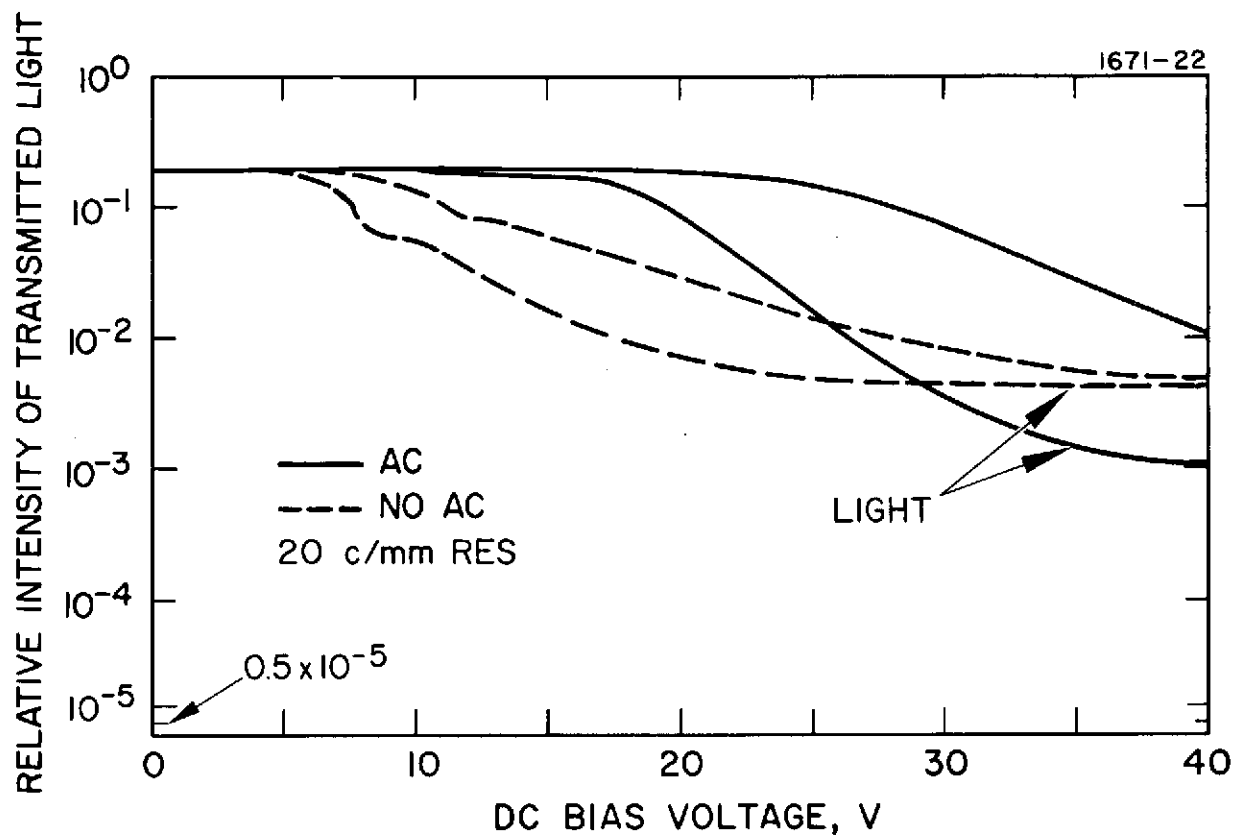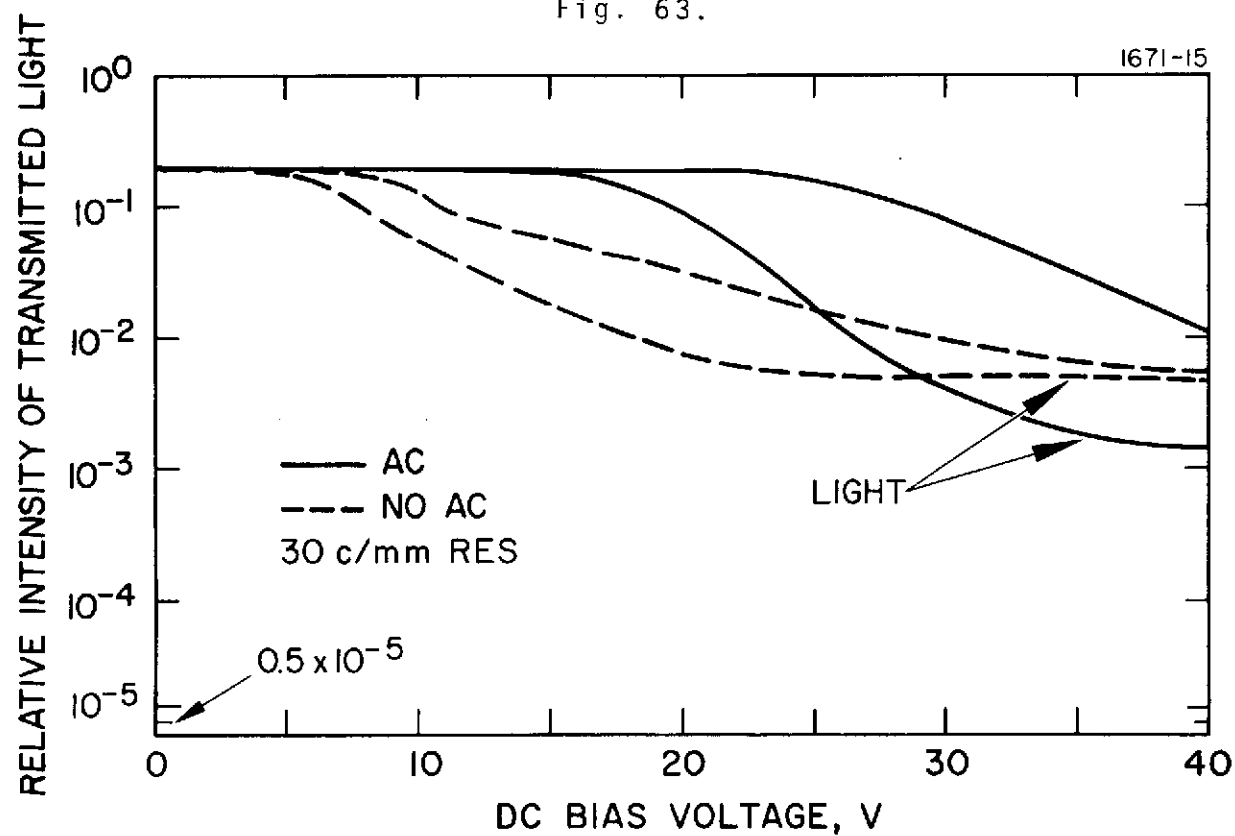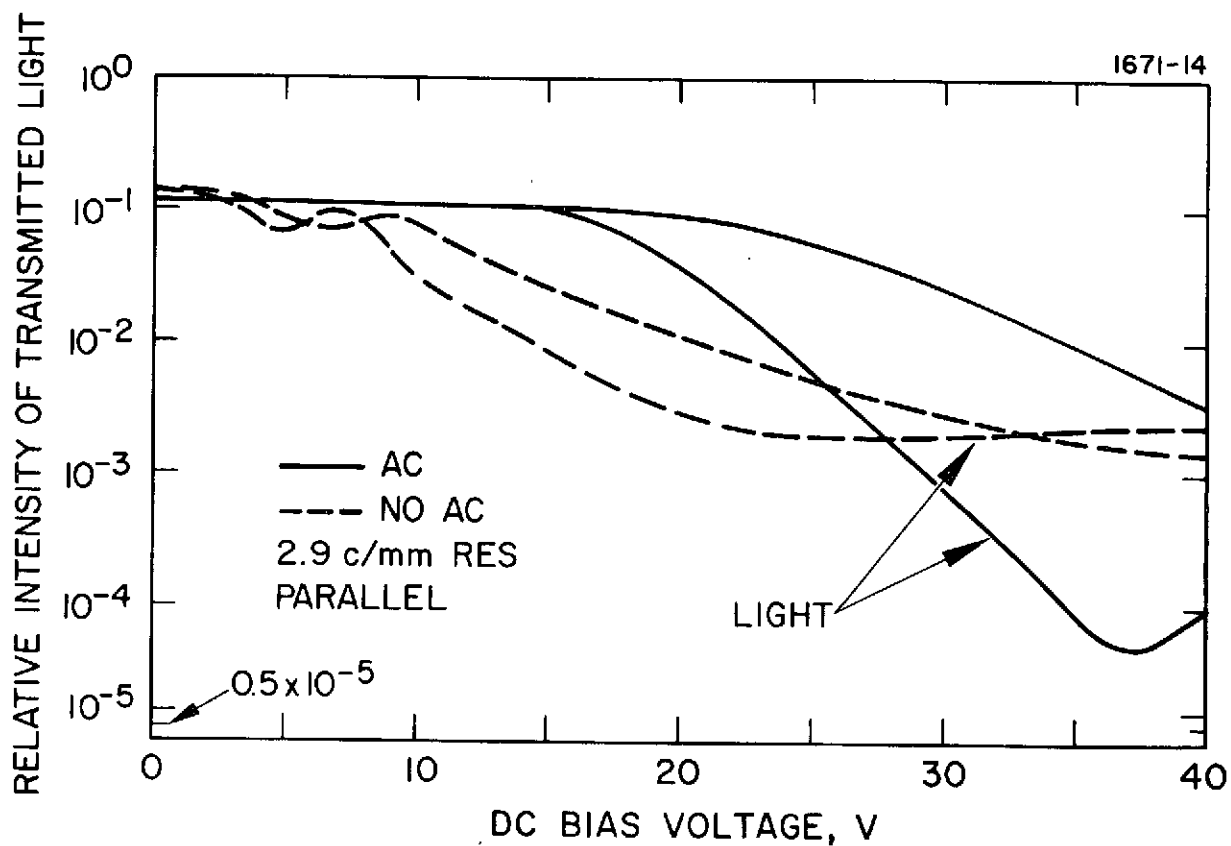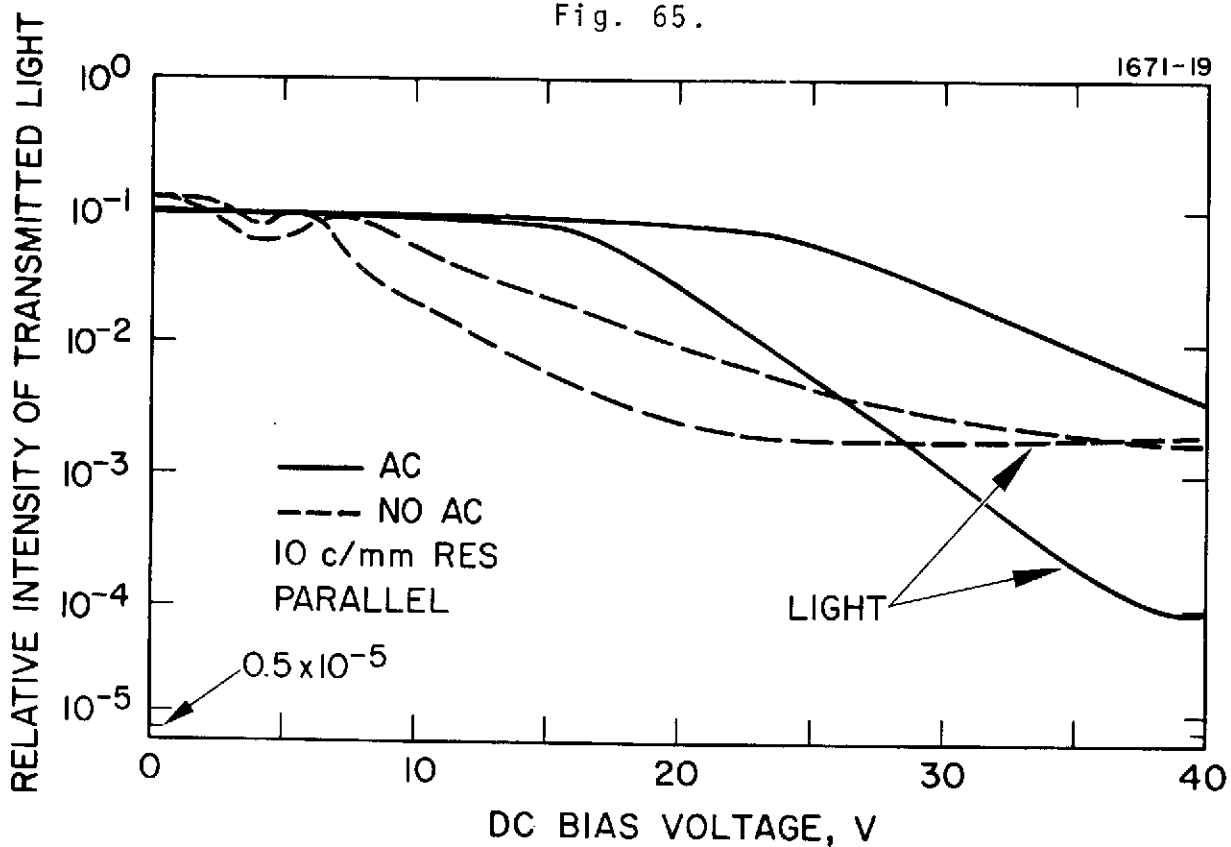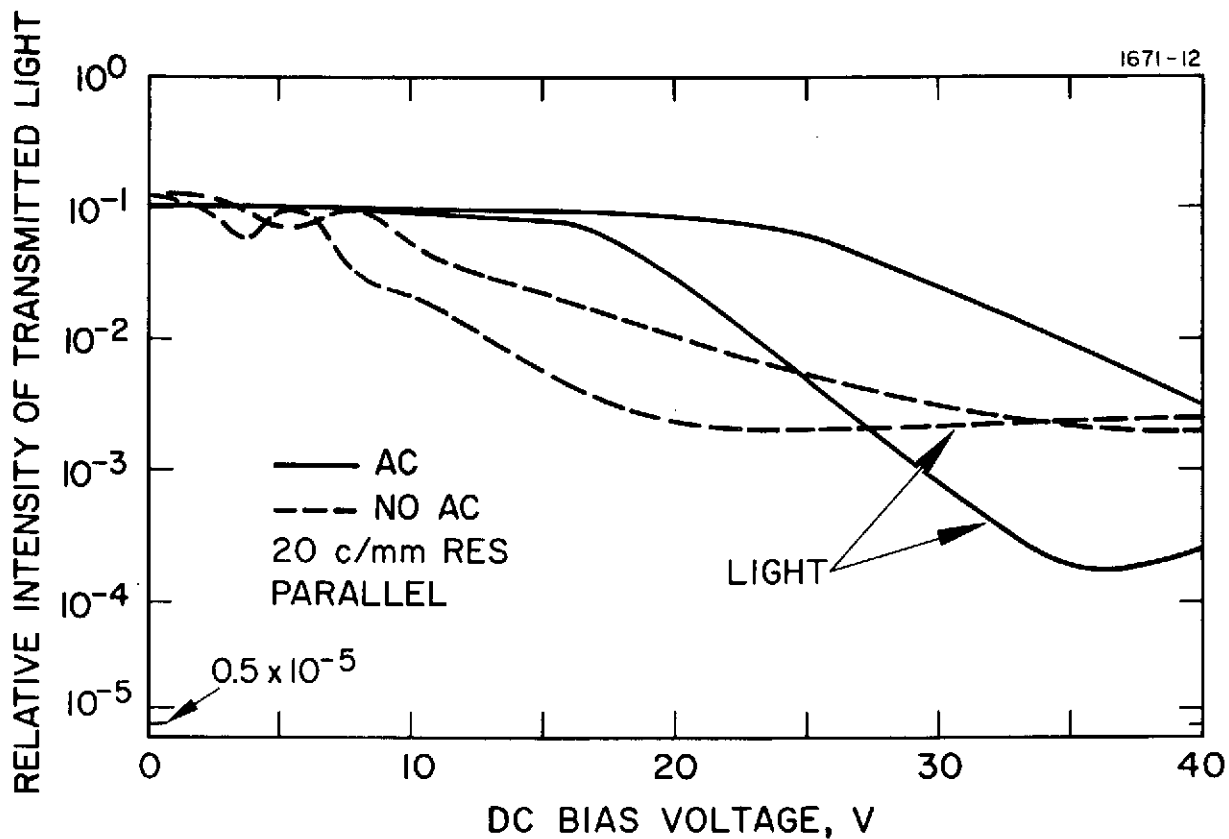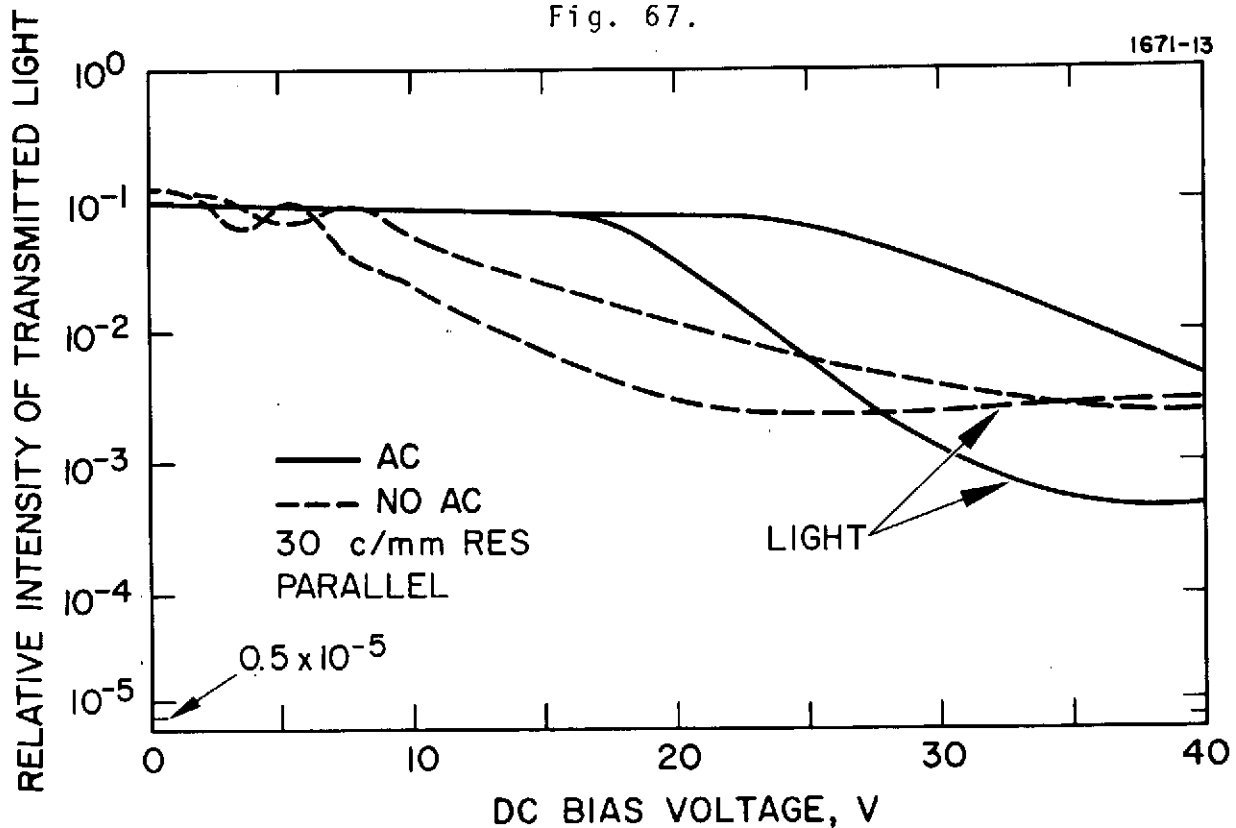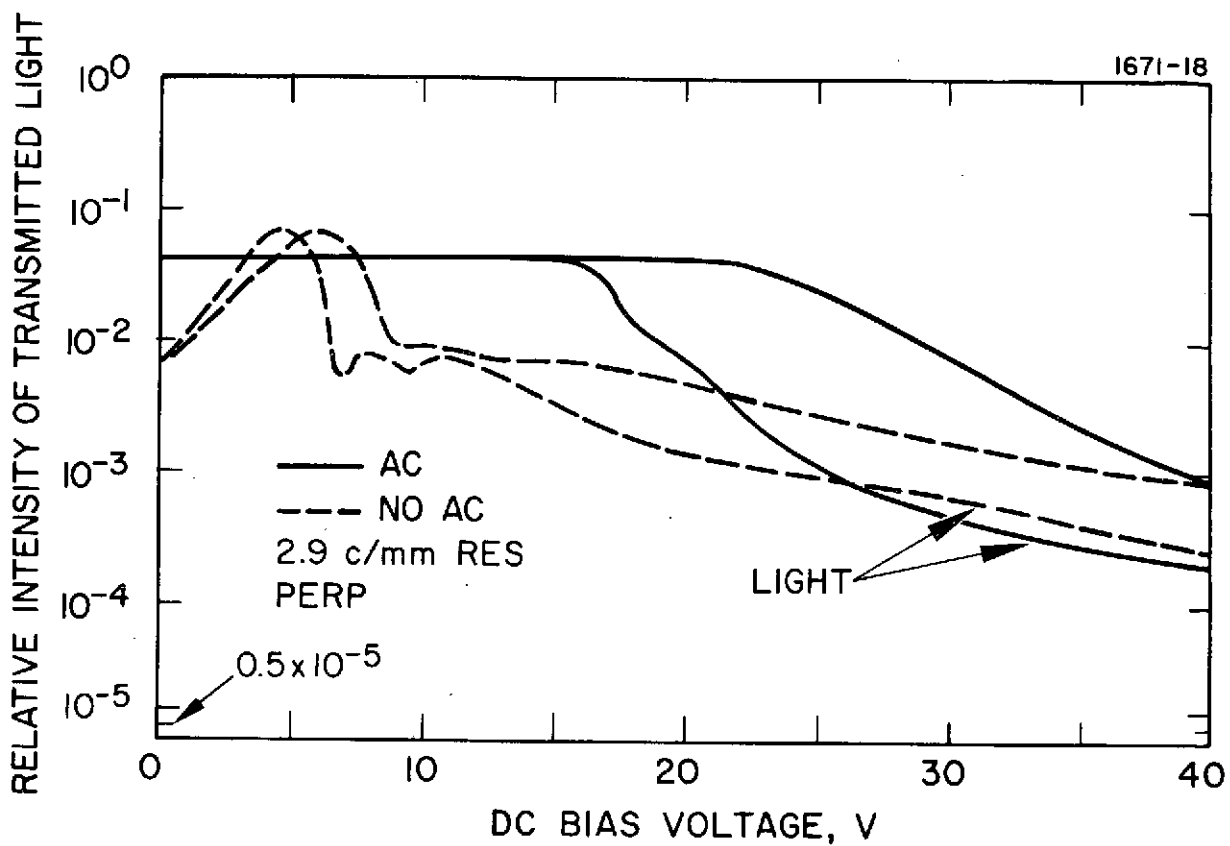
REFERENCES

1. P. Chatelain, Bull. Soc. Franc. Miner. Crist. 77, 323 (1954).

2. G.W. Gray, "Molecular Structure and the Properties of Liquid Crystals," Academic Press, N.Y. 1962, Chap. IV.

3. N.H. Hartshorne and A. Stuart, "Crystals and the Polarizing Microscope," 2nd Ed., Ed. Arnold, London, 1960.

4. R. Williams and G. Heilmeier, J. Chem Phys. 44, 638 (1966).

5. R.A. Soref, in "The Physics of Opto-Electronic Materials," Plenum Press, 1971, p. 207.

6. See for example "Surface Chemistry," ACS Monograph 153, L.I. Osipow, Reinhold Publishing Corp., New York, 1962.

7. P. Chatelaine, Bull. Soc. Franc. Miner. Crist. 66, 105 (1943).

8. P.A. Penz, Phys. Rev. Letters 24, 140 (1970).

9. L.C. Creogh, A.R. Kmetz and R.A. Reynolds, IEEE Trans. Elec. Devices, ED-18, 672 (1971).

10. M.J. Rafuse and R.A. Soref, Electrically Controlled Birefringence of Thin Nematic Films, Sperry Rand Research Report No. SRRC-RR-71-24, June 1971.

11. W. Hass, J. Adams, and J.B. Flannery, Phys. Rev. Letters Vol. 25, No. 19, 1326 (1970).

12. H. Gruler and G. Meier, Molecular Crystals and Liquid Crystals, 16, 299 (1972).

13. G.V. Jorgenson and G.K. Wehner - Tenth National Symposium on Vacuum Technology 1963, G.H. Bancroft, ed. (Pergamon Press, N.Y. 1963) p. 388.

14. R. Williams, J. Chem Phys 32, 1505 (1960).

15. H. Gerischer, J. Electrochem. Soc 113, 1174 (1966).

16. H. Gerischer, Physical Chemistry, Vol IX A, Eyring, Henderson and Jost, eds, (Academic Press, N.Y. 1970) p. 463.

17.   A. Many, J. Phys. Chem. Solids <u>26</u>, 587 (1965).

18.   J. DeWald, <u>Surface Chemistry of Metals and Semicon-</u>
<u>ductors</u>, H. Gatos, ed, (J. Wiley, N.Y., 1960) p. 205.